SHEAR RESISTANCE OF DISCONTINUITIES IN ROCK

by

JEFFREY WILLIAM NELSON

B.S., University of Colorado
(1974)

SUBMITTED IN PARTIAL FULFILLMENT
OF THE REQUIREMENTS FOR THE
DEGREE OF

MASTER OF SCIENCE

at the

MASSACHUSETTS INSTITUTE OF TECHNOLOGY

MAY 1977

Signature redacted

Signature of Author.....
Department of Civil Engineering, May 12, 1977

Signature redacted

Certified by.....
Thesis Supervisor

Signature redacted

Accepted by.....
Chairman, Departmental Committee on Graduate Students of the
Department of Civil Engineering

Thesis
CE
1977
M5.

ABSTRACT

SHEAR RESISTANCE OF DISCONTINUITIES IN ROCK

by

JEFFREY WILLIAM NELSON

Submitted to the Department of Civil Engineering on May 12, 1977
in partial fulfillment of the requirements
for the degree of Master of Science

This thesis is concerned with the development of an analytical model for the shear resistance of an individual rock discontinuity. Two basic mechanisms of resistance, the sliding mechanism and the shearing mechanism, have been identified, studied individually, and combined to describe discontinuity shear resistance.

The sliding mechanism represents sliding on horizontal and inclined surfaces of a discontinuity. Friction, as an important part of the sliding mechanism, has been studied through theory and experimental observations, revealing that friction in rocks is not clearly understood. Experimental observations of friction in minerals indicates that surface conditions of cleanliness, roughness, and moisture play an important role in controlling sliding resistance.

The shearing mechanism represents shearing through asperities on a discontinuity. Different methods for theoretically calculating single asperity shear resistance have been presented and compared. The base shear method, a simple and commonly used method which assumes a failure surface parallel to the plane of the discontinuity, has been shown to significantly overestimate asperity shear resistance in some cases.

The two mechanisms of sliding and shearing have been combined in an analytical relationship describing the shear resistance of a discontinuity. Evaluation of the parameters affecting this relationship has indicated that shear resistance is strongly dependent on the displacement of the discontinuity during shear. A shear simulation process has been proposed to account for this displacement dependence. A geometric representation of a discontinuity is sheared in increments of displacement, with the direction of displacement determined by establishing the direction of minimum resistance through an iterative procedure.

Thesis Supervisor: Herbert H. Einstein

Title: Associate Professor of Civil Engineering

ACKNOWLEDGEMENTS

Professor Herbert H. Einstein receives my sincere appreciation for the guidance which he has provided in the completion of this thesis. His generous contributions of time and personal interest are a credit to himself and an example to his profession.

I have received financial support for this research and for my studies at M.I.T. from NSF Grant No. ENG 75-19112 ("Research on Rock Discontinuities") and from a HEW Domestic Mining and Mineral and Mineral Fuel Resources Fellowship. This support is gratefully acknowledged.

Credit and thanks are also due to Charles Schwartz, who performed the finite element analysis described in Appendix A, and to William Dershowitz, who performed numerical computations for Chapter 5.

Finally, I wish to thank my wife, Deborah, who typed the manuscript, provided editorial assistance, and otherwise supported me in this effort.

TABLE OF CONTENTS

LIST OF FIGURES

LIST OF TABLES

NOTATION

A	Total area of a discontinuity
A_r	Area of a discontinuity where sliding occurs
A_s	Area of a discontinuity where shearing of asperities occurs
a_c	Contact area ratio ($= (A_r + A_s)/A$)
a_s	Shear area ratio ($= A_s/A$)
c_i	Cohesion of the intact material
i	Inclination of an asperity face, measured from the plane of a discontinuity
i^*	Dilation angle
N	Total normal force acting on a discontinuity
N_r	Normal force acting on the sliding area (A_r) of a discontinuity
N_s	Normal force acting on the shearing area (A_s) of a discontinuity
n	Component of q which acts in a direction perpendicular to the plane of a discontinuity
p	As a subscript, denotes the value of a quantity at peak discontinuity shear resistance
q	Uniform stress applied to an asperity face
S	Total shear resistance of a discontinuity
S_r	Shear resistance due to sliding on a discontinuity
S_s	Shear resistance due to shearing of asperities on a discontinuity
s	Component of q which acts in a direction parallel to the plane of a discontinuity
u	Displacement of a discontinuity in a direction parallel to the plane of a discontinuity
v	Displacement of a discontinuity in a direction perpendicular to the plane of the discontinuity

$\dot{v}$	Dilation rate, rate of change of v with respect to u ($=\frac{\Delta v}{\Delta u}$)
α	Inclination of q from the normal of the asperity face on which q acts
μ	Coefficient of friction, the ratio of friction force to normal force
σ	Normal stress acting on a discontinuity (= N/A)
σ_c	Unconfined compressive strength of the intact material
σ_t	Tensile strength of the intact material
σ_T	Transition stress, σ for which $\tau = \tau_i$
τ	Specific shear resistance of a discontinuity (= S/A)
τ_i	Specific shear resistance of the intact material
ϕ_i	Angle of internal friction of the intact material
ϕ_μ	Friction angle for sliding on flat, smooth surfaces
χ	Horizontal tip displacement of an asperity at failure

CHAPTER 1

INTRODUCTION

In the majority of engineering problems involving rock masses, recognition of the discontinuous nature of the rock mass is of utmost importance to the understanding of the rock mass behavior. The behavior of the mass is governed by the behavior of the discontinuities as well as the behavior of the intact rock. In general, the discontinuities have properties of strength and deformability which are quite different from those of the intact rock, and in many cases, the discontinuities will completely dominate the engineering considerations of the rock mass.

Although the importance of discontinuities in controlling rock mass behavior is well recognized, analytical description of discontinuity behavior is inadequate in many respects, and thus considerable research in this area is necessary. The purpose of this thesis is to develop an analytic description of the shear resistance of an individual discontinuity in rock.

The method of approach to this problem is to: identify the important mechanisms responsible for shear resistance, study these mechanisms and develop analytical descriptions of them individually, and combine these mechanisms to form an analytical description of a discontinuity as a whole.

The structure of the thesis reflects the method of approach described above. In Chapter 2, two basic mechanisms of shear resistance in rock discontinuities are identified, the sliding mechanism and the shearing mechanism, and the important factors which influence these mechanisms are discussed. In addition, the basic terminology which is used to quantitatively describe shear behavior is defined. Chapter 3 reviews existing analytical models for rock discontinuities by other researchers. Chapters 2 and 3 provide the background for the remainder of the thesis. In Chapters 4 and 5, the two basic mechanisms of shear resistance, sliding and shearing, are examined in detail individually. Analytical descriptions of each of these mechanisms are then combined in Chapter 6, where a procedure for modelling the behavior of a single discontinuity is formulated.

CHAPTER 2

MECHANISMS IN THE SHEARING PROCESS

As a starting point in this study of the shear resistance of rock discontinuities, it is useful to identify the mechanisms involved in the shearing process. By examining these mechanisms, the shear behavior of discontinuities will be better understood. This chapter attempts to identify the important mechanisms, as well as the various factors which influence these mechanisms.

In addition to identifying factors and mechanisms, this chapter defines the basic terminology used to describe shear behavior and explains the emphasis of the approach used in this study.

2.1 DEFINITION OF TERMS

As a basis for following discussions of the mechanical behavior of discontinuities, it is necessary to define the terminology used to describe the shearing process. The direct shear test will be used here as an example to illustrate these terms, although in their general sense the terms apply to any shearing of discontinuities.

A schematic representation of a direct shear test is shown in Fig. 2-1a. The normal force (N) is normal to the plane of the discontinuity, and shear force (S) is coplanar with the discontinuity plane. If the area of the discontinuity surface is defined as A, then the normal stress (σ)

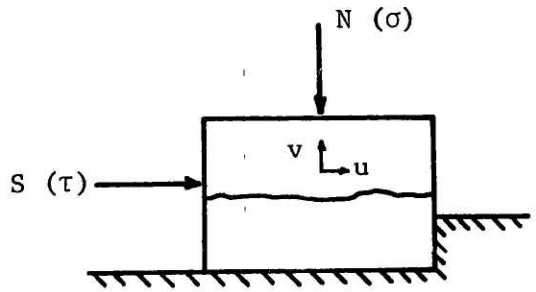

(a)

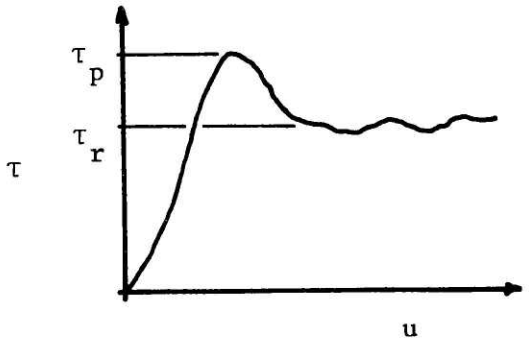

(b)

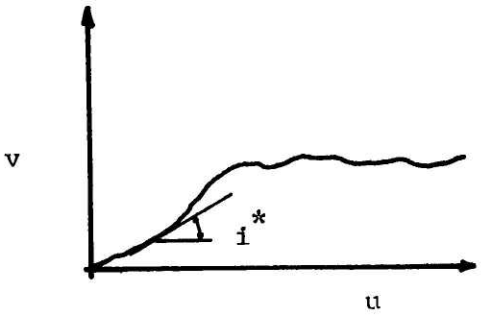

(c)

Figure 2-1. Schematic of direct shear test, with typical plots of shear stress vs. shear dispalcement and normal displacement vs. shear displacement.

and shear stress (τ) on the discontinuity plane are given by $\frac{N}{A}$ and $\frac{S}{A}$, respectively.

The usual procedure in a direct shear test is to apply a constant N, and measure S while the top block is displaced over the bottom block. Displacements of the top block which take place during shear can be measured in a direction normal to the discontinuity plane and parallel to the discontinuity plane. These are defined as the normal displacement (v) and the shear displacement (u), respectively.

An example of a plot of τ vs. u from a direct shear test is shown in Fig. 2-1b. As u increases, τ increases to a "peak" value (τ_p), and then decreases to a relatively constant "residual" value (τ_r). It should be noted that "residual" does not necessarily imply a constant value with increasing displacement, but only the value attained after some arbitrarily large displacement. Not all shear tests will exhibit a "peak" value of shear resistance. Some tests will show a τ - u curve which increases monotonically to a final value.

Figure 2-1c illustrates a plot of v vs. u during a direct shear test. Positive normal displacement (upward) of the top block is termed dilation, while negative normal displacement (downward) is termed contraction. The slope of the v - u curve at any particular point is defined as the dilation rate ($\dot{v}$). The dilation angle (i^*), illustrated in Fig. 2-1c, is given by

$$i^* = \arctan \dot{v} = \arctan \left(\frac{\Delta v}{\Delta u} \right)$$

The values of $\dot{v}$ and i^* at peak shear resistance (τ_p) are denoted by $\dot{v}_p$ and i^*_p.

A series of direct shear tests performed at different normal stresses

can be used to determine the dependence of shear strength on normal stress. These results are plotted on a Mohr diagram, as shown in Fig. 2-2, to define the strength envelope for that particular type of discontinuity. It is possible to obtain envelopes for both peak and residual strengths. The peak strength envelopes are generally curved, particularly in the lower normal stress range. The residual envelopes tend to be much flatter, being approximately linear in many cases. The nature of these envelopes will be treated further in later sections of this thesis.

2.2 BASIC MECHANISMS

In order to understand the shearing process and what causes different behavior in different discontinuities, it is useful to study the mechanisms involved. This section identifies those mechanisms which appear to be important in the shearing of rock discontinuities.

Patton (1966) was one of the first to systematically study the different shear mechanisms in rock discontinuities. Through laboratory tests on discontinuities cast from a model material, he identified two different mechanisms of shear resistance. The discontinuities that he tested had regularly shaped asperities, or "teeth", on their surfaces, as illustrated in Fig. 2-3a. By performing direct shear tests on these model discontinuities, Patton found that the mechanism of peak shear resistance was dependent on the level of normal stress acting on the discontinuity.

At low normal stresses (Test 1 in Fig. 2-3), peak resistance was mobilized while the upper block was sliding upward on the teeth of the lower block, as illustrated in Fig. 2-3b. The shear force-shear displacement curve for this test is shown in Fig. 2-3d. The initial, steep portion of

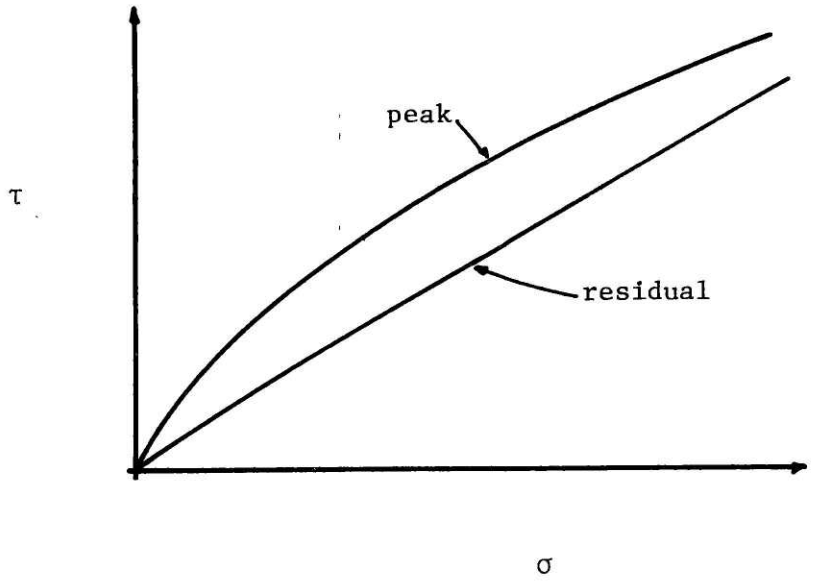

Figure 2-2 Mohr diagram illustrating peak and residual failure envelopes.

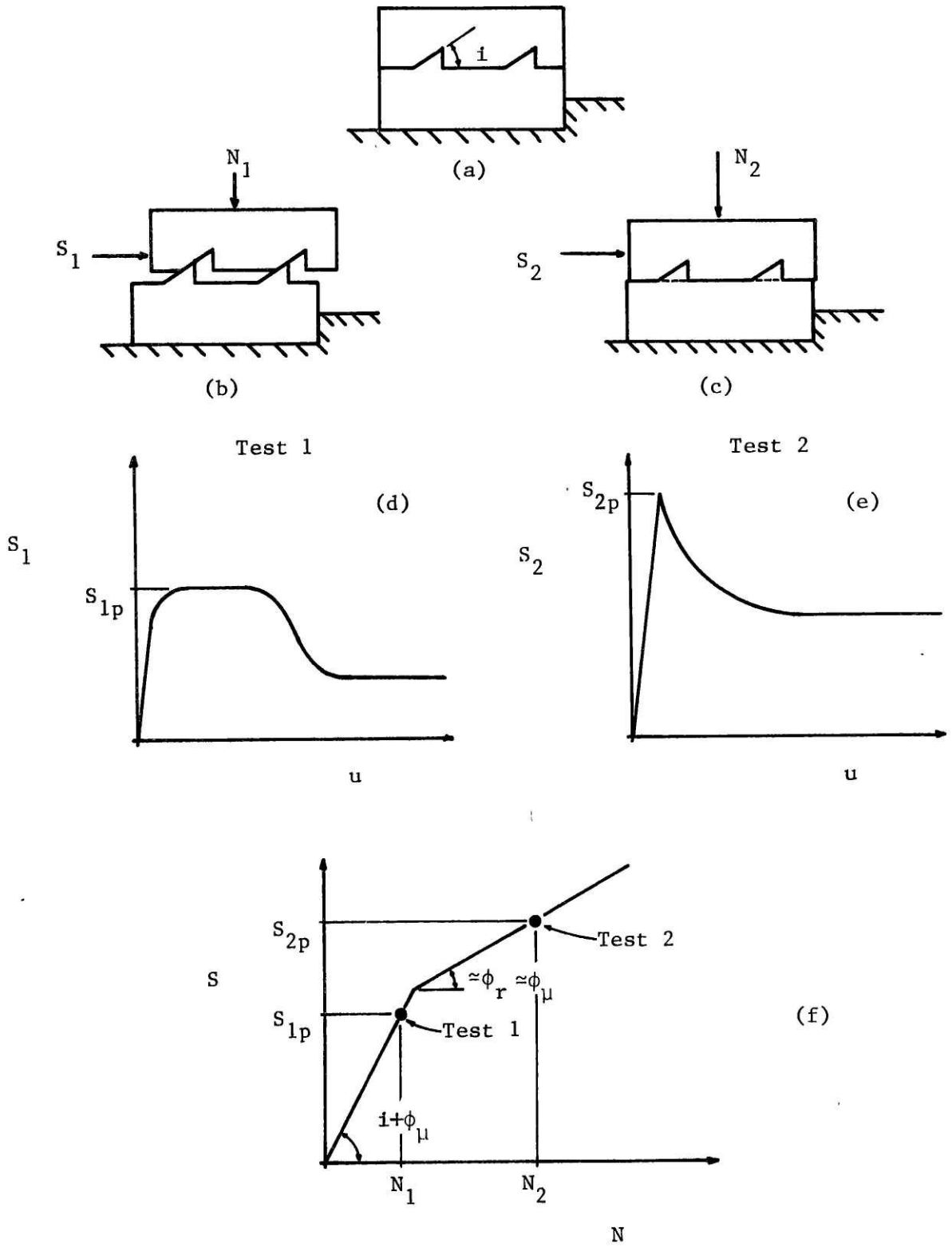

Figure 2-3 Model tests performed by Patton (1966).

the curve represents "elastic" distortion prior to sliding. The following flat portion represents the displacement due to sliding of the top block upward, where the discontinuity is dilating. Eventually the teeth are sheared through or overridden, the discontinuity no longer dilates, and the resistance drops towards a residual value.

At high normal stresses (Test 2 in Fig. 2-3), there is no sliding up the inclined teeth. Peak resistance is mobilized by shearing through the teeth at their base, as illustrated in Fig. 2-3c. The shear force-shear displacement curve for this test is shown in Fig. 2-3e. It shows a steep initial "elastic" portion, but there is no flat portion corresponding to sliding during dilation. At peak resistance, there is virtually no dilation, and once the peak is reached the resistance drops quickly towards a residual value.

The values of peak resistance (S_p) for the two tests described above can be plotted on a Mohr diagram, as in Fig. 2-3f. Patton found that the failure envelope defined by a number of tests on identical discontinuities at different normal stresses could be represented by two straight lines as shown. This is the well-known bilinear envelope representing the two mechanisms of shear resistance described above. For low N, the mechanism of peak resistance is sliding up the inclined teeth. It can be shown that the relation between shear force (S) and normal force (N) for sliding up inclined surfaces can be represented by the following equation:

$$S = N \tan (i + \phi_\mu) \qquad (2.1)$$

where i is the inclination of the sliding surface and ϕ_μ is the friction angle for sliding on a flat, smooth surface. (As used here, a "flat, smooth" surface is one which is macroscopically smooth, but microscopically

irregular (unpolished). The scale of smoothness at which ϕ_μ is measured is important, and this topic will be discussed in Chapter 4.) Patton found that eq. 2.1 fit his data well for tests where sliding was the mechanism of peak shear resistance.

For high values of N, the mechanism of peak resistance is shearing through the base of the teeth. The form of the failure envelope for this mechanism is controlled by the shear strength of the teeth. Patton found that in his tests this portion of the failure envelope could be approximated by a linear function of N, with a slope angle (ϕ) that was approximately equal to the residual friction angle (ϕ_r) as well as the sliding friction angle (ϕ_μ). This is expressed by

$$S = C_x + N \tan \phi$$

where C_x is the intercept of the envelope on the S-axis.

In summary, the initial portion of the bilinear failure envelope is controlled by the angle i and the friction angle ϕ_μ . The second portion of the envelope is controlled in a more complex way by the strength of the teeth as determined by their size and the specific shear strength of the intact material.

The bilinear envelope described above was obtained from tests where the asperities (teeth) were uniform in size and inclination. The two mechanisms of shear resistance occurred separately at different levels of normal stress. In real rock discontinuities, asperities have many different sizes and shapes, with the result that the two mechanisms of shear resistance occur simultaneously on different asperities. This causes the failure envelope to be curved rather than bilinear for actual discontinuities.

In the above discussion, two different mechanisms of shear resistance have been identified. The first mechanism was sliding accompanied by dilation. The second mechanism was shearing, without dilation in this case, although it is possible to have dilation associated with shearing as well (see Chapter 6). Dilation can be an important component of both the sliding and the shearing mechanism, in that it increases the shear resistance in both cases. The two mechanisms described above are considered to be the two major mechanisms involved in the shearing of rock discontinuities. In this thesis, they will be known as the sliding mechanism and the shearing mechanism. These two mechanisms will be examined in detail in Chapters 4 and 5. It will be seen that the distinction between sliding and shearing is a somewhat arbitrary one, in that a sliding mechanism on one scale can be considered a combination of sliding and shearing on a smaller scale. However, it is still useful to make the distinction between the two mechanisms as outlined above.

2.3 FACTORS INFLUENCING BEHAVIOR

As well as identifying the mechanisms involved in the shearing process, it is important to identify the physical factors which influence these mechanisms. This section presents a brief discussion of five important factors: character of the rock through which the discontinuity passes, surface geometry of the discontinuity, filler material, water, and the state of applied stress.

The character of the rock through which the discontinuity passes, called the "wall rock", influences shear behavior in several direct and indirect ways. Wall rock type, as described by its texture and mineralogy,

influences behavior in two direct ways. One effect is related to the sliding mechanism, because sliding properties are dependent on rock type. This effect is examined in Chapter 4. Another effect of rock type involves the shearing mechanism, because the strength of surface irregularities is influenced by rock type.

There are also a number of indirect effects of the wall rock type. One effect concerns the change in character of the rock with weathering. Different rock types have different rates of weathering and different weathering products. Another effect of rock type is the influence it has on the surface geometry of the discontinuity during the creation of the discontinuity. The size and shape of surface irregularities are influenced by the texture of the intact rock and by cracks and other flaws in the intact rock. A final effect of rock type is the influence it has on the type and amount of gouge produced during shearing of discontinuity. This gouge can have a significant influence on the shear behavior.

The surface geometry of the discontinuity has an important effect on shear behavior on several different scales. It is convenient to divide the scale of surface irregularities into three groups: roughness, on a microscopic scale; asperities, on an intermediate scale; and undulations, on a large scale. Irregularities play an important role in both the sliding and the shearing mechanism on all scales. Surface geometry is particularly important in determining dilation and shear strength of asperities. The effect of surface geometry, as it relates to shearing and sliding, is examined in Chapters 4 and 5.

The type and amount of filler material can greatly influence discontinuity behavior. As used here, filler material represents weathering

products, gouge, or foreign material transported into the discontinuity. If the filler material thickness is greater than the height of surface irregularities, the characteristics of the filler can completely dominate the behavior of the discontinuity. If the filler thickness is less than that height, then the filler material and the irregularities will interact in some way. In either case, the presence of filler can have an important effect. However, effects of filler material will not be examined in this thesis.

The presence of water in the discontinuity influences behavior in both direct and indirect ways. A direct effect is through cleft water pressure which influences the effective stresses in the discontinuity. Other direct effects include the alteration of sliding properties and strength properties of the rock by encouraging the process of weathering. Water can also cause swelling of the filler material or the wall rock itself. The effects of water will only be examined on a limited basis, in so far as they influence the sliding properties (Chapter 4).

The state of applied stress is a factor which is related to all of the preceding factors. The relative importance of these factors, in general, will be related to the magnitude of stresses acting on the discontinuity. The influence of stress on the mechanism of shear failure was illustrated in the preceding section describing Patton's work. The exact nature of the dependence of the preceding factors on the applied stresses is of major interest. Its treatment is a part of the remaining portions of this thesis.

2.4 MODEL DEVELOPMENT

The material in the preceding sections of this chapter was presented to provide a background for the study of the shear behavior of rock discontinuities. In following chapters, the mechanisms will be examined more closely in an attempt to formulate a model which can describe and predict the shear resistance of discontinuities. Before continuing, a few general comments will be made concerning model development.

Any model which is useful must properly represent the process that is to be modelled, leading to certain requirements:

1. The model should account for the important factors which influence the shear behavior of discontinuities, and it must do so in a way which is consistent with observations of actual discontinuities.
2. The physical description of the discontinuity, which will be the necessary input to the model, must be practically obtainable. That is, input parameters must be measurable in a practical way.

These two requirements will be kept in mind in the course of the following model development.

There is more than one type of approach which could be used to develop a model which satisfies the above requirements, as will now be discussed.

In the development thus far in this chapter, emphasis has been placed on what might be called a "mechanistic" approach. In this approach, the overall shearing process is separated into different mechanisms, each of which can be described in an analytical way. These mechanisms can then be combined to form a model for the overall process.

Another somewhat different approach might be called a "phenomenological" or "empirical" approach. This approach involves the selection of some analytic model which relates certain measurable parameters to quantities of interest in the shearing process. The model has to predict shear behavior in a way which agrees with observations, but it may have no conceptual or physical similarity with the actual process being modelled.

From a practical standpoint, the relative merit of each approach depends on the usefulness of the resulting model and the success it has in each individual situation. However, it is believed that the mechanistic approach is one which will provide a better physical understanding of the process being modelled, and probably one which will find a more general application. Therefore, the mechanistic approach is the approach employed in this thesis.

CHAPTER 3

REVIEW OF EXISTING DISCONTINUITY MODELS

At present there are few models available which attempt to describe the shear strength of rock discontinuities. This chapter reviews three of these models, examining their usefulness and pointing out the limitations of each.

First, the laboratory work of Patton is recalled, and its application to actual rock discontinuities is discussed. Then, models developed by Ladanyi and Archambault (1970) and Barton (1971, 1973) are presented. These latter two models are good examples of the two different approaches discussed in Section 2.4. Ladanyi and Archambault use a mechanistic approach, while Barton uses an empirical (phenomenological) approach.

3.1 PATTON

The laboratory work of Patton (1966) has been described in Section 2.2. For model discontinuities with several identical asperities, the failure envelope was bilinear. The initial linear portion was described by:

$$S = N \tan (i + \phi_\mu) \qquad (3.1)$$

This equation can be applied to actual rock discontinuities if, over a certain range of normal stress, a sliding mechanism operates and no shearing of asperities occurs. This is likely to be true if a discontinuity has asperities with a uniform inclination (i), or asperities with different but very low inclinations such that none of the asperities are

likely to shear. If it can be established that only a sliding mechanism occurs over the normal stress range that is of interest, then eq. 3.1 can be used to predict the failure envelope, and only the parameters i and ϕ_μ are required. Estimates of i can be made from measurements of the surface geometry of the discontinuity. ϕ_μ can be measured in sliding tests on samples of the wall rock. (As defined in Section 2.2, ϕ_μ is the friction angle for sliding on flat, smooth surfaces. The scale at which a surface is considered "flat" and "smooth" must be specified, because a surface will always be irregular on a very small scale. In this thesis, a flat smooth surface is a surface which is smooth on a macroscopic scale, but irregular on a microscopic scale (unpolished). This matter will be discussed further in Chapter 4.)

3.2 LADANYI AND ARCHAMBAULT MODEL

Ladanyi and Archambault (1970) developed an equation to describe the shear strength of rock discontinuities using an energy approach, where they account for shearing and sliding taking place simultaneously over the surface of the discontinuity. Their approach is patterned after that taken by Rowe et al. (1964), where energy components in a direct shear test on granular material were analysed.

Ladanyi and Archambault divide the total shear resistance (S) of a rock discontinuity into four components:

S_1 = component due to external work done in dilation

$$= N \dot{v} \tag{3.2}$$

S_2 = component due to internal work done in dilation

$$= S \dot{v} \tan \phi_f \tag{3.3}$$

S_3 = component due to internal friction under no volume change

$$= N \tan \phi_\mu \tag{3.4}$$

S_4 = component due to shearing through surface irregularities

$= A\ \tau_i$ (3.5)

where N = total normal force

$\dot{v}$ = dilation rate (defined in Section 2.1)

S = total shear force

ϕ_f = statistical average of the friction angle when sliding occurs along the irregularities of different orientations

A = total discontinuity area

τ_i = specific shear strength of the intact material

Two of these parameters need to be discussed, ϕ_f and τ_i.

ϕ_f: Rowe (1962) investigated ϕ_f for granular material and found that $\phi_f \simeq \phi_\mu$ for dense packings. From this information, Ladanyi and Archambault conclude that $\phi_f \simeq \phi_\mu$ for tightly interlocked rock surfaces as well. However, because of the rigid nature of the sliding rock surfaces, sliding will only occur along irregularities of a single orientation, and ϕ_f should equal ϕ_μ in <u>all</u> cases.

τ_i: Ladanyi and Archambault chose to use Fairhurst's parabolic criterion (Fairhurst, 1964) for the strength of the intact material:

$$\tau_i = \sigma_c \left[\frac{(n+1)^{\frac{1}{2}} - 1}{n}\right]\left[1 + \frac{n\,\sigma}{\sigma_c}\right]^{\frac{1}{2}} \qquad (3.6)$$

where $n = \dfrac{\sigma_c}{-\sigma_t}$, the ratio of unconfined compressive strength to tensile strength.

Referring back to the four shear components, the first three components (S_1, S_2, S_3) arise from sliding on certain portions of the discontinuity while the fourth component (S_4) arises from shearing of irregularities on other portions of the discontinuity. If the shearing area is designated A_s, and sliding is assumed to act over the remainder of the area $(A - A_s)$, then the following can be written:

$$S = (S_1 + S_2 + S_3)\ (1 - a_s) + S_4\ a_s \qquad (3.7)$$

where $a_s = A_s/A$, the shear area ratio.

If N and S are assumed to act uniformly over A, then eqs. 3.2 - 3.5 can be substituted into eq. 3.7 with the following result:

$$\tau = \frac{S}{A} = \frac{\sigma(\dot{v} + \tan \phi_\mu)(1 - a_s) + a_s \tau_i}{1 - (1 - a_s)\, \dot{v} \tan \phi_f} \tag{3.8}$$

Equation 3.8 requires a number of parameters which must be determined to predict τ_i. The parameters ϕ_μ and τ_i can be measured through laboratory tests on samples of the intact material. As previously discussed, ϕ_f can be assumed equal to ϕ_μ. The parameters $\dot{v}$ and a_s are much more difficult to determine. Ladanyi and Archambault suggest the following two empirical expressions for these parameters ($\dot{v}_p$, a_{sp}) at peak shear resistance.

$$\dot{v}_p = \left(1 - \frac{\sigma}{\sigma_T}\right)^K \tan i \tag{3.9}$$

$$a_{sp} = 1 - \left(1 - \frac{\sigma}{\sigma_T}\right)^L \tag{3.10}$$

where K and L are empirically determined constants, i is the inclination of surfaces on which sliding occurs as σ approaches zero, and σ_T is the transition pressure, or the normal stress for which the shear strength of the discontinuity equals that of the intact rock.

Ladanyi and Archambault indicate that, based on available experimental data, K = 4 and L = 1.5. However, they acknowledge that the numerical values of these coefficients, as well as the entire form of the equations for $\dot{v}$ and a_s (eqs. 3.9 and 3.10), are based on a limited amount of data and may not be applicable to all discontinuities.

Figure 3.1a illustrates the variation of $\dot{v}$ and a_s with σ as indicated by eqs. 3.9 and 3.10 with K = 4 and L = 1.5. Using these relationships for $\dot{v}$ and a_s, Fig. 3.1b illustrates the general form of eq. 3.8 on a plot

(b)

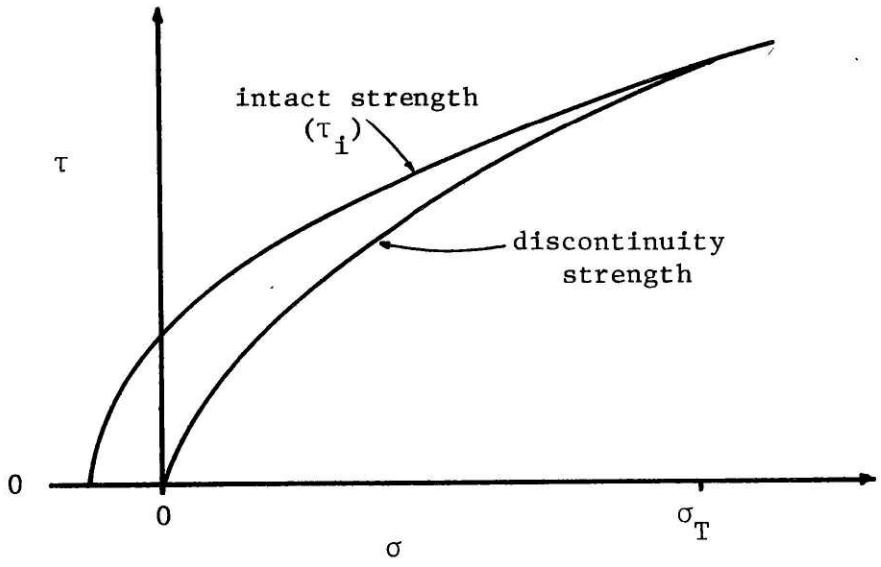

discontinuity strength: $\tau = \frac{S}{A} = \frac{\sigma(\dot{v} + \tan \phi_\mu)(1 - a_s) + a_s \tau_i}{1 - (1 - a_s)\, \dot{v} \tan \phi_f}$

(a)

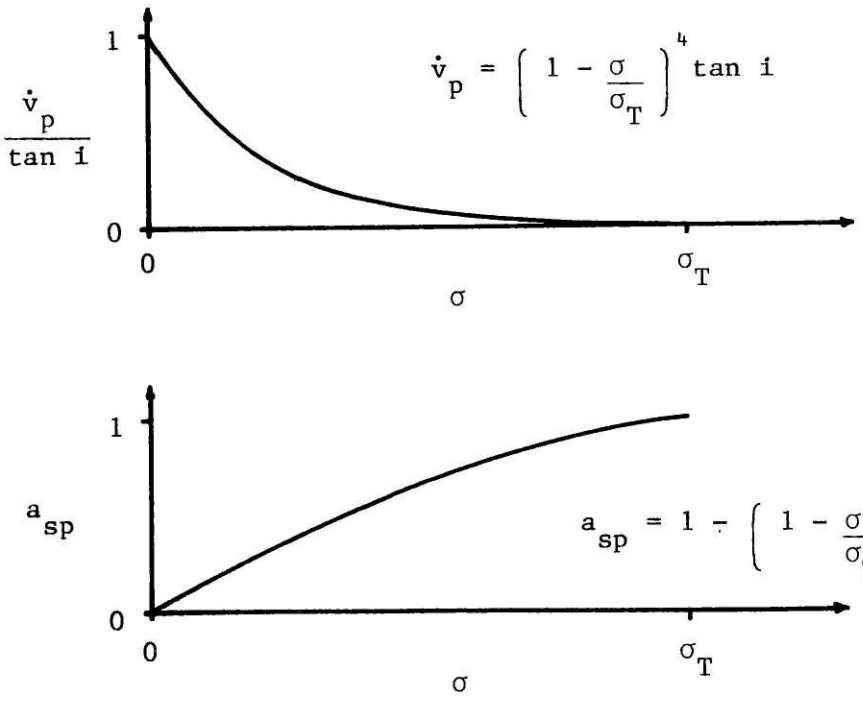

Figure 3-1 Discontinuity shear equation of Ladanyi and Archambault (1970), with suggested empirical relationships for shear area ratio (a_s) and dilation rate ($\dot{v}$).

of τ vs. σ , as well as the form of the intact strength envelope as given by eq. 3.6.

Ladanyi and Archambault performed a series of direct shear tests on simulated discontinuities, using rectangular concrete prisms to simulate asperities, and found good agreement between the observed failure envelope and the failure envelope predicted by eq. 3.8.

Equation 3.8 represents a mechanistic model which accounts for shearing and sliding mechanisms occurring simultaneously over different portions of the discontinuity. In the development of eq. 3.8, a fully interlocking discontinuity is assumed, i.e., all portions of the discontinuity are either shearing or sliding. Ladanyi and Archambault present a modification to eq. 3.8 to account for partial interlocking, but this will not be discussed here. Another assumption made is that both S and N are distributed uniformly over the total area. This, of course, is an approximation, but one which is diffcult to improve upon because the high degree of static indeterminancy in the distribution of stresses over the discontinuity. A final assumption that is of interest concerns the shearing component, S_4. This component is assumed to be equal to the shearing area times the specific shear strength of the intact material, and is assumed to act parallel to S. This is a simplification with respect to both magnitude and direction. This topic will be discussed further in Chapters 5 and 6.

There is another point connected with this last comment concerning the shearing component that deserves mention. Ladanyi and Archambault assume that the dilation component $(S_1 = N \dot{v})$, acts over only the sliding portion of the discontinuity (see eq. 3.7). If the discontinuity is dilating during shear, then the <u>entire</u> discontinuity is dilating because of the

rigid nature of the intact rock. Therefore, S_1 acts over the entire area and the following equation would appear to be correct, rather than eq. 3.7:

$$S = (S_1 + S_2 + S_3)\ (1 - a_s) + (S_1 + S_4)\ a_s$$

It seems that the reason Ladanyi and Archambault did not include S_1 with S_4 is that they assumed a horizontal shearing action (S_4 parallel to S), so that that portion of N which acts on the shearing areas is not being dilated against. This does not seem correct, because in reality, the entire N will be dilated against as the entire discontinuity dilates.

The most serious limitation to the practical use of eq. 3.8 is the determination of $\dot{v}$ and a_s, as mentioned on p. 19. It is not known whether the empirical relationships given by eqs. 3.9 and 3.10 are generally applicable to rock discontinuities. The measurement of $\dot{v}$ in shear tests is an increasingly common procedure, so that $\dot{v}$ data is available to compare with equation 3.9. However, the direct measurement of a_s is a very difficult task and seldom done, so there is very little information on a_s at present.

In general, the variation of $\dot{v}$ and a_s with σ is expected to depend on such factors as ϕ_μ, τ_i, and the surface geometry of the discontinuity. For example, low ϕ_μ, high τ_i, and slightly inclined asperities will tend to favor sliding with dilation ($\dot{v}$) rather than shearing (a_s). High ϕ_μ, low τ_i, and steeply inclined asperities will tend to favor shearing (a_s) rather than dilation ($\dot{v}$). Therefore, even if the form of eqs. 3.9 and 3.10 were found to apply to all discontinuities, the constants K and L are likely to be different for different discontinuities. The problem of predicting $\dot{v}$ and a_s will be further discussed in Chapter 6.

3.3 BARTON MODEL

Barton (1971) empolyed an empirical approach in the development of an equation to describe the shear strength of rock discontinuities. He performed a series of direct shear tests on discontinuities in a model material. The discontinuities were created by tensile splitting of the material, resulting in rough, irregular surfaces. Analyzing the data from these tests, Barton observed that the following relationships could be approximated:

$$\arctan\left(\frac{\tau_p}{\sigma} \right) = 2\ i_p^* + 30^o \tag{3.11}$$

and

$$i_p^* = 10 \log_{10} \frac{\sigma_c}{\sigma} \tag{3.12}$$

where τ_p = peak shear resistance
σ = normal stress, held constant during each test
i_p^* = dilation angle at peak shear resistance
σ_c = unconfined compressive strength of the intact material

Equations 3.11 and 3.12 can be combined to give:

$$\tau_p = \sigma \tan\left(20 \log_{10} \frac{\sigma_c}{\sigma} + 30^o \right) \tag{3.13}$$

This equation describes a relationship between τ_p, σ, and σ_c which approximately fits Barton's model discontinuity test data. The discontinuities, although irregular, all had the same order of roughness and approximately the same ϕ_μ ($\simeq 30^o$).

Barton (1973) hypothesized that eq. 3.13 could be modified for discontinuities with different roughness and different ϕ_μ, and proposed a more general relationship:

$$\tau_p = \sigma \tan\left(\text{JRC} \log_{10} \frac{\text{JCS}}{\sigma} + \phi_\mu \right) \qquad (3.14)$$

where JRC = joint roughness coefficient

JCS = joint wall compressive strength

ϕ_μ = friction angle for sliding on flat smooth surfaces

JRC accounts for discontinuities with different surface roughness. Barton suggests that JRC varies from 0 for smooth planar discontinuities to 20 for rough undulating discontinuities. At present there is no method for determining JRC from measurements of the surface geometry. JRC can be back-figured from one or more direct shear tests on discontinuities and an average value can then be used for similar discontinuities. This method presumes that JCS and ϕ_μ are well established, and that the model is valid. Barton (1976a) proposes an alternate method for determining JRC from "tilt tests". These are simulated direct shear tests at very low normal loads, where the normal and shear forces are supplied through gravity by tilting the discontinuity until sliding occurs. The angle of tilt can be used to back-figure a value of JRC for that test. This value of JRC is then assumed to be valid for higher stress ranges, and used in eq. 3.14. This method is still in development, and it is not yet clear whether JRC obtained in this way is valid for higher stress ranges. (By higher stress ranges, it is meant only those higher stress ranges for which eq. 3.14 applies. Barton (1976b) has proposed a different empirical relation from eq. 3.14 for very high normal stresses, which will not be discussed here.)

JCS is a measure of the strength of the surface irregularities. Barton suggests that JCS will vary from σ_c for unweathered discontinuities to approximately $\frac{1}{4}\sigma_c$ for weathered discontinuities, and that it can be estimated from Schmidt hammer tests on the wall rock.

Finally, ϕ_μ can be determined from sliding tests on samples of the wall rock.

Figure 3-2 illustrates the general form of eq. 3.14 on a shear stress-normal stress diagram for various combinations of JRC and JCS, ($\phi_\mu = 30^o$). Figure 3-2 also contains a qualitative description of joint roughness corresponding to JRC = 5,10,and 20.

In order to evaluate the general applicability of eq. 3.14, Barton (1973) reviewed published data from shear tests on a number of different types of rock. This review involved a comparison of experimental failure envelopes with failure envelopes predicted by eq. 3.14. Barton found that eq. 3.14 accounts for surface roughness, strength of the wall rock, effects of weathering, sliding properties of the wall rock, and the dependence of the failure envelope curvature on normal stress, all in a way which at least qualitatively agrees with observed discontinuity behavior. With appropiate selection of JRC and JCS values, the failure envelope given by eq. 3.14 was found to agree quantitatively quite closely in many cases. However, further investigation of the applicability of eq. 3.14 to other discontinuities needs to be done before any assessment of its general validity can be made.

An important consideration in the usefulness of eq. 3.14 lies in the ability to obtain values for JRC, JCS, and ϕ_μ for particular discontinuities. While direct measurements of JCS and ϕ_μ may be relatively easy to obtain, there is no method for directly determining JRC. JRC must be back-figured from direct shear tests, or possibly from tilt tests. The accurate determination of JRC is quite important, as the failure envelopes illustrated in Fig. 3-2 are sensitive to JRC, particularly for higher JCS.

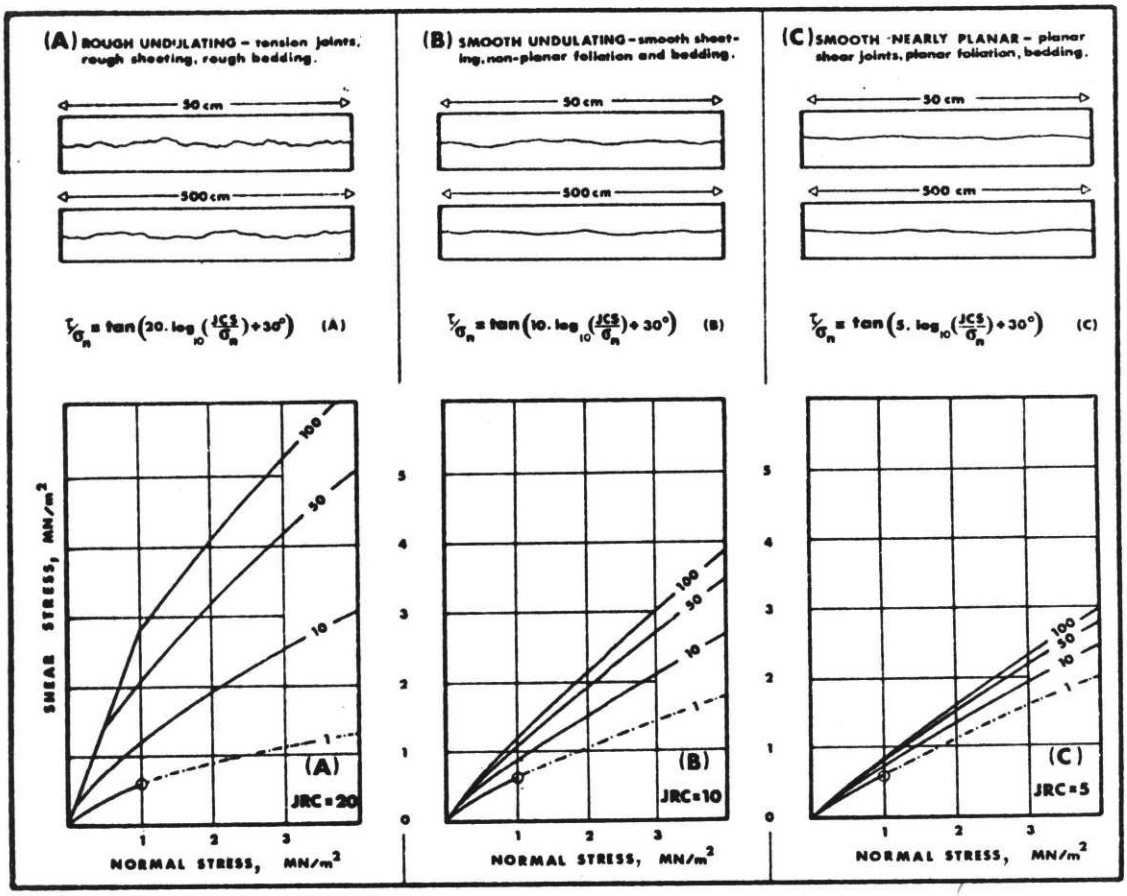

(Numbers on curves are values of JCS.)

Figure 3-2 Discontinuity shear equation of Barton (1973). (from Barton, 1976b)

It is felt that further development, in the area of establishing the general applicability of eq. 3.14 and also establishing a reliable method for determining JRC, is needed before eq. 3.14 can be a useful method for predicting rock discontinuity strength.

3.4 SUMMARY

The models of Patton (1966) and Landanyi and Archambault (1970) use a mechanistic approach to the problem of describing rock discontinuity shear strength. Patton's model is too simplified to accurately represent the failure envelope of most rock discontinuities. Ladanyi and Archambault's model has a much more general application, but difficulties in predicting dilation rate ($\dot{v}$) and shear area ratio (a_s) seriously limit its practical use. In spite of these limitations, the concepts developed by Patton and Ladanyi and Archambault are fundamentally sound, and are used as a basis for a part of the research reported in this thesis.

The model of Barton (1971, 1973) uses an empirical approach. In spite of the fact that this model may prove to be a useful method of predicting discontinuity shear strength, it provides little insight into the mechanisms involved in the shearing process, and therefore is not considered further in this thesis.

CHAPTER 4

THE SLIDING MECHANISM

Two mechanisms have been identified in Chapter 2 as being the major mechanisms involved in the shearing of rock discontinuities. These are the sliding mechanism and the shearing mechanism. The sliding mechanism is the mechanism by which shear resistance is developed when flat smooth surfaces are forced to slide over each other. The sliding mechanism can be divided into two submechanisms: a friction submechanism and a dilation submechanism.

The dilation submechanism results from sliding in a direction which is not parallel to the plane of the discontinuity. It is accounted for by the angle i in Patton's equation for sliding (eq. 3.1), and by the component S_1 in Ladanyi and Archambault's model (eq. 3.2). The dilation submechanism is directly and simply related to the dilation rate ($\dot{v}$), (or dilation angle, i^*), and will be discussed in more detail in Chapter 6.

This chapter examines the friction submechanism. The physical processes responsible for friction are studied in general, and how they apply to rocks in particular. The phenomenon of stick-slip is also investigated, in order to understand the role that friction plays in it, and since it helps in turn to understand friction. Finally, experimental measurements of the sliding friction angle for minerals are reviewed.

The purpose of this study of the friction submechanism is to gain a better understanding of friction in rocks, to determine which mechanisms are important in friction, and which factors have an important influence

on these mechanisms.

4.1 FRICTION

Friction is the resistance to motion which exists when a solid object is moved tangentially with respect to the surface of another which it touches, or when an attempt is made to produce such motion (Rabinowicz, 1965). Its importance in almost all physical processes is well recognized, but the mechanism of friction itself is not well understood, as will be shown in this chapter.

Experimental observation of friction has led to the proposal of two "laws" under which friction is often assumed to operate. These two laws are generally credited to Amontons, as published in 1699, although Leonardo da Vinci actually noted them two centuries earlier. (For a historical review of the subject, see Bowden and Tabor, 1964, p. 502.) The two laws are:

1. Friction force (F) is directly proportional to normal force (N); i.e., $F = \mu N$, where μ is the coefficient of friction. ($\mu = \tan \phi_{\mu}$).
2. Friction force is independent of the apparent area of contact on the sliding surface. (Apparent area of contact is the gross or macroscopic area of contact, not the microscopic or actual area of contact, to be discussed further below.)

These two laws are obviously related. The first law implies that F is only dependent on μ and N, and thus is independent of contact area. While there are exceptions to both of these laws, they provide a set of rules under which engineers generally consider friction.

Attempts to explain these laws in terms of physical mechanisms have led to a theory of friction known as the adhesion theory of friction.

This theory will now be explained.

Adhesion Theory of Friction

All surfaces, even those which appear to be very smooth, are irregular on a microscopic scale. When two surfaces are placed in contact, only tips of opposing surface irregularities (asperities) touch each other. Initially, the number of contacts, as well as the actual contact area, is very small. The contact stresses are very high, so that ductile plastic yielding of the asperities occurs. The effect of asperity yielding is to increase the actual contact area and to decrease the contact stress until yielding stops (see Fig. 4-1). If yielding is controlled only by normal stresses on the asperity, then the final actual contact area (A_c) is given by

$$A_c = \frac{N}{p} \tag{4.1}$$

where N is the normal force between the surfaces and p is the indentation or penetration hardness of the material. (The actual contact area due to ductile plastic yielding can be influenced by factors other than N and p. The contact area can be dependent on the shear stress across the contact, although this effect is usually neglected. Bowden and Tabor (1964, p. 74) discuss this effect. The contact area can also be time dependent, due to creep or time-dependent breakdown of surface films. This effect will be discussed further in Section 4.2.)

Adhesive bonds form across these areas of contact, creating "adhesion junctions" which resist any applied force tending to cause sliding. If these adhesion junctions are assumed to have a constant specific shear strength (s), then the friction force provided by these junctions is

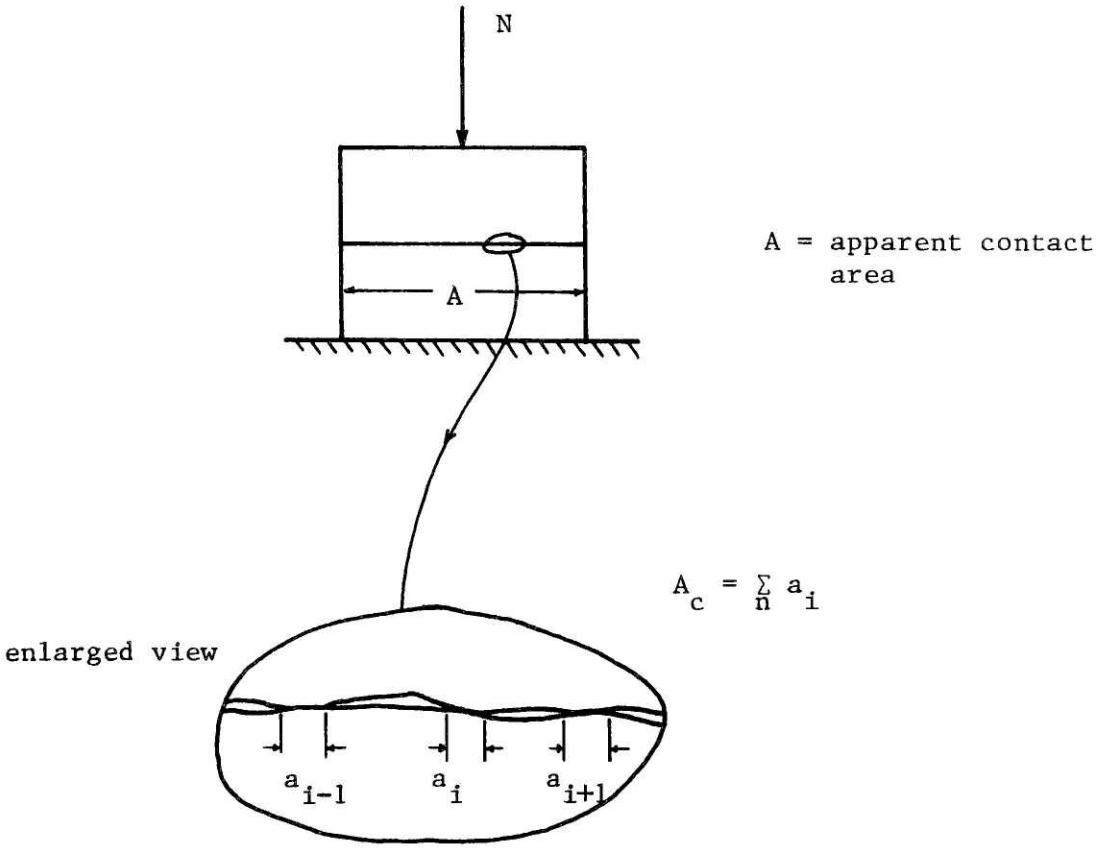

Figure 4-1 Actual contact area between surfaces.

given by

$$F = s\, A_c \tag{4.2}$$

Equations 4.1 and 4.2 combine to give

$$\mu = \frac{F}{N} = \frac{s\, A_c}{p\, A_c} = \frac{s}{p}$$

Because s and p have been assumed to be constants for a given material, μ will also be a constant for a given material (up to the limit of full contact between surfaces, where $A_c = A$ in Fig. 4-1.)

This simple theory readily explains the direct proportionality between F and N, as well as the non-dependence of F on the apparent area of contact. It is this theory, the adhesion theory of friction, which is widely accepted as the basic mechanism of friction in most materials.

Components of Friction Force

Rabinowicz (1965) states that friction force can be derived from four possible components. One of these is the adhesion component, due to adhesive forces between surfaces as just described in the adhesion theory of friction. There are three other possible components: the roughness component, the plowing component, and the electrical component. These other components will now be discussed.

The roughness component arises when contacting surfaces are irregular enough that one surface must be lifted over the irregularities on the roughness scale of the other surface for sliding to occur. This requires an additional force, beyond the adhesion component. If the scale of the surface irregularities is small relative to the sliding displacement, then the roughness component will have both positive and negative contributions

which will tend to cancel each other out as sliding progresses.

The plowing component contributes to the friction force when asperities on one surface "plow " into the material of the opposing surface. The force required for deformation by plowing must be supplied by the friction force. The plowing component differs from the adhesion component in that there is gross permanent deformation of the material due to plowing, whereas the deformation associated with adhesion only involves the tips of small asperities, being permanent but much smaller in scale. The plowing component can be important for rough surfaces where asperities interlock rather than simply contact at their tips.

The electrical component arises when there is electrical attraction and/or repulsion across the two sliding surfaces. This component is very small in most cases.

Separation of the friction force into components is analogous to the separation of rock discontinuity shear resistance into mechanisms and submechanisms. The adhesion component and the roughness component together correspond to the sliding mechanism, where adhesion is analogous to the friction submechanism and roughness is analogous to the dilation submechanism. The plowing component corresponds to the shearing mechanism. If the scale is chosen small enough, the "sliding" mechanism can in turn be subdivided into both shearing and sliding. The definition of shearing and sliding in any particular case is thus a question of the scale considered.

Friction in Rocks and Minerals

The adhesion theory of friction, which accounts for an adhesion component but not for the other three components, is generally recognized as being valid for metals, because metals are ductile and the other three

components are usually negligible. However, there is some dispute as to whether it can be correctly applied to friction in rocks and minerals. Rocks and minerals are characterized as brittle materials, thus the notion of ductile plastic flow at the contact points may not apply to them. The contact stresses required to produce ductile plastic deformation in quartz, for example, are on the order of 1,500,000 psi (Brace, 1963). In copper, they are only 1,400 psi. There is also some question as to whether ductile plastic flow observed in quartz is actually ductility or perhaps micro-fracturing on a scale too small to be seen (Brace, 1963). At any rate, it is unclear whether or not all the contact points behave in a ductile manner. If they do not, then the contact area (A_c) is no longer proportional to the normal force (N), and the adhesion theory of friction no longer strictly applies.

In addition to the possibility that contact area is not directly proportional to normal load, there is a question as to whether the friction force is due to adhesion bonds. Bromwell (1966) states that frictional resistance of brittle materials is probably due to adhesive forces acting at the contact points, just as in metals. He notes that the cleaning of surfaces in various brittle materials produced a marked increase in the coefficient of friction. (The cleaning was accomplished by placing the material under high vacuum.) This increase in friction is presumably caused by an increase in adhesion junction strength due to cleaner surfaces.

Byerlee (1967b) has proposed that brittle fracture, rather than ductile plastic flow, is the dominant mechanism of friction in most rocks. He developed a theory of friction based on brittle fracture. The theory applies to very smooth surfaces of brittle material, where only the tips of

microscopic irregularities touch each other (no interlocking), just as in the adhesion theory of friction. Instead of ductile deformation however, the asperities crush at their tips. Sliding then occurs when these asperities fail by brittle fracture, as tangential forces are applied to their crushed tips. By determining the normal and shear forces at the tips of the asperity at failure, a coefficient of friction was theoretically calculated to range from 0.10 to 0.15, the magnitude depending primarily on asperity shape. Friction tests were performed on samples of granite, calcite, and other minerals which appeared to verify his theory. For very smooth surfaces on these materials, μ ranged from 0.10 to 0.15. For surfaces with greater roughness, μ increased with roughness. The implications of this theory for natural surfaces, which are much rougher than those for which Byerlee found his theory applicable, is not clear. However, Byerlee contends that brittle fracture is the controlling mechanism of friction in brittle materials, even in the case of interlocking asperities, and that the adhesion theory of friction therefore does not apply to most rocks.

Friction experiments by other researchers on very smooth surfaces of brittle material do not support Byerlee's theory. In Section 4.3, it will be seen that very smooth, clean surfaces of quartz produce very high coefficients of friction, sometimes greater than 1.0.

It is apparent from the preceding discussion of friction that the mechanisms involved in the sliding of rocks and minerals are not entirely clear. Further investigation of this subject will now be made through the study of the stick-slip phenomenon, which is the subject of Section 4.2. By studying the results of these investigations and attempting to describe the mechanism of stick-slip, a better understanding of friction may be obtained.

4.2 THE STICK-SLIP PHENONMENON

"Stick-slip" is a term which refers to the "jerky" motion of alternately sticking and slipping of two surfaces as they are forced to slide over each other. This type of motion has been observed in laboratory friction experiments on a variety of materials, including metals and rocks. The observation of stick-slip in rocks has given rise to the theory that stick-slip occurring in the earth's crust along faults is a mechanism of earthquakes (for example, see Brace and Byerlee, 1966). This theory has prompted numerous investigations of the frictional sliding behavior of rocks in an effort to describe the conditions under which stick-slip occurs. This section reports the results of those investigations, as well as discussing the mechanics of stick-slip, to gain insight into friction in rocks.

The Mechanics of Stick-Slip

Stick-slip is the result of mechanical instability between a force tending to cause sliding and the friction force which is resisting sliding. To illustrate the stick-slip process, a friction experiment is shown schematically in Fig. 4-2. A block of weight W rests on a rigid flat surface. The normal force (N) on the plane of sliding is equal to W. A tangential force (T) can be applied through the spring between points A and B. The friction force (F) which resists sliding is given by $F = \mu N$.

When point B is moved to the right at a constant velocity (v), the block remains stationary until T is sufficient to overcome F. At this point, sliding occurs.

If μ does not change as sliding begins, then the block will slide with a constant velocity equal to v. T is equal to F, and "stable" sliding

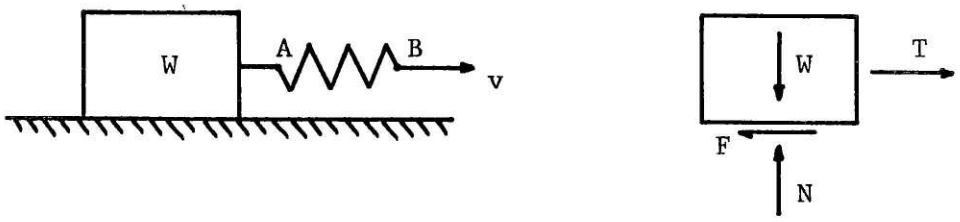

(a) (b)

Figure 4-2 Schematic of friction experiment.

takes place.

If μ decreases as sliding begins, F will decrease, and it is possible that the difference between F and T will cause the block to accelerate to velocity greater than v, or "slip". This will only happen if F decreases with sliding more rapidly than T. As the block slips, T decreases as the spring contracts until eventually it is less than F, and a "stick" occurs. Then T increases until it is sufficient ot overcome F again, and the entire stick-slip cycle is repeated.

It is the interaction of the forces F and T and the way that they vary during sliding which determines whether or not stick-slip occurs. Changes which occur in F depend on the frictional characteristics of the sliding material. Changes which occur in T depend on the stiffness of the spring and the relative displacements of points A and B as sliding takes place.

Effects of Stiffness on Stick-Slip

If T can be controlled so that it always decreases at the same rate as F with sliding, then stick-slip can be prevented. In the friction experiment, T can be controlled through the stiffness of the spring. Increasing the spring stiffness will increase the rate at which T decreases during sliding, possibly eliminating stick-slip.

Rabinowicz (1965) investigated stick-slip of steel on steel, using various spring stiffnesses, and found that it was possible to eliminate stick-slip using a spring stiffness of 170 kg/cm (950 lb/in).

Byerlee and Brace (1968) investigated the effect of loading machine stiffness in triaxial tests on ground surfaces of granite. With stiffness as high as 2×10^5 kg/cm (11×10^5 lb/in), they were unable to eliminate

stick-slip. In fact, they were unable to observe any influence of machine stiffness on stick-slip behavior, contrary to what is expected. Apparently the machine stiffness required to eliminate stick-slip in those tests was much higher than the stiffnesses used, indicating that the drop in friction force as sliding began was extremely abrupt.

The preceding discussion of stick-slip presumed a spring stiffness or loading machine stiffness acting in a friction experiment. Loading systems in nature also have a certain stiffness associated with them, so the above comments apply to natural situations as well as to friction experiments, although it is difficult to estimate the stiffness of rock masses as they might apply to a particular sliding situation.

Effect of Frictional Characteristics on Stick-Slip

The classic explanation of stick-slip is that there are two types of friction, static friction and kinetic sliding friction. It is assumed that the coefficient of static friction (μ_s) is greater than the coefficient of kinetic friction (μ_k). Any force tending to cause sliding is resisted by static friction until sliding begins, at which point the friction force falls to the lower kinetic value, causing slip.

While this simple idea of $\mu_s > \mu_k$ can account for the occurrence of stick-slip, the process by which this takes place must still be explained. This process must be compatible with any friction mechanism which is assumed to apply to the material. Indeed, any proposed mechanism must be related to the friction mechanism, accounting for changes in friction force which take place as sliding is initiated.

Rabinowicz (1965) makes a distinction between two types of stick-slip processes, time-controlled and displacement-controlled. Possible

friction mechanisms for each type will be discussed here.

It is possible to account for stick-slip if friction is time-dependent. If the coefficient of friction is a function of the time of contact between surfaces, increasing with increasing time of contact, then the friction force will be smaller when sliding than when not sliding. This would explain how the friction force can drop suddenly when sliding begins, as the contact time is much less during slip than during stick.

Bowden and Tabor (1964) suggest possible explanations for a time dependence of friction which are based on the adhesion theory of friction. These explanations require that the size of the adhesion junctions is dependent on time, rather than only on normal force and penetration hardness as described in Section 4.1. One explanation is that creep occurs at the adhesion junctions, resulting in an increase in actual contact area with time. Another possibility is that there is a time factor in the breakdown of surface films, also resulting in an increase in contact area with time. A final explanation is that diffusion across the interfaces of the junctions leads to a strengthening of the junctions with time.

Rabinowicz (1965) presents the data of Dokos (1946) to show that steel exhibits time-dependent friction properties. The coefficient of friction for steel was observed to be proportional to the logarithmn of stationary contact time.

Dietrich (1972) investigated time-dependency of friction in rocks in a series of direct shear tests. Sandstone, quartzite, graywacke, and granite were tested at normal pressures of 20 - 850 bars (300 - 12,300 psi). For clean, rough surfaces (ground with #80 abrasive), no dependence of on contact time was observed. However, if an accumulation of gouge from

previous sliding was present, then μ_s showed a distinct time dependency for all the rocks tested. This time dependency of μ_s, which clearly required the presence of gouge, gave rise to stick-slip behavior. In these tests, time dependent friction apparently played an important role in causing stick-slip.

Another approach to the friction mechanism responsible for stick-slip assumes that μ is a function of displacement. Two different models, one based on adhesional friction and the other based on a brittle fracture mechanism, are presented here.

In the adhesion theory of friction, friction force originates from adhesion junctions, and initially (before sliding) the size of the adhesion junctions is assumed to be dependent on the normal force and the penetration hardness of the material. As sliding takes place, some junctions are broken while others are being formed, and the size of the junctions may be dependent on other factors such as the size of the asperities and the shear stress across the junctions. If the size of these junctions varies in some way with displacement, then the friction force will also vary, and in this way stick-slip could develop.

Byerlee (1970) proposed a similar model of the friction force varying with displacement based on a brittle fracture mechanism. In this model, the friction force is the result of interlocking asperities on the sliding surface. When the asperities fail, the friction force decreases, and slip occurs. Sliding continues until enough frictional reisitance due to the interlock of new asperities is generated. Then stick occurs and the whole process is repeated.

The two displacement controlled models for stick-slip, as described

above, are similar. They both rely on the interaction of asperities which produces a friction force that varies with displacement. The difference is the mode of asperity failure, ductile plastic flow in one case and brittle fracture in another. Either model can account for stick-slip behavior.

Observations from Stick-Slip Experiments

In order to gain a better understanding of the stick-slip mechanism in rocks, the results of stick-slip studies reported in the literature will be discussed. Friction experiments have been performed on a variety of rocks, under a wide range of testing conditions. Experimental apparatus, loading procedure, stress conditions, temperature, rock type, and sliding surface preparation vary from experiment to experiment. This makes it difficult to make direct comparisons of experimental data. The effects of four major parameters are described here. These are: rock type, pressure, temperature, and surface conditions.

Rock Type

Brace (1972) reviewed the literature concerning stick-slip observations and concluded that weak minerals in rocks cause stable sliding rather than stick-slip. These weak minerals include calcite, dolomite, and such platy silicates as talc or serpentine.

Byerlee and Brace (1968) performed triaxial friction experiments on ground surfaces of two types of dunite, one which contained 3% serpentine while the other contained none. At 3 kbar (44,000 psi) confining pressure, the dunite without serpentine exhibited stick-slip and the other dunite did not. Apparently only a small amount of a weak mineral, serpentine, was able to cause stable sliding.

Stesky et al. (1974) tested a variety of rocks, including granite, gabbro, quartzite, dunite, peridotite, and anorthosite, in the same manner as Byerlee and Brace (1968). Only the peridotite showed stable sliding at room temperature. All the other rock types slid by stick-slip. This was attributed to a small amount (<1%) of serpentine in the peridotite.

Pressure

The effect of pressure, as used here, refers to the normal pressure on the sliding plane, as determined by the applied normal pressure in a direct shear test, or the confining pressure and axial stress in a triaxial test.

Byerlee and Brace (1968) reviewed a number of triaxial tests and reported that stick-slip was absent in all of the rocks below a confining pressure of 0.8 kbar (12,000 psi), for pressures ranging to 6 kbar (87,000 psi). The effect of increasing the confining pressure from 0.8 kbar to 6 kbar was to cause severe stick-slip behavior in a number of rock types.

Scholz, Molnar, and Johnson (1972) performed direct shear tests on granite with normal pressures up to 1 kbar (15,000 psi). For normal pressures less than 15 bars (220 psi), sliding was stable. Above 15 bars, stick-slip was predominant.

Drennon and Handy (1972) performed direct shear tests on limestone with normal pressures ranging from 0.75 - 20.0 kg/cm^2 (10 - 280 psi). They also observed a transition from stable sliding to stick-slip with an increase in normal pressure. The transition pressure was quite variable, decreasing with increasing temperature of the specimen during the test.

Surface Conditions

Two factors relating to surface conditions have been observed to influence frictional behavior and stick-slip: surface roughness and the presence of gouge.

Hoskins, Jaeger, and Rosengren (1968) tested five different rock types (granite, gabbro, trachyte, sandstone, marble) with two degrees of surface finish (rough ground, polished) in direct shear tests with normal stresses ranging from 125 to 750 psi. For the rough surfaces, stable sliding occurred at all normal pressures. For the same rocks with polished surfaces, stick-slip was observed. There was also a marked decrease in the coefficient of friction associated with the change from rough to polished surfaces.

Dietrich (1972) also investigated the effect of surface roughness in direct shear tests on sandstone, quartzite, graywacke, and granite. Whereas clean rough surfaces showed stable sliding, highly polished surfaces showed stick-slip. In these tests, the coefficient of friction was found to be greater for polished surfaces than for rough surfaces. As noted previously, the effect of gouge production in these tests was to make the coefficient of static friction dependent on the time of contact between surfaces. The presence of gouge was necessary to produce stick-slip with rough surfaces, but not for smooth surfaces.

Scholz, Molnar, and Johnson (1972) reported that in their direct shear tests the accumulation of gouge tended to reduce the stress drop (drop in friction force) during slip. Drennon and Handy (1972) also found

that gouge reduced the stress drop in their direct shear tests. These two observations seem to conflict with those of Dietrich, as they imply that gouge formation favors stable sliding rather than stick-slip.

Temperature

Stesky et al. (1974) performed an extensive study of the effect of temperature on stick-slip, through triaxial tests on a number of rock types. In all of the rock types which showed stick-slip at room temperature (granite, gabbro, quartzite, anorthosite, dunite), an increase in temperature caused a transition to stable sliding. The transition temperature varied from 100° - 600°C., depending on rock type, for a confining pressure of 3 kbar (44,000 psi).

Drennon and Handy (1972) found a different effect of temperature in direct shear tests on limestone. As the temperature of the tests was increased from 25° to 100°C., a transition from stable sliding to stick-slip occurred. The range of normal pressure was 0.75 - 20.0 kg/cm^2 (10 - 280 psi).

Thus, the above two investigations showed the opposite effect of temperature, but the temperature range, pressure range, and rock type were different in each case, and therefore cannot be directly compared.

Summary of Effects

In any particular case of frictional sliding, the four parameters described above will interact to determine whether sliding is stable or by stick-slip. However, it is possible to make certain generalizations about the influence of each of these factors separately.

Rock type plays an important role in sliding behavior. Certain weak

minerals, when present in rocks, will cause stable sliding rather than stick-slip. The effect of pressure on frictional sliding is clear. Higher pressures promote stick-slip rather than stable sliding. Surface roughness seems to play an important role, with very smooth surfaces being favorable to stick-slip. The influence of gouge on the sliding surface is not clearly defined. In some instances, it has been observed to promote stick-slip, in others, it promoted stable sliding. In general, temperature increase has the effect of eliminating stick-slip behavior, although an exception to this has been observed.

Concluding Remarks on Friction Mechanisms in Stick-Slip

Considering the two types of stick-slip processes mentioned previously, time-controlled and displacement-controlled, it can be concluded that time-controlled stick-slip is not always important. Although Dietrich (1972) observed a time dependence of friction in a variety of rocks, it was only under conditions where there was an accumulation of gouge. Those conditions did not apply to a majority of experiments where stick-slip was observed. While time-controlled stick-slip may play an important role in certain situations, it appears that a model of displacement controlled stick-slip would generally be more applicable. The displacement-controlled model can involve adhesional friction or friction based on brittle fracture, but at this point it is not clear which best fits the observations.

Few of the investigators of the stick-slip phenomenon address the problem of describing the friction mechanism responsible for stick-slip. This is probably due to the fact that it is diffcult to come to any conclu-

sion based on observations to date.

Drennon and Handy (1972), from their studies of stick-slip in direct shear tests on limestone, stated that adhesion seemed to be the friction mechanism controlling stick-slip. It was observed that high temperature and high normal loads caused an increase in the coefficient of friction, which was in some way responsible for stick-slip. They postulated that a film of adsorbed water on the surface of the limestone caused stable sliding by decreasing the area available for adhesion. High temperature would drive off this adsorbed water, and high normal pressures would cause the film to be penetrated. Both have the same effect of creating a larger adhesional friction force which is responsible for stick-slip.

Byerlee (1967a) discussed the mechanism involved in his tests of frictional sliding of granite. He concluded that brittle fracture, rather than ductile plastic deformation, is the controlling mechanism. This was, in part, based on observations of the type of wear particles produced during sliding, which were angular in shape and showed no evidence of plastic flow.

Summary

Theory and observations of the role of friction in stick-slip were reviewed in this section. Two different mechanisms, adhesion associated with ductile plastic flow and brittle fracture, have been identified as possible mechanisms controlling friction. The study of friction experiments conducted to investigate stick-slip has revealed that it is not clear which mechanisms are responsible for friction in rocks. It has been shown that there are certain factors (such as rock type and pressure) which have a well-defined influence on frictional behavior, while other factors (such as

surface conditions and temperature) influence behavior in a way which is not well understood. In addition, the effects of these factors are difficult to relate to the mechanisms of friction.

Clearly, there is no single theory or mechanism which can be used to explain friction in rocks. Apparently the friction process is a highly complex one, and further investigation of this subject needs to be done before the physical mechanisms involved can be well defined.

4.3 MEASUREMENTS OF FRICTION OF MINERALS

This section contains the results of a survey of data from sliding experiments on minerals which have been reported in the literature. The experiments reported were performed on a variety of minerals, under a variety of conditions. The aim of these experiments was to determine values of ϕ_μ for particular minerals. (As used in this section, ϕ_μ is the friction angle determined from the sliding tests, with no requirements regarding surface roughness, although all of the minerals tested were macroscopically smooth.) The results of the reported experiments, along with a description of the testing conditions, will be presented and discussed, and conclusions concerning ϕ_μ for each mineral will be made.

One of the purposes of this survey is to provide a basis for estimating ϕ_μ values for rocks. It is thought that if values of ϕ_μ can be established for the rock-forming minerals, then it might be possible to predict ϕ_μ for rocks of known mineral content. Although a method for making this prediction has not been developed, the first step is to investigate ϕ_μ for individual minerals.

Another purpose of this survey is to study the friction mechanism in

minerals, to see which factors influence ϕ_μ and what effect these factors have.

Examination of data from mineral sliding experiments reveals that, for any particular mineral, a wide range in values of ϕ_μ has been measured. Experiments have been performed with a variety of experimental set-ups, and thus under a variety of test conditions. Test conditions, equipment-related and otherwise, were observed to play an important role in the sliding behavior of the minerals in these tests. In particular, mineral surface conditions greatly influenced behavior. These surface conditions include roughness, cleanliness, and the presence of moisture.

Data has been gathered from mineral sliding experiments for individual minerals, with particular reference to surface roughness, surface cleaning prior to test, surface moisture conditions, and the type of sliding test employed. This information is presented in Tables 4-1 and 4-2. (All of the data presented are from single mineral sliding tests; e.g., quartz sliding against quartz, calcite sliding against calcite, etc.) Discussion of the information in Tables 4-1 and 4-2 is divided into three mineral groups: quartz, other massive structured minerals, and layer-lattice minerals.

Quartz

Quartz is the mineral which has been tested most extensively for sliding behavior. Table 4-1 shows a wide range of values of ϕ_μ which have been obtained by various investigators. As an example of the two extremes, a value of $\phi_\mu = 38^\circ$ was measured by Hardy and Doubleday (1922), while a value of $\phi_\mu = 6^\circ$ was measured by Tschebotarioff and Welch (1948). Both of these tests were performed on dry surfaces, with at least one of the

MINERAL	TYPE OF TEST	SURFACE ROUGHNESS	SURFACE CLEANING	SURFACE MOISTURE CONDITIONS	ϕ_p (°)	REMARKS	REFERENCE
Quartz	hemisphere against plane surface	polished	heated in chromic acid, scrubbed under running tap water	dry	38		Hardy and Doubleday (1922)
	block against many particles embedded in mortar	polished block, irregular particles	? (probably none)	dry (in dessicator) moist (air dry) saturated	6 24 24		Tschebotarioff and Welch (1948)
		roughened with carborundum stone	? (probably none)	dry saturated	20 26		
	"flat" surface against "flat" surface	"flat"	washed with soap and water	saturated oven-dry	33 11		Penman (1953)
	3 chips, bedded in plaster against "flat" surface		wash with soap and water	saturated	19-33		
	mass of loose particles against plane	plane w/same roughness as particles	?	saturated	22 31	pebbles silt-size particles	Rowe (1962)
	3 hemispheres against plane surface	polished with tin oxide abrasive	washed with soap and water, scrubbed during rinse	oven-dried oven-dried, air-equilibrated saturated	6-8 6-9 23-27		Horn and Deere (1962)
		ground with #240 grit	washed with soap and water, scrubbed during rinse	oven-dried, air-equilibrated saturated	28 35		
		polished surfaces etched in ammonium bifluoride	washed with soap and water, scrubbed during rinse	oven-dried, air-equilibrated saturated	7 33		
	block against block	ground with #600 grit, asperity height <1000Å	chemically cleaned	oven-dried air-dried saturated	25 36 37		Bromwell (1966)
		ground with #220 grit	chemically cleaned	air-dried saturated	25 30		
	block against block	see figure 4-2					Dickey (1966)
	block against block	ground with #220 grit	?	air dry (relative humidity=0)	27		Byerlee (1966)
	particle against particle and plane against plane	irregular particles, polished plane	wiped with acetone, boiled in distilled water	oven-dried saturated saturated	17 22 26	particle-plane particle-plane particle-particle	Procter and Barton (1974)
Feldspar	3 hemispheres against plane surface	polished	washed with soap and water, rubbed during rinse	oven-dried oven-dried, air-equilibrated saturated	6-7 7 37	microcline feldspar	Horn and Deere (1962)
	particle against plane	irregular particles, polished plane	wiped with acetone, boiled in distilled water	saturated	29	particle-plane	Procter and Barton (1974)
Calcite	hemisphere against plane surface	polished	? (probably none)	dry moist saturated	6 15 15		Tschebotarioff and Welch (1948)
	3 hemispheres against plane surface	polished	washed with soap and water, rubbed during rinse	oven-dried oven-dried, air-equilibrated saturated	8 8-12 31-34		Horn and Deere (1962)

Table 4-1 Sliding Friction Angles for Various Massive-Structured Minerals

MINERAL	TYPE OF TEST	SURFACE ROUGHNESS	SURFACE CLEANING	SURFACE MOISTURE CONDITIONS	ϕ_μ	REFERENCE
Chlorite	3 hemispheres against plane surface	polished	washed with soap and water, rubbed during rinse	oven-dried oven-dried, air equilibrated saturated	28 19 12	Horn and Deere (1962)
Biotite	3 hemispheres against plane surface	cleavage planes used	no cleaning, cleavage performed immediately before test	oven-dried oven dried, air equilibrated saturated	17 15 7	Horn and Deere (1962)
Muscovite	3 hemispheres against plane surface	cleavage planes used	no cleaning, cleavage performed immediately before test	oven-dried oven-dried, air equilibrated saturated	22-24 17-20 12-15	Horn and Deere (1962)
Phlogopite	3 hemispheres against plane surface	cleavage planes used	no cleaning, cleavage performed immediately before test	oven-dried oven-dried, air equilibrated saturated	16-17 12-14 9	Horn and Deere (1962)
Steatite	hemisphere against plane surface	polished	?	dry moist saturated	11 9 9	Tscheborarioff and Welch (1948)
	3 hemispheres against plane surface	polished	washed with soap and water, rubbed during rinse	oven-dried oven-dried, air equilibrated saturated	21 15 13	Horn and Deere (1962)
Talc	3 hemispheres against plane surface	polished	washed with soap and water, rubbed during rinse	oven-dried oven-dried, air equilibrated saturated	20 14 9	Horn and Deere (1962)
Serpentine	3 hemispheres against plane surface	polished	washed with soap and water, rubbed during rinse	oven-dried oven-dried, air equilibrated saturated	32-37 27-33 16-26	Horn and Deere (1962)
Pyrophyllite	hemisphere against plane surface	polished	?	dry moist saturated	9 7 7	Tschebotarioff and Welch (1948)

Table 4-2 Sliding Friction Angles for Various Layer-Lattice Minerals

surfaces polished, although the type of test and surface cleaning were different in each case. This kind of sensitivity to surface conditions, although to a lesser degree, is reflected in most of the data for quartz.

It is difficult to determine the exact causes of discrepancies between values of ϕ_μ measured by different investigators, because of the difference in testing techniques. Causes of variability in ϕ_μ can more readily be distinguished within the tests performed by one particular investigator. For example, Horn and Deere (1962) varied the surface moisture conditions while holding other testing conditions constant. The results show an increase in ϕ_μ from 6° for oven-dry quartz to 27° for saturated quartz.

Bromwell (1966) and Dickey (1966) are the only investigators who studied the effects of all three surface conditions, namely roughness, cleanliness, and moisture. Their findings are best illustrated by the data of Dickey (1966), as presented in Figure 4-3. For very smooth surfaces, cleanliness is an important factor. Very smooth surfaces which are unclean show a much lower ϕ_μ than clean ones. The presence of water has no effect on very smooth, clean surfaces. However, if very smooth surfaces are unclean, then water causes an increase in ϕ_μ from the dry condition. For very rough surfaces, neither the degree of cleanliness nor the presence of water have a significant effect on ϕ_μ. A value of $\phi_\mu = 25^\circ$ is indicated for <u>all</u> very rough surfaces. (The roughness corresponding to the "very rough" condition in Fig. 4-3 was obtained by grinding the quartz specimen with No. 120 grit on a diamond wheel. The values of "average roughness" indicated in Fig. 4-3 represent the average deviation of the surface roughness profile from a straight line.)

Other investigators (Tscheborarioff and Welch, 1948; Horn and Deere,

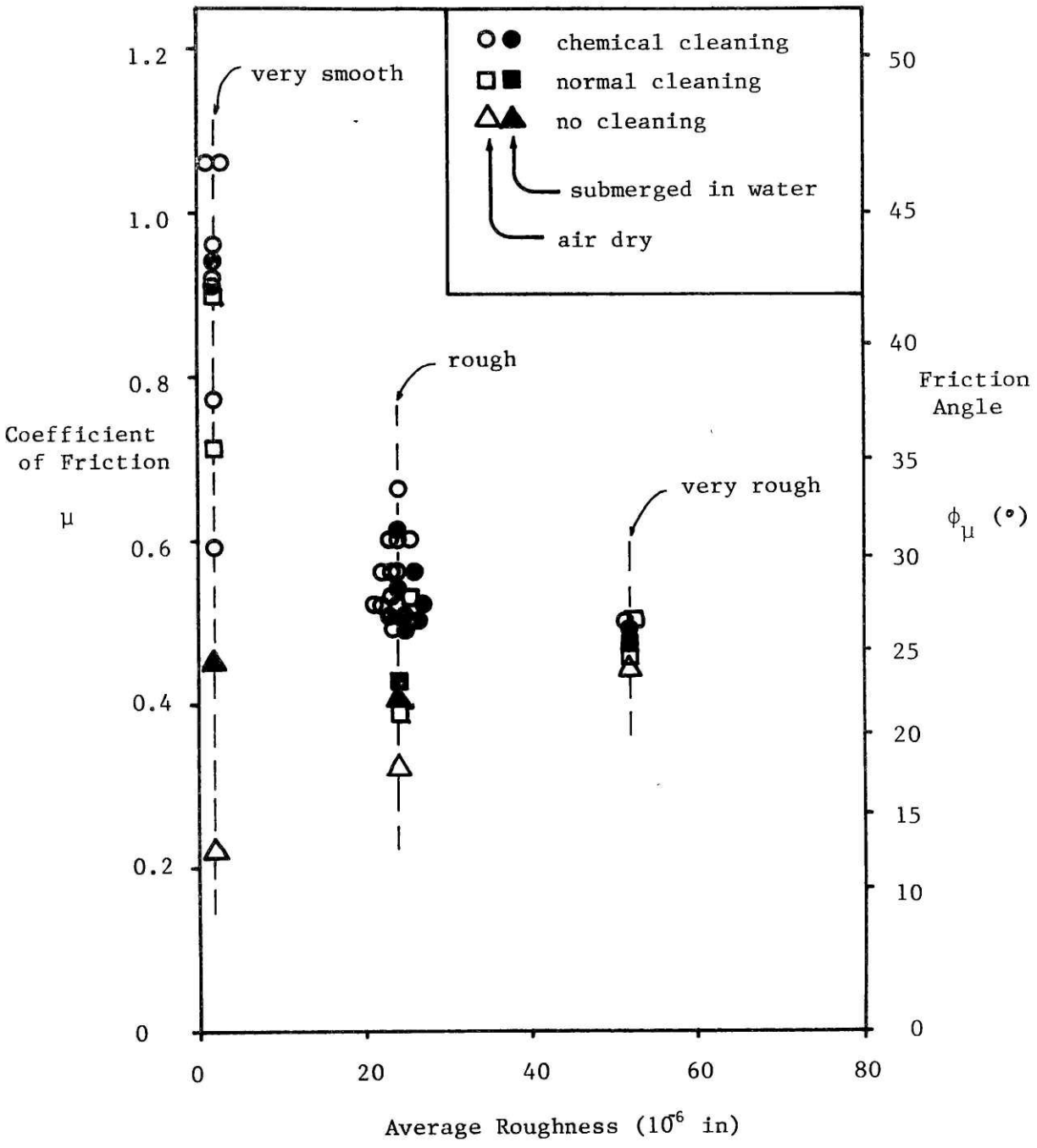

Figure 4-3 Coefficient of friction vs. surface roughness for quartz sliding on quartz, data from Dickey (1966).

1962) tested rough quartz surfaces, but it appears that the surfaces they tested were not as rough as the "very rough" surfaces of Dickey (1966). While no measurements of the roughness of natural quartz are available, it seems reasonable to conclude that it is probably "very rough" and therefore $\phi_\mu = 25^\circ$ for naturally occurring quartz.

Other Massive Structured Minerals

Data on massive structured minerals, other than quartz, are quite scarce. A few sliding tests have been performed on feldspar and calcite (see Table 4-1), with a wide range of values reported. Feldspar shows $\phi_\mu = 6^\circ - 37^\circ$ and calcite shows $\phi_\mu = 6^\circ - 34^\circ$, apparently being sensitive to surface conditions in the same way as quartz. In the tests reported by Horn and Deere (1962) and Tscheborarioff and Welch (1948), both calcite and feldspar show a higher value of ϕ_μ in tests on saturated surfaces than in tests on dry surfaces. This is the same effect observed by these investigators with quartz.

There has not been sufficient investigation of the influence of all surface conditions on the sliding behavior of either feldspar or calcite, and therefore no conclusions can be made concerning the exact effect of these conditions on ϕ_μ.

Layer-Lattice Minerals

Data on layer-lattice minerals are also quite scarce. Minerals which have been investigated include chlorite, biotite, muscovite, phlogopite, steatite, talc, serpentine, and pyrophyllite (see Table 4-2).

In the experiments performed, the effect of surface moisture was the only surface condition effect that was studied. For all of the layer-lattice

minerals, a higher value of ϕ_μ was measured in dry tests than in saturated tests. This is the opposite of what was observed in tests on massive-structured minerals.

In general, the magnitude and range of ϕ_μ for the layer-lattice minerals is less than that observed for massive-structured minerals. All of the values for ϕ_μ lie between 8° and 28°, except for serpentine, which showed a maximum of 37°.

There is insufficient data on the layer-lattice minerals to fully define the effect of surface conditions on their sliding behavior.

Conclusions

From this survey of mineral sliding tests, it is apparent that ϕ_μ measured for a given mineral is dependent on the surface conditions under which the mineral is tested. In particular, roughness, cleanliness, and moisture are three important factors.

There has been a thorough investigation of the effects of all three of these surface conditions for only one mineral, quartz. It was observed that for very rough surfaces in quartz, corresponding to those believed to occur in nature, $\phi_\mu = 25^\circ$, independent of the cleanliness of the surface and the presence of moisture.

For other minerals, the effects of all surface conditions have not been determined. Only a wide range of ϕ_μ for these minerals can be established at present. Further research in this area needs to be done before more definite conclusions can be drawn.

4.4 SUMMARY

This chapter has examined various aspects of the friction submechanism, which is a part of the sliding mechanism. Investigation of friction through study of current theory has revealed that the mechanisms responsible for friction in rocks cannot be clearly determined. Information from stick-slip experiments has provided insight into possible mechanisms and important factors influencing stick-slip, but it has not given a clear picture of the friction process. Information from sliding experiments on minerals has pointed out the importance of a number of factors (especially surface conditions) on the values of ϕ_μ measured, indicating that ϕ_μ for a given mineral can vary considerably under different sliding conditions.

CHAPTER 5

THE SHEARING MECHANISM

The shearing mechanism was defined in Chapter 2 as being the mechanism of shear resistance when intact material composing asperities on the surface of the discontinuity is sheared through. This chapter examines different methods for determining the shear resistance of a single asperity. In the following three sections, three different methods with different degrees of complexity are presented. The three methods are then compared, and the implications of the results of the analyses are discussed with regard to rock discontinuity shear.

5.1 ASPERITY DESCRIPTION

The shear resistance of a single asperity will depend on many factors, including size and shape of the asperity, distribution of applied stresses on the asperity, and the strength of the asperity material. Certain simplifications are made with respect to the above-mentioned factors for the analyses presented in this chapter, and these simplifications will now be described.

The size and shape of asperities on the surface of a discontinuity are controlled by such factors as the texture and mineralogy of the intact rock and the process by which the discontinuity was created. Asperities may be highly irregular in both size and shape. However, it is necessary

to confine the analyses presented herein to a certain idealized shape. This shape is a symetric wedge, whose cross-section is shown in Fig. 5-1a. A plane strain condition is assumed, so that the wedge is infinitely long in the direction perpendicular to the plane of the figure. The shape of the asperity is completely defined by the inclination (i) of its faces. (The size of the asperity, as defined by its face length in Fig. 5-1a, will be discussed in Section 5.5.)

The assumed applied stress conditions on the asperity are illustrated in Fig. 5-1b. A uniform applied stress (q) acts over a certain distance (B) on the left face of the asperity, with a certain inclination (α) from the normal to the asperity face. The right face of the asperity is not stressed.

This loading condition is based on consideration of how an asperity on the surface of a discontinuity might be sheared. Figure 5-2 shows a discontinuity with a single asperity in a direct shear test. Under application of normal force (N) only, the two mating surfaces are in full contact (Fig. 5-2a). As the shear force (S) is applied, there will be elastic deformation and possibly a small amount of sliding, with the result that there will probably be no contact between the two surfaces at the right face of the asperity (Fig. 5-2b). If N is large enough to prohibit dilation by sliding on the asperity surface, the asperity will be sheared (Fig. 5-2c). (The exact nature of this shear failure will be treated in the following sections of this chapter.) Therefore, the assumption made here is that, at failure, the asperity is only loaded on one face. An additional assumption made is that the applied loading causing failure of the asperity is a uniform stress on the asperity face. A simplifying assumption

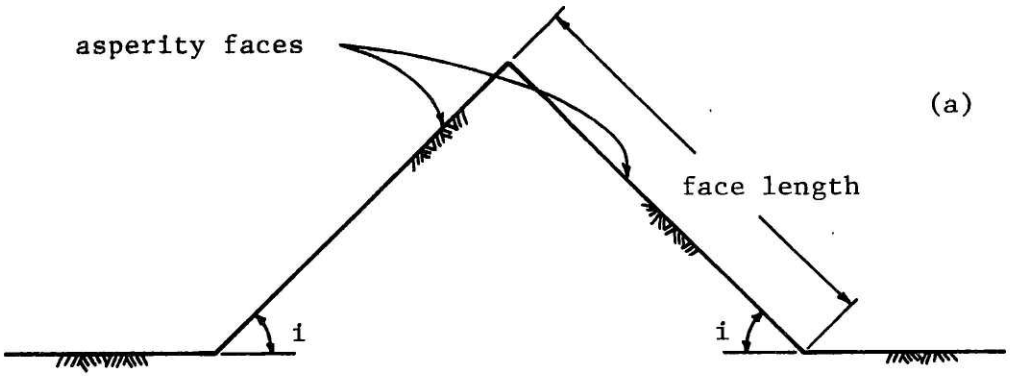

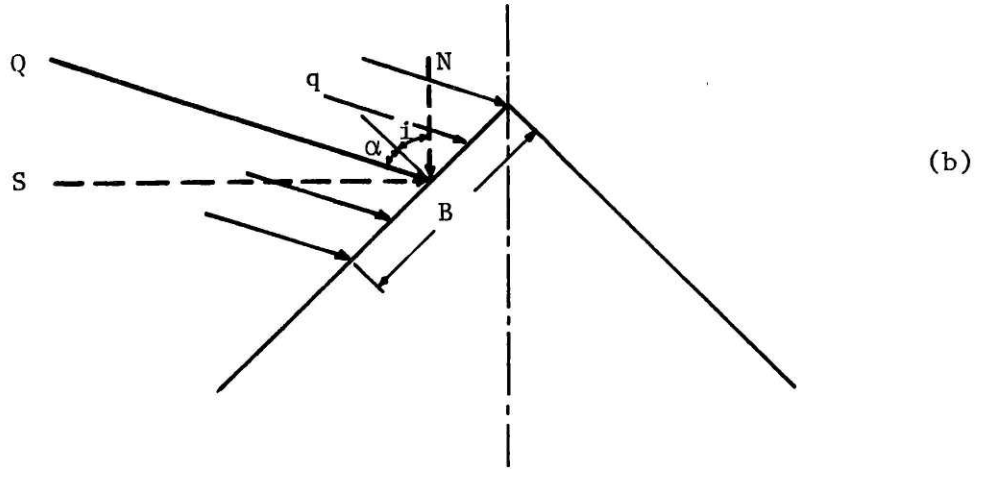

Figure 5-1 Asperity shape and loading conditions assumed in asperity shear analyses.

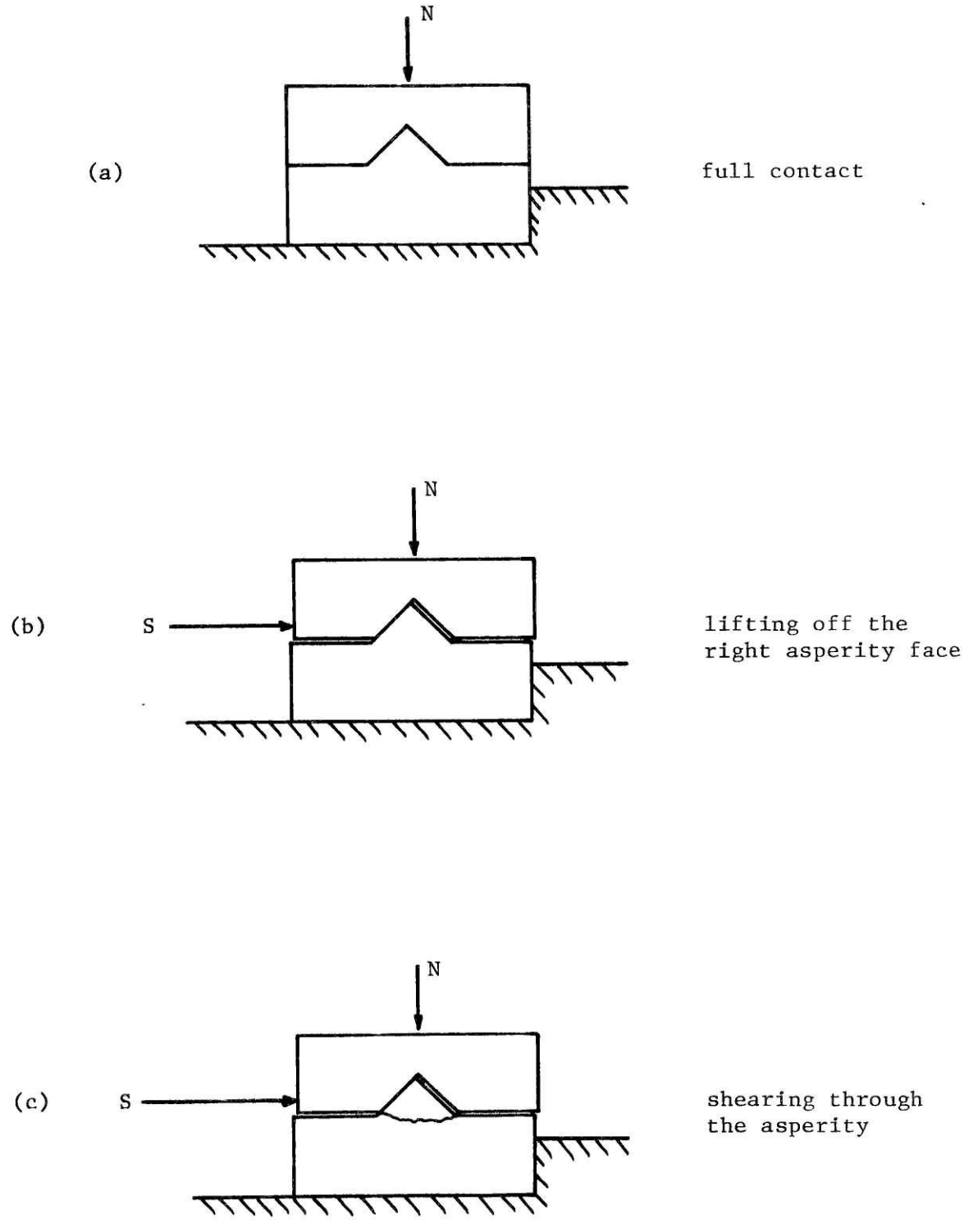

Figure 5-2 Asperity shear in a direct shear test.

is made because the actual distribution of applied stresses is not known.

Referring again to Fig. 5-1, a normal direction and a shear direction will now be defined with respect to the asperity. The normal direction is the direction parallel to the centerline of the asperity. The shear direction is perpendicular to the normal direction (and is parallel to the base of the asperity in Fig. 5-1a). The uniform applied stress (q) has a resultant force (Q) which has a component (N) in the normal direction and a component (S) in the shear direction, as illustrated in Fig. 5-2b.

$$Q = q\ B$$

$$N = Q \cos(i + \alpha)$$

$$S = Q \sin(i + \alpha)$$

(Note that forces such as N, S and Q used in this chapter are in units of force per unit length perpendicular to the plane of the figures.) The normal component (n) and the shear component (s) of the uniform applied stress (q) are given by

$$n = \frac{N}{B} = q \cos(i + \alpha) \qquad (5.1)$$

$$s = \frac{S}{B} = q \sin(i + \alpha) \qquad (5.2)$$

From which

$$s = n \tan(i + \alpha) \qquad (5.3)$$

The material composing the asperity is assumed to be weightless and to follow the Coulomb failure criterion, which is given by

$$\tau_i = c_i + \sigma \tan \phi_i \qquad (5.4)$$

where c_i is the cohesion and ϕ_i is the angle of internal friction of the intact material.

The following three sections present different methods of calculating asperity shear resistance, based on the above-described asperity shape, loading conditions, and material properties. In each section, a method for determining q as a function of α , i, c_i, and ϕ_i will be developed. From this value of q and the associated value of α , the quantities n and s can be calculated from eqs. 5.1 and 5.2. These values of n and s will then be used in Section 5.5 to compare the three methods to each other.

5.2 BASE SHEAR

The simplest method of calculating asperity shear resistance is to assume a planar failure surface through the asperity which is parallel to the shear direction. (As defined in Section 5.1, the shear direction is the direction perpendicular to the centerline of the asperity.) This type of failure surface is illustrated in Fig. 5-3a, and is referred to as base shear. As drawn in the figure, the failure plane begins at the lower boundary of the applied stress (q). Actually, every plane which is parallel to and above the one drawn is a failure plane as well, but the selection of any failure plane among these does not affect the results of the analysis.

In order to calculate the maximum allowable q that the asperity can resist, a limiting equilibrium approach is used. The tip of the asperity, bounded by the assumed failure plane, is shown in Fig. 5-3b. Q is the resultant force of the applied stress q (Q = q B), and $\sigma(x)$ and $\tau(x)$ represent the distribution of normal and shear stresses along the failure plane.

From equilibrium in the y - direction,

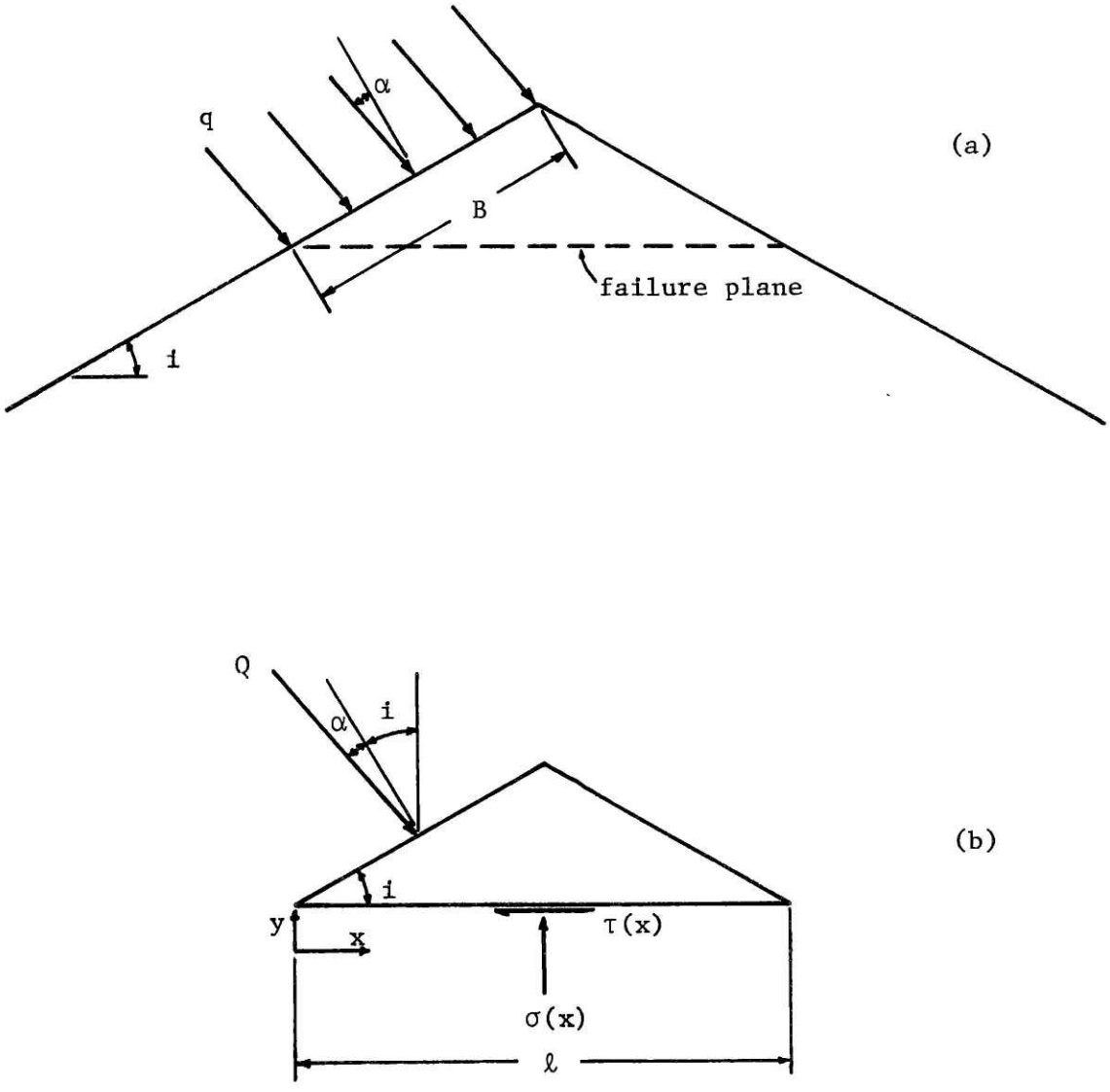

Figure 5-3 Base shear analysis.

$$Q \cos(i + \alpha) = \int_0^{\ell} \sigma(x)\, dx \qquad (5.5)$$

(Forces such as Q, N and S, have units of force per unit length.)

From equilibrium in the x - direction,

$$Q \sin(i + \alpha) = \int_0^{\ell} \tau(x)\, dx \qquad (5.6)$$

It is assumed that full shearing resistance is mobilized along the entire failure plane, such that

$$\tau(x) = c_i + \sigma(x) \tan \phi_i \qquad (5.7)$$

Equations 5.6 and 5.7 combine to give

$$Q \sin(i + \alpha) = \int_0^{\ell} \{ c_i + \sigma(x) \tan \phi_i \}\, dx$$

$$= c_i \ell + \tan \phi_i \int_0^{\ell} \sigma(x)\, dx$$

Using eq. 5.5,

$$Q \sin(i + \alpha) = c_i \ell + \tan \phi_i\, Q \cos(i + \alpha) \qquad (5.8)$$

Noting that $\ell = 2B \cos i$ and that $Q = qB$, eq. 5.8 can be simplified and rearranged to give

$$q = \frac{2 \cos i \; c_i}{\sin(i + \alpha) - \cos(i + \alpha) \tan \phi_i} \qquad (5.9)$$

Combining eq. 5.9 with eqs. 5.1 and 5.3 produces

$$s = 2 \cos i \; c_i + n \tan \phi_i \qquad (5.10)$$

From eq. 5.10, it is seen that s is a unique function of i, c_i, n, and ϕ_i. In physical terms, the shear resistance of the asperity depends thus only on the normal stress acting on the asperity, the inclination of the asperity, and the strength of the asperity material. With the base shear method, shear resistance (s) can be expressed in eq. 5.10 without explicitly involving α. In the following two methods to be presented, an analytic relationship between s and n

cannot be developed without explicitly involving α. This will be apparent when the other two methods are presented in the following two sections.

The simplicity of the base shear method, as indicated by eq. 5.10, is the direct result of choosing a planar failure surface which is parallel to the shear direction. The shear component of the applied stress does not generate any frictional resistance on the failure plane, only the normal component does. This results in a simple dependence of s on n.

The assumption of a Coulomb failure criterion also plays an important role in the simplicity of this method (as well as the other methods). Because the dependence of shear stress on normal stress is linear, the distribution of normal stresses on the failure plane need not be known, only the resultant normal force on the failure plane.

The base shear method described above is the same method used by Ladanyi and Archambault (1970) for describing the component due to asperity shear in the development of their shear equation (see Section 3.2). They assumed that the component of resistance due to shearing of asperities (S_4) was given by

$$S_4 = \tau_i A \qquad (3.5)$$

That is, the shear resistance is equal to the shear area of the asperities multiplied by the specific shear strength of the intact material. (However, Ladanyi and Archambault use a different relationship for τ_i than that used in this section.)

5.3 PLANE SHEAR

The base shear method assumes a planar failure surface which is parallel to the shear direction. Another approach to the problem is to

again assume a planar failure surface, but one which is not required to be parallel to the asperity base. In this method, the plane shear method, the failure surface is allowed to take any inclination which results in a minimum value of q at failure. The plane shear method always results in a value of q which is equal to or less than that obtained by the base shear method, and the base shear method becomes thus a special case of the plane shear method.

Figure 5-4 illustrates the failure surface for the plane shear method. The inclination of this surface is defined by the angle θ . From Fig. 5-4 and equilibrium in the y - direction:

$$Q \cos(\alpha + \theta) = \int_0^{\ell} \sigma(x)\, dx \qquad (5.10)$$

From equilibrium in the x - direction:

$$Q \sin(\alpha + \theta) = \int_0^{\ell} \tau(x)\, dx \qquad (5.11)$$

The resistance along the failure plane is assumed to be fully mobilized, so that eq. 5.7, 5.10, and 5.11 can be combined in the same way as for the base shear method to produce:

$$Q \sin(\theta + \alpha) = c_i \ell + \tan \phi_i \, Q \cos(\theta + \alpha) \qquad (5.12)$$

From Fig. 5-4b,

$$\ell = \frac{\sin \gamma}{\sin(180 - \gamma - \theta)} B = \frac{\sin \gamma}{\sin(\gamma + \theta)} B \qquad (5.13)$$

where $\gamma = 180^{\circ} - 2i$, because of asperity symetry.

Noting that $Q = q B$ and using eq. 5.13, eq. 5.12 can be put into the following form:

$$q = \frac{\sin \gamma}{\sin(\theta+ \gamma) \sin(\theta+ \alpha) - \cos(\theta+ \alpha) \tan \phi_i} \frac{c_i}{} \qquad (5.14)$$

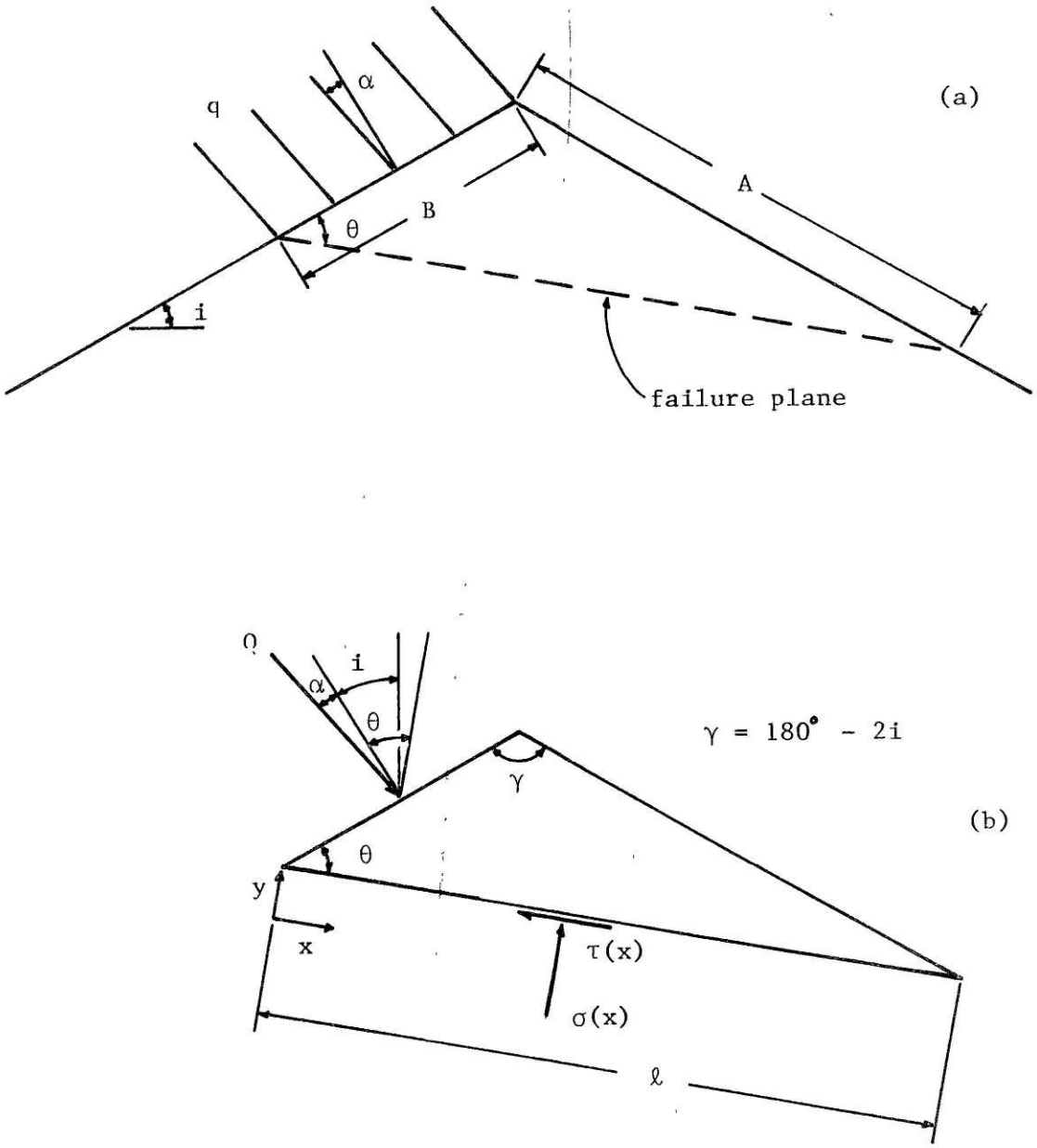

Figure 5-4 Plane shear analysis.

It is convenient to now define a new quantity N_c, where

$$N_c = \frac{q}{c_i}$$

so that

$$N_c = \frac{\sin \gamma}{\sin(\theta+\gamma)} \quad \frac{1}{\sin(\theta+\alpha) - \cos(\theta+\alpha) \tan \phi_i} \tag{5.15}$$

To determine the value of θ for which q is a minimum, eq. 5.15 can be minimized with respect to θ, for which

$$\theta = 90^\circ + (\phi_i - \gamma - \alpha)/2$$

or

$$\theta = \tfrac{1}{2}(\phi_i + 2i - \alpha) \tag{5.16}$$

by noting that $\gamma = 180^\circ - 2i$. Equation 5.16 can now be substituted into eq. 5.15 with the following result:

(5.17)

$$N_c = \frac{\sin 2i}{\sin \tfrac{1}{2}(\alpha+2i-\phi_i)} \quad \frac{1}{\sin \tfrac{1}{2}(\alpha+2i+\phi_i) - \cos \tfrac{1}{2}(\alpha+2i+\phi_i) \tan \phi_i}$$

Thus, N_c can be calculated from given values of i, α, and ϕ_i. (From Fig. 5-4, θ cannot be negative. Therefore, eq. 5.17 is only valid for combinations of α, i, and ϕ_i for which θ is positive in eq. 5.16.) Since $q = N_c c_i$, eqs. 5.1 and 5.2 can be written in the form

$$n = N_c c_i \cos(i + \alpha) \tag{5.18}$$

$$s = N_c c_i \sin(i + \alpha) \tag{5.19}$$

It is not possible to express s directly in terms of i, c_i, n and ϕ_i in the plane shear method as was done in the base shear method. However,

for any given combination of i, α, c_i, and ϕ_i, n and s can be calculated using eqs. 5.17 - 5.19.

From eq. 5.16, it is apparent that when ϕ_i is greater than i, the distance A in Fig. 5-4a is larger than the distance B, which has practical significance in situations where the distance A required by this method is greater than the length of the asperity face. (Asperity face length is illustrated in Fig. 5-1a.) The ratio of $\frac{A}{B}$, defined as R, will be used as an indicator of the applicability of the plane shear method when available asperity face length is considered. From Fig. 5-4,

$$\frac{A}{\sin \theta} = \frac{B}{\sin(180^\circ - \gamma - \theta)}$$

Combining this equation with eq. 5.16, and simplifying,

$$R = \frac{A}{B} = \frac{\sin \tfrac{1}{2} (\phi_i + 2i - \alpha)}{\sin \tfrac{1}{2} (- \phi_i + 2i + \alpha)} \qquad (5.20)$$

Thus, R is greater than 1 if $\phi_i > \alpha$. The importance of R in the interpretation and comparison of the plane shear method will be discussed in Section 5.5.

The plane shear method is somewhat more complex than the base shear method, but it results in a value of shear resistance which is more "correct" because it does not restrict the inclination of the failure plane. However, both the base shear method and the plane shear method are inexact, in that they do not agree with a more rigorous analysis using plasticity theory. Plasticity theory predicts a curvi-linear failure

surface which yields a lower value of shear resistance than both the base and the plane shear method. The method of analysis which employs plasticity theory is presented in the next section.

5.4 ZONE SHEAR

A third method of determining asperity shear resistance, herein referred to as the zone shear method, does not assume a planar failure surface, but instead assumes zones of shear failure by employing a more rigorous approach based on plasticity theory. When the load q is applied to the asperity (see Fig. 5-5), three different zones develop. All of the points in these zones are in a state of limiting equilibrium, or "failure". The problem consists of determining the maximum allowable states of stress in these zones from which the maximum allowable value of q is determined. This is the same approach used by Prandtl (1920) in his solution to the indentation problem in a frictional, weightless material, which was later applied to the bearing capacity of footings by Terzaghi (1925). The problem illustrated in Fig. 5-5 is analogous to a bearing capacity problem at the top of a slope, with an inclined loading. Sokolovskii (1965) and Brinch Hansen (1960) treat a number of problems similar to this, using plasticity theory in a frictional material, but do not present a solution to this problem. Meyerhof (1951,53) outlines a method of solving the problem of inclined loading at the top of a slope, however, the published results of his analysis are not in a form which can be directly applied to the asperity shear problem. Therefore, the solution will be developed in this section.

The approach used here is one where failure zones (i.e., zones where all points are in a state of limiting equilibrium) are " pieced" together

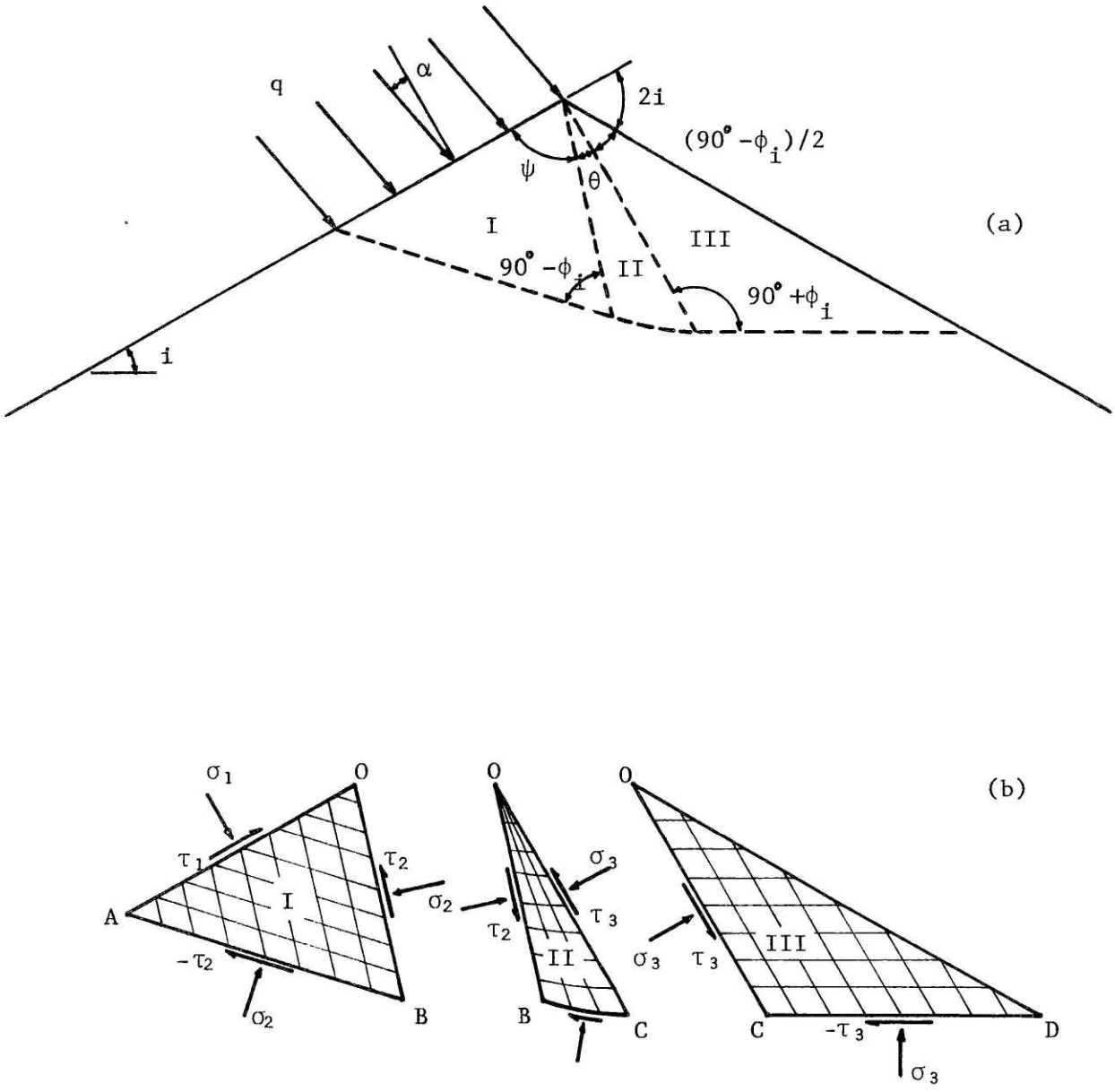

Figure 5-5 Zone shear analysis.

to form a failure mechanism which satisfies static equilibrium throughout the region of the solution, and also conforms to external boundary conditions. A truly rigorous solution would also account for the kinematics of the problem, which require that the velocity conditions are consistent throughout the region of the solution. That has not been done here. However, Hill (1950) developed an "exact" solution to Prandtl's indentation problem which considered both statics and kinematics, and found that his solution yielded the same value for ultimate load as did Prandtl's solution. Therefore, it is believed that the solution presented here for an asperity is "exact", in spite of the fact that kinematics are not considered. (Note that this solution is exact only for a weightless material. For an asperity composed of rock, the effects of weight are neglible.)

The solution is developed in the following way. Referring to Fig. 5-5, there are three different zones of failure developed in the asperity, labelled zones I, II, and III.

Zone I, immediately below the loaded area on the asperity, is a region of uniform stress. All points in this zone have the same stress state, the Mohr's circle for which is drawn in Fig. 5-6. There are two sets of straight slip lines in zone I, as shown in Fig. 5-5b.

Zone III, on the unloaded side of the asperity, is also a region of uniform stress. The Mohr's circle for this zone is also drawn in Fig. 5-6. This zone also has two sets of straight slip lines, as shown in Fig. 5-5b.

Zone II is a region of non-uniform stress. It is known as the radial shear zone, or the transition zone (providing a transition of the stress state in zone I to that in zone III). All points along any single radial line (a line passing through point 0 in Fig. 5-5b) have the same

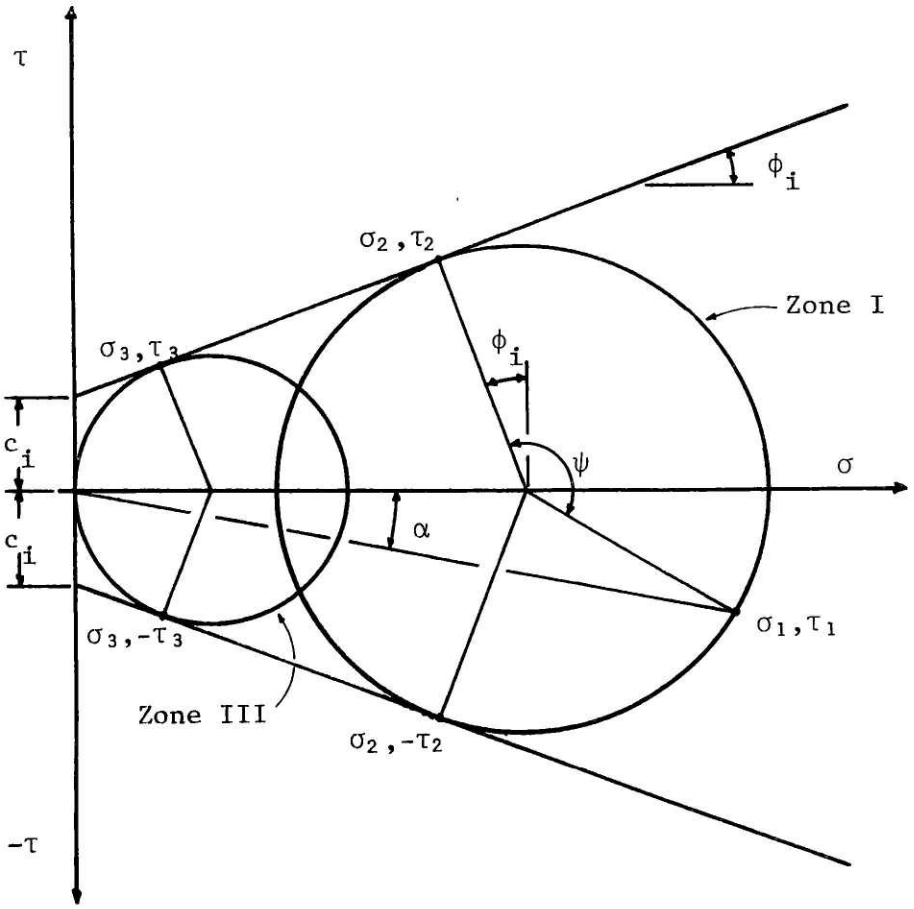

Figure 5-6 Mohr's circles for zone I and zone III.

stress state, but the stress state is continuously changing in any non-radial direction. The Mohr's circles for points in zone II, if drawn, would be a series of circles lying inbetween the circles for zone I and zone III in Fig. 5-6. The slip lines in zone II, shown in Fig. 5-5b, are a set of radial lines and a set of logarithmic spirals.

Figure 5-5b indicates the stresses acting on the boundaries of the three zones. By determining σ_1 and τ_1 for the limiting condition, the maximum allowable q can be determined.

$$\sigma_1 = q \cos \alpha$$

$$\tau_1 = q \sin \alpha$$

and

$$\tau_1 = \sigma_1 \tan \alpha \tag{5.21}$$

From Mohr's circle for zone I (see Fig. 5-6):

$$\frac{\tau_1}{\cos(180^\circ + \phi_i - 2\psi)} = \frac{\tau_2}{\cos \phi_i} \tag{5.22}$$

and

$$\sigma_1 = \sigma_2 + \tau_2 \tan \phi_i + \tau_1 \tan(180^\circ + \phi_i - 2\psi) \tag{5.23}$$

where ψ is the angle formed by planes OA and OB in zone I in Figure 5-5. σ_2 and τ_2 lie on the failure envelope, and are therefore related by

$$\tau_2 = c_i + \sigma_2 \tan \phi_i \tag{5.24}$$

τ_2 and τ_3 are the shear stresses acting on the radial boundaries of zone II, and can be shown (Prandtl, 1920) to be related by

$$\tau_2 = \tau_3 \exp(2\theta \tan \phi_i) \tag{5.25}$$

where θ is the angle formed by zone II, between planes OB and OC. From Fig. 5-5a,

$$\psi + \theta + (90^\circ - \phi_i)/2 + 2i = 180^\circ$$

or

$$\theta = 135^\circ - 2i - \psi + \phi_i/2 \tag{5.26}$$

From Mohr's circle for zone III (see Fig. 5-6):

$$\frac{\tau_3}{\cos \phi} = \sigma_3 + \tau_3 \tan \phi_i \tag{5.27}$$

and

$$\tau_3 = c_i + \sigma_3 \tan \phi_i \tag{5.28}$$

Equations 5.27 and 5.28 can be combined to give:

$$\tau_3 = c_i(1 + \sin \phi_i) \tag{5.29}$$

Equations 5.22, 5.25, and 5,28 can now be combined to give:

$$\tau_1 = \frac{\cos(180^\circ + \phi_i - 2\psi)}{\cos \phi_i} c_i(1 + \sin \phi_i) \exp(2\theta \tan \phi_i) \tag{5.30}$$

where θ is given by eq. 5.26. In order to solve for τ_1, the quantities c_i, ϕ_i, i, and ψ must be known. While c_i, ϕ_i, and i (as well as α) are a part of the problem definition, ψ must be calculated from the quantities α, i and ϕ_i. This can be done by combining eqs. 5.21, 5.22, 5.23, 5.24, 5.25, and 5.29 to give:

(5.31)

$$\exp(2\theta \tan \phi_i)\left[\sin(2\psi-\phi_i) + \frac{1}{\sin \phi_i} + \cos(2\psi-\phi_i) \cot \alpha\right] - \frac{(1-\sin \phi_i)}{\sin \phi_i} = 0$$

where again θ is given by eq. 5-26. The solution of eq. 5.31, for given values of α, i and ϕ_i, will give a value of ψ which can then be used in eq. 5.30 to calculate τ_1.

From τ_1, q can be calculated:

$$q = \frac{\tau_1}{\sin \alpha}$$

$$q = \frac{\cos(180^\circ + \phi_i - 2\psi)\ c_i(1 + \sin\phi_i)\ \exp(2\theta \tan\phi_i)}{\sin\alpha\ \cos\phi_i}$$

or

$$q = N_c\ c_i$$

where

$$N_c = \frac{\cos(180^\circ + \phi_i - 2\psi)\ (1 + \sin\phi_i)\ \exp(2\theta\ \tan\phi_i)}{\sin\alpha\ \cos\phi_i} \qquad (5.32)$$

Equations 5.18 and 5.19 can be used to calculate n and s, as with the plane shear method, but using the N_c just developed for this method.

The zone shear method is not applicable for all combinations of i, α, and ϕ_i. With some combinations, the value of ψ obtained from eq. 5.31 will indicate that $\psi + (90^\circ - \phi_i)/2 + 2i > 180^\circ$, or that $\theta + (90^\circ - \phi_i)/2 + 2i > 180^\circ$, both of which represent a physically impossible configuration (see Fig. 5-5). In effect, the asperity apex angle (γ) is not large enough to accomodate the shear zones required for this method. An "overlap" of zones occurs, causing ψ and/or θ to be negative. Therefore, any solution using the zone shear method where ψ or θ are negative is physically impossible, and thus not admissible.

As with the plane shear method, the distance from the tip of the asperity to the point of emergence of the failure surface on the unloaded face of the asperity can be calculated. From Fig. 5-5,

$$R = \frac{A}{B} = \frac{\overline{OD}}{\overline{OA}}$$

From zone I

$$\frac{\overline{OA}}{\sin(90^\circ - \phi_i)} = \frac{\overline{OB}}{\sin(90^\circ + \phi_i - \psi)} \qquad (5.33)$$

From the logarithmic spiral

$$\overline{OC} = \overline{OB} \exp(\theta \tan \phi_i) \tag{5.34}$$

From zone III

$$\frac{\overline{OD}}{\sin(90^\circ + \phi_i)} = \frac{\overline{OC}}{\sin \tfrac{1}{2}(90^\circ - \phi_1)} \tag{5.35}$$

Equations 5.33 - 5.35 can be combined to give

$$R = \frac{\overline{OD}}{\overline{OA}} = \frac{\cos(\phi_i - \psi)}{\sin \tfrac{1}{2}(90^\circ - \phi_i)} \exp(\theta \tan \phi_i) \tag{5.36}$$

The importance of R will be discussed in the next section.

5.5 COMPARISON OF METHODS

In the preceding sections, three different methods for determining the shear resistance of an idealized asperity were presented. Each of these three methods makes a different assumption concerning the failure mechanism in the asperity, and each gives a different result. These three methods will now be compared. Differences will be pointed out, and the implications of these differences for asperity shear on rock discontinuities will be discussed.

The basis of comparison for the three methods is the relationship between n and s (as defined in Section 5.1) for an asperity of given inclination (i) and angle of internal friction (ϕ_i). Methods of calculating s and n for given values of i, c_i, and ϕ_i were presented in the three preceding sections. Since n and s are linear functions of c_i, it is convienient to normalize n and s by dividing them by c_i. The methods can

then be compared through plots of s/c_i vs. n/c_i for various combinations of i and ϕ_i. Figure 5-7 presents a plot of s/c_i vs. n/c_i for $i = 15^\circ$ and $\phi_i = 30^\circ$. Three curves are presented, labelled plane shear, base shear, and zone shear. The base shear curve was obtained directly from eq. 5.10. The plane shear curve was obtained by calculating N_c for various values of α (given i and ϕ_i) using eq. 5.17. Then eqs. 5.18 and 5.19 were used to calculate n/c_i and s/c_i yielding different points on the curve. The zone shear curve was obtained by calculating N_c for various values of α (given i and ϕ_i) using eq. 5.32. Then eqs. 5.33 and 5.34 were used to calculate n/c_i and s/c_i in the same way as for the plane shear method.

The curves in Fig. 5-7 indicate that, for each method, s/c_i is a unique function of i, ϕ_i and n/c_i. Each point on the curves also has a value of α associated with it. By noting that

$$\frac{s}{n} = \tan(i + \alpha)$$

it is seen that the angle formed by the n/c_i axis and a line from the origin to the point in question is equal to $\alpha + i$. The angles i and α are shown on Fig. 5-7. In this way, the angle α associated with each point of the curves is apparent.

The base shear method yields the highest values of s/c_i for any n/c_i. The zone shear method yields the lowest values, while the plane shear method yields intermediate values. The base shear method is an upper limit solution to the problem, while the zone shear method is exact (within the assumptions specified in Section 5-1). The zone shear method does not apply to all combinations of i, α, and ϕ_i, due to limitations of geometry on the development of shear zones, as mentioned in Section 5.4. For

this reason, the zone shear method only applies to limited range of n/c_i; for example, see Fig. 5-9. This limited range depends on i and ϕ_i as well as n/c_i, and therefore the range is different for other figures which follow. (The plane shear method is also not valid for all combinations of α, i and ϕ_i, as pointed out in Section 5.3, and therefore is also not defined for all values of n/c_i in some of the figures which follow.)

Plots of s/c_i vs. n/c_i have been prepared for all combinations of $i = 15°, 30°, 45°$ and $\phi_i = 20°, 30°, 40°$. These are presented in Figs. 5-7 through 5-15. In all of the plots, the three curves lie close together for low values of n/c_i, but they diverge considerably as n/c_i increases.

For given values of ϕ_i, the divergence of the curves increases with increasing i. For given values of i, the divergence of the curves increases with decreasing ϕ_i. In more physical terms, the difference between the three different shear methods is greater for steep asperities and low internal friction angles than it is for low-angle asperities and high internal friction angles.

An important difference in the three methods occurs at high values of n/c_i. For both the zone and plane shear methods, there is a "maximum allowable" value of n/c_i, i.e., n/c_i has a finite value for $s/c_i = 0$. (It is not shown on all figures due to the scale chosen.) This means that under normal stress alone, the asperity can fail, as in a crushing action or a bearing capacity type failure. In contrast, the base shear method indicates steadily increasing shear resistance with increasing normal stress.

Some restriction in the region of the s/c_i vs. n/c_i plots can be made by considering possible values of α in the problem, where α

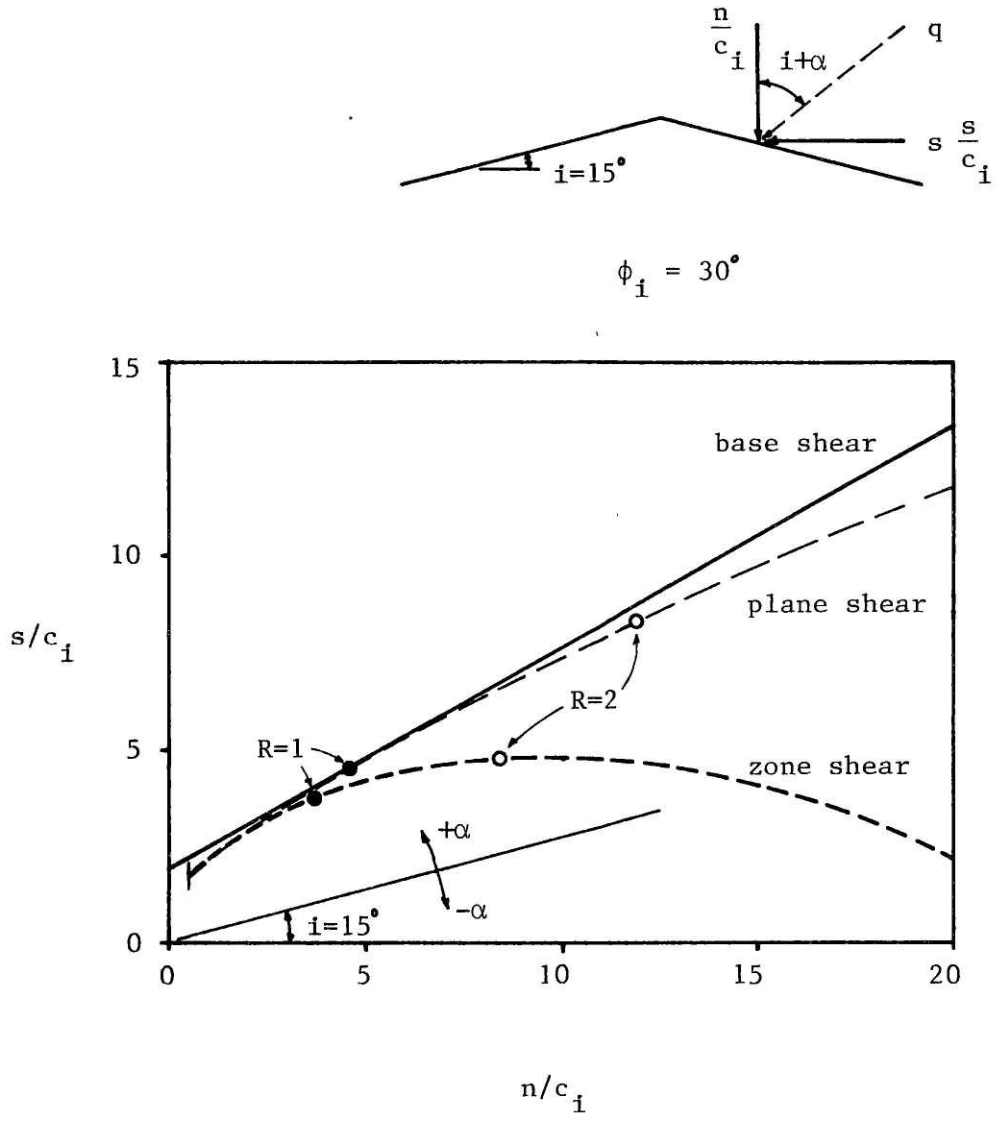

Figure 5-7 Plot of s/c_i vs. n/c_i for $i = 15^\circ$ and $\phi_i = 30^\circ$.

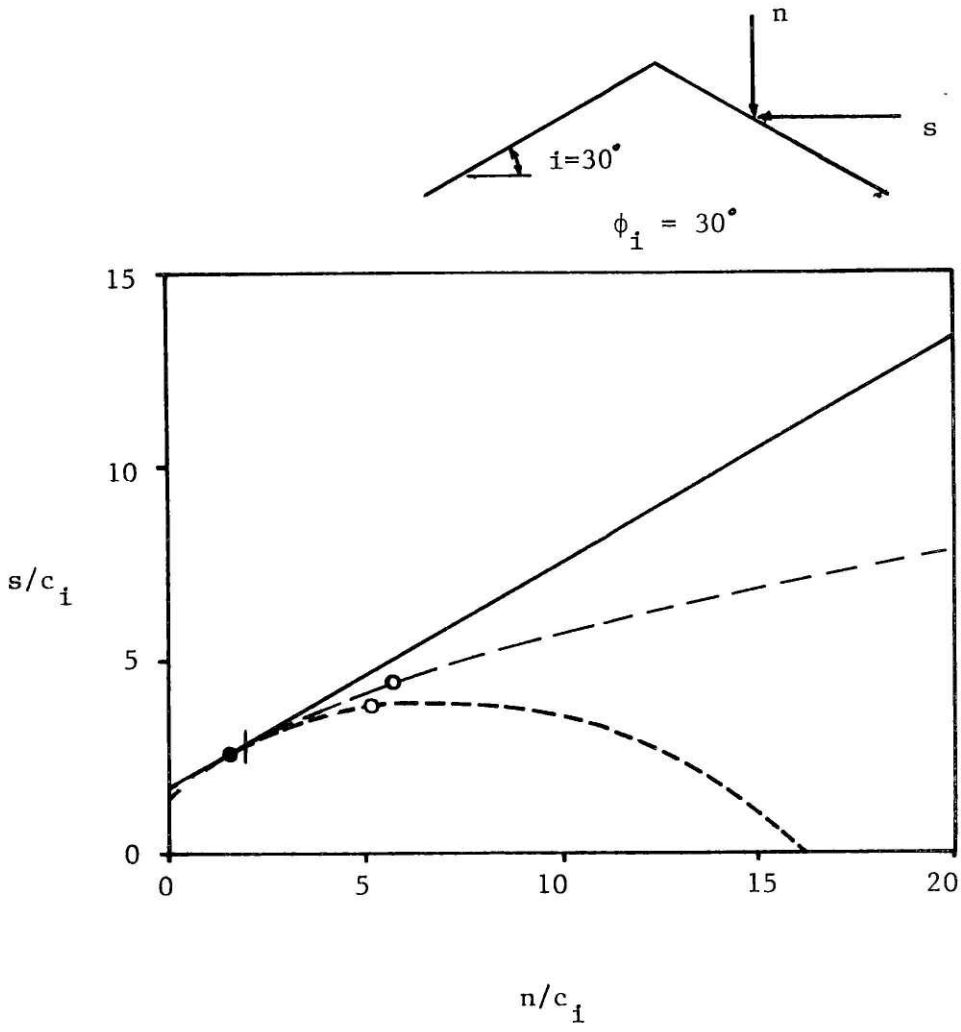

Figure 5-8 Plot of s/c_i vs. n/c_i for $i = 30^\circ$ and $\phi_i = 30^\circ$.

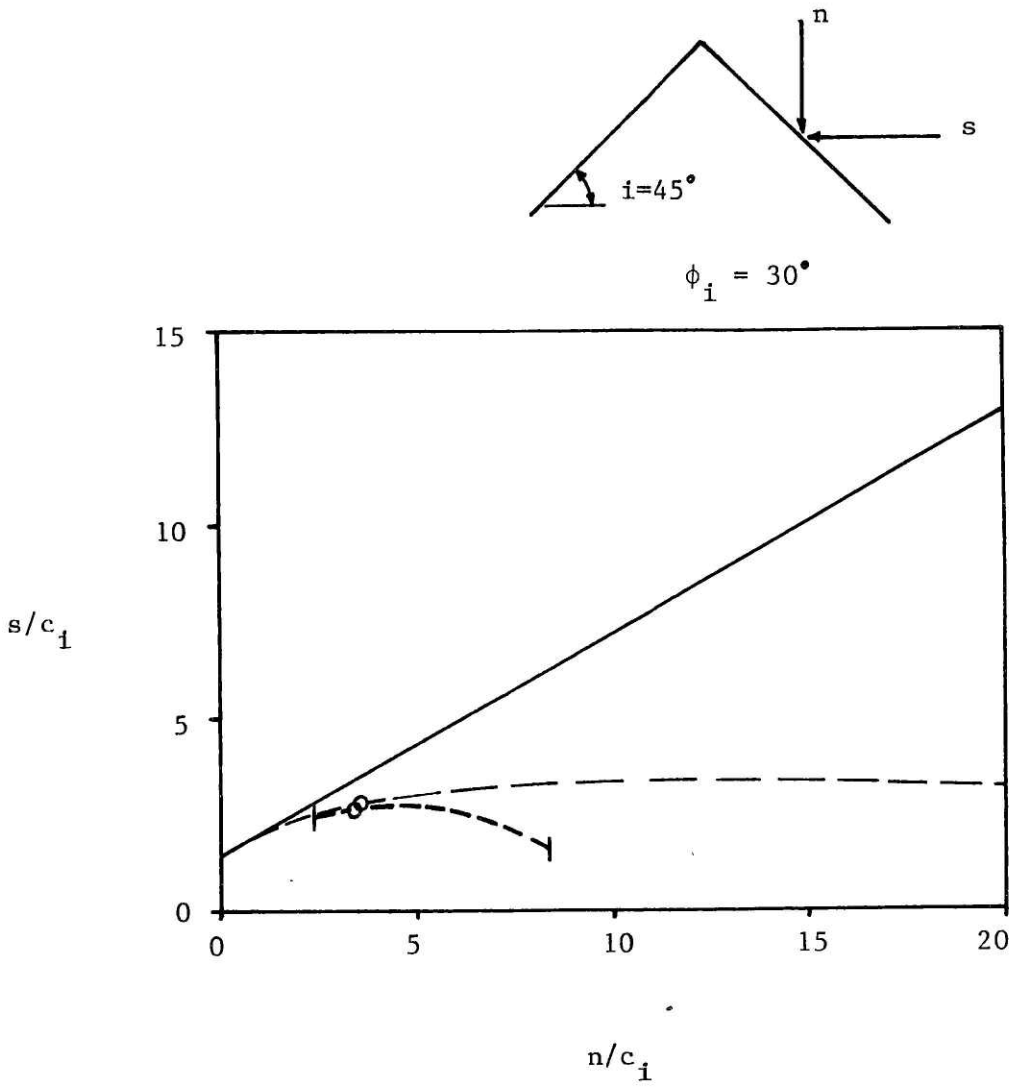

Figure 5-9 Plot of s/c_i vs. n/c_i for $i = 45^\circ$ and $\phi_i = 30^\circ$.

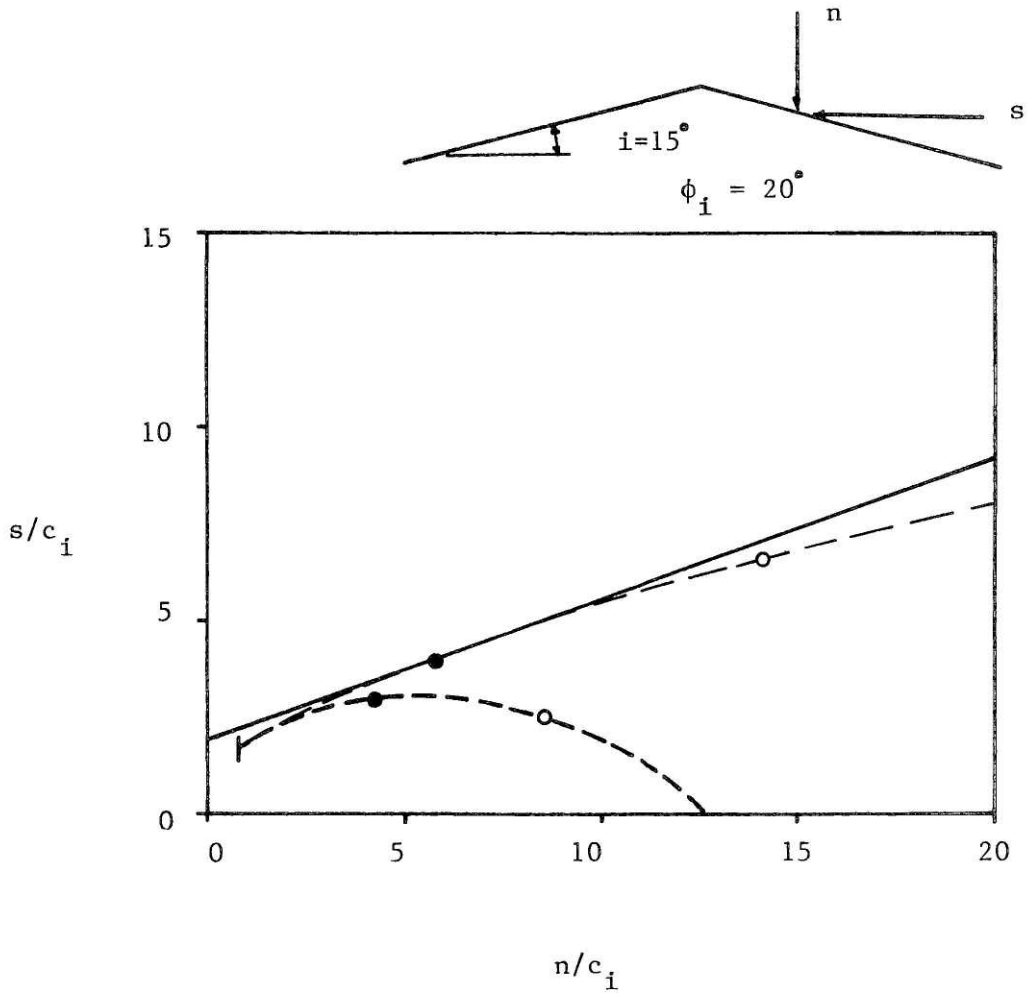

Figure 5-10 Plot of s/c_i vs. n/c_i for $i = 15^\circ$ and $\phi_i = 20^\circ$.

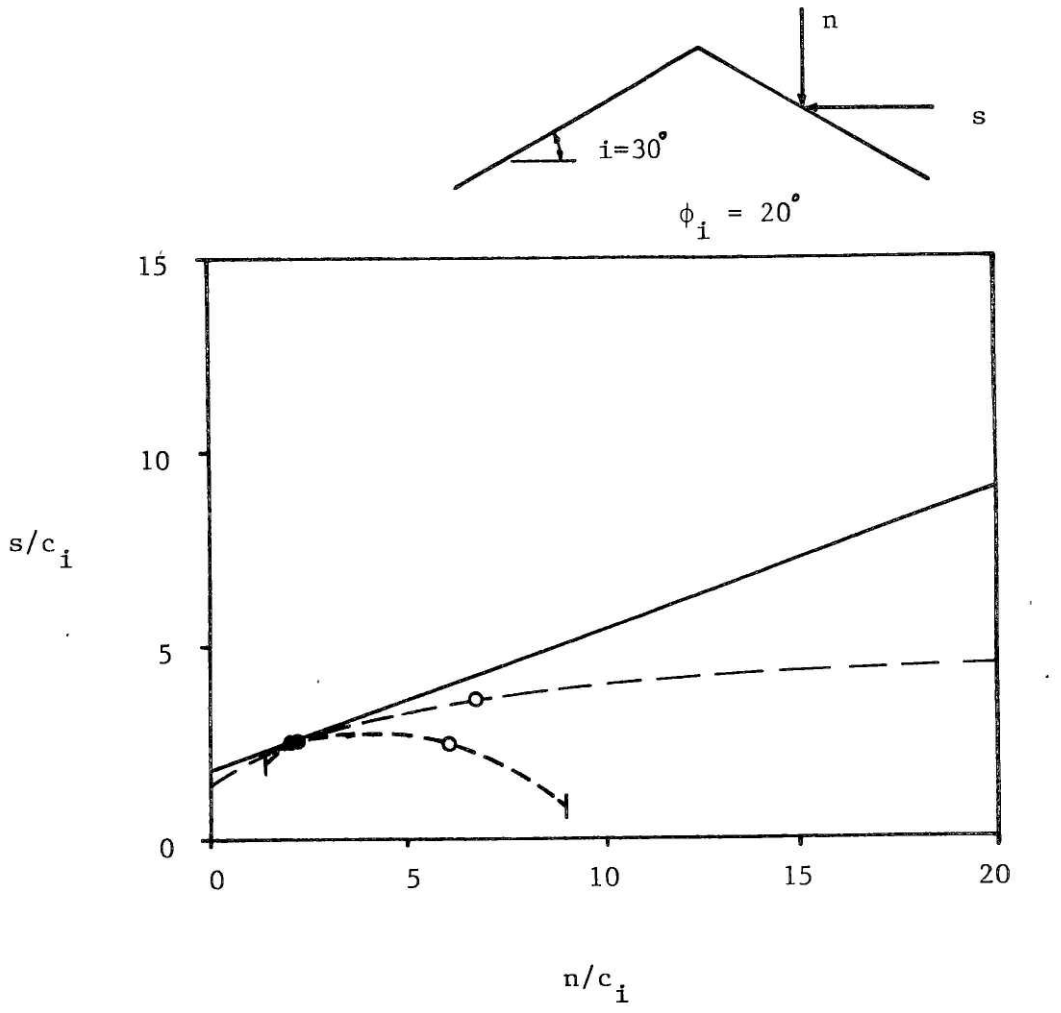

Figure 5-11 Plot of s/c_i vs. n/c_i for i = 30° and ϕ_i = 20°.

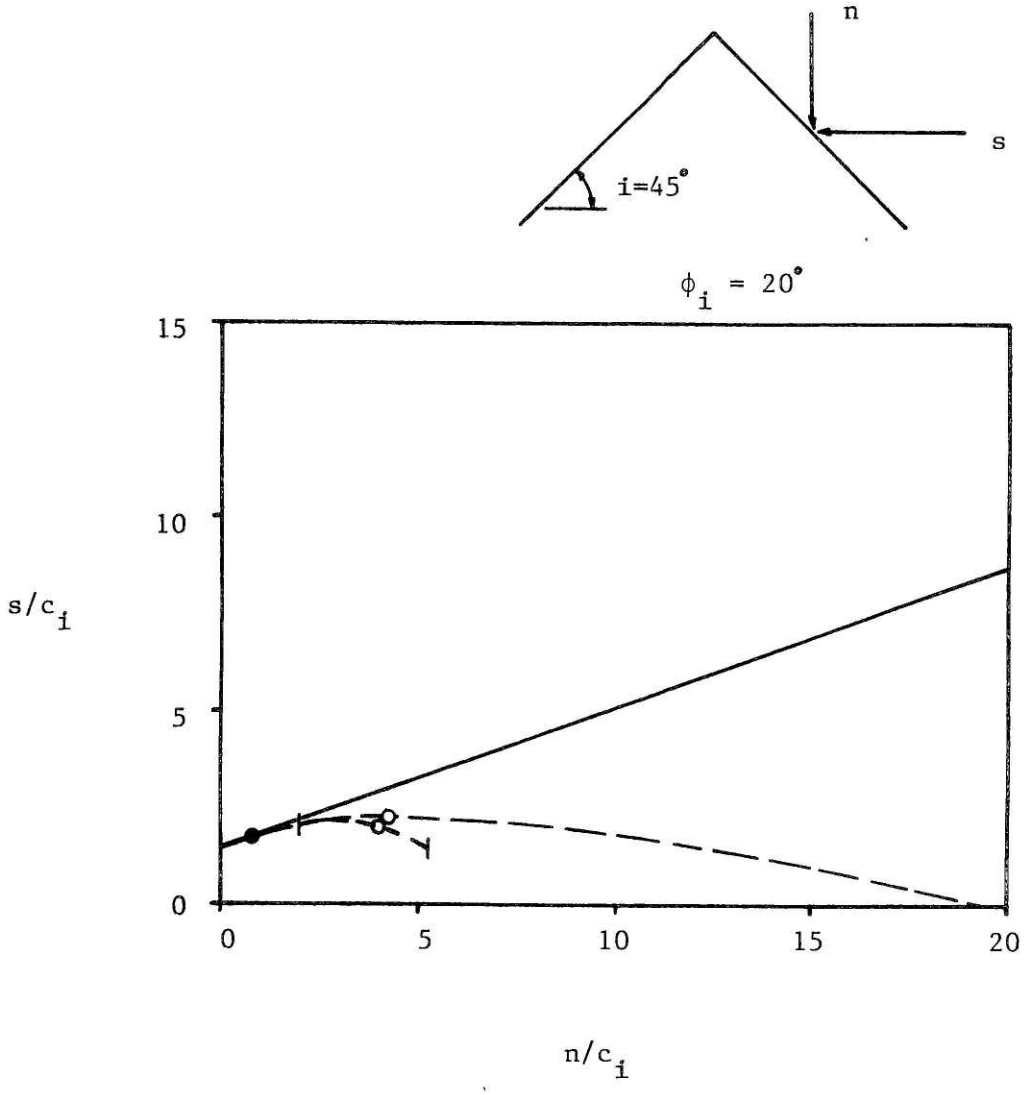

Figure 5-12 Plot of s/c_i vs. n/c_i for $i = 45^\circ$ and $\phi_i = 20^\circ$.

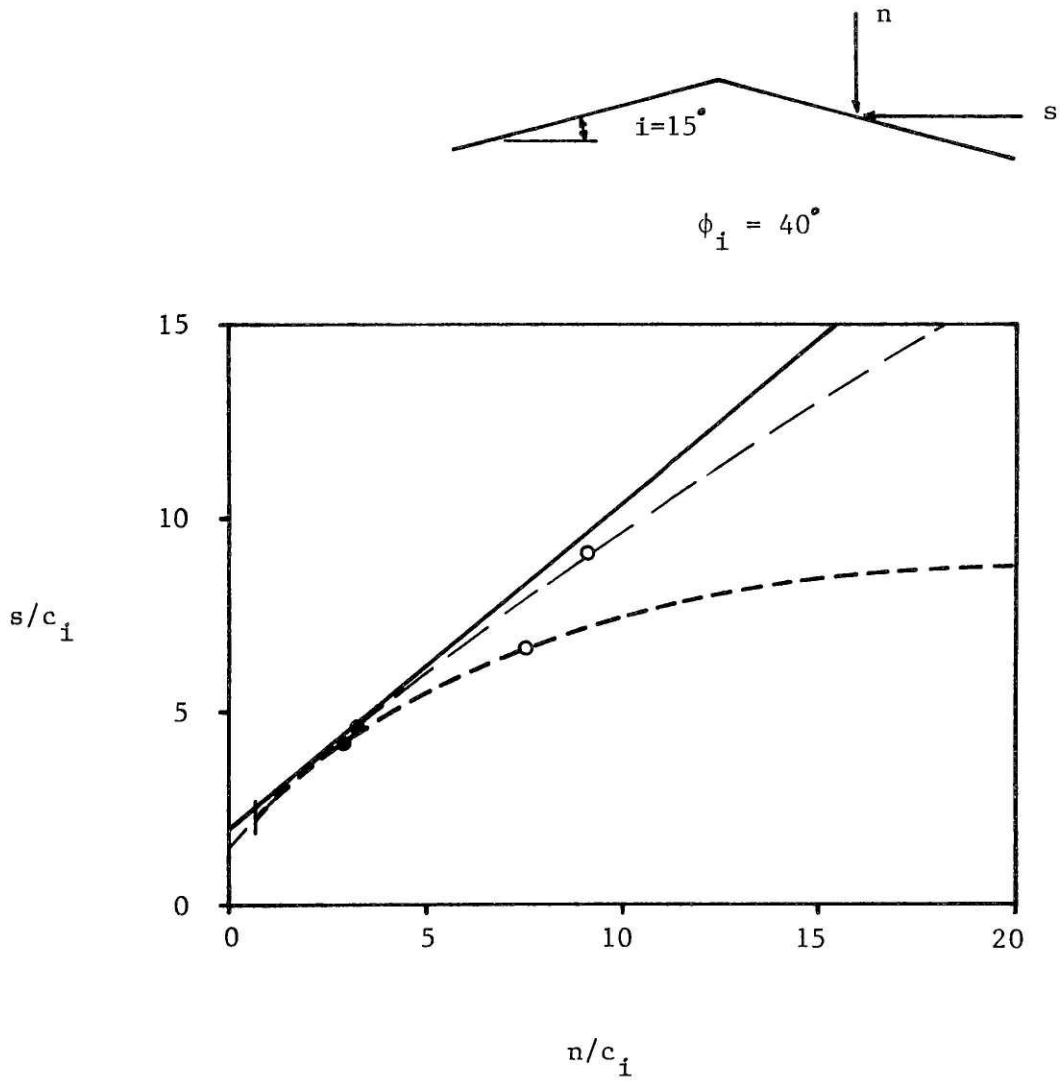

Figure 5-13 Plot of s/c_i vs. n/c_i for $i = 15^\circ$ and $\phi_i = 40^\circ$.

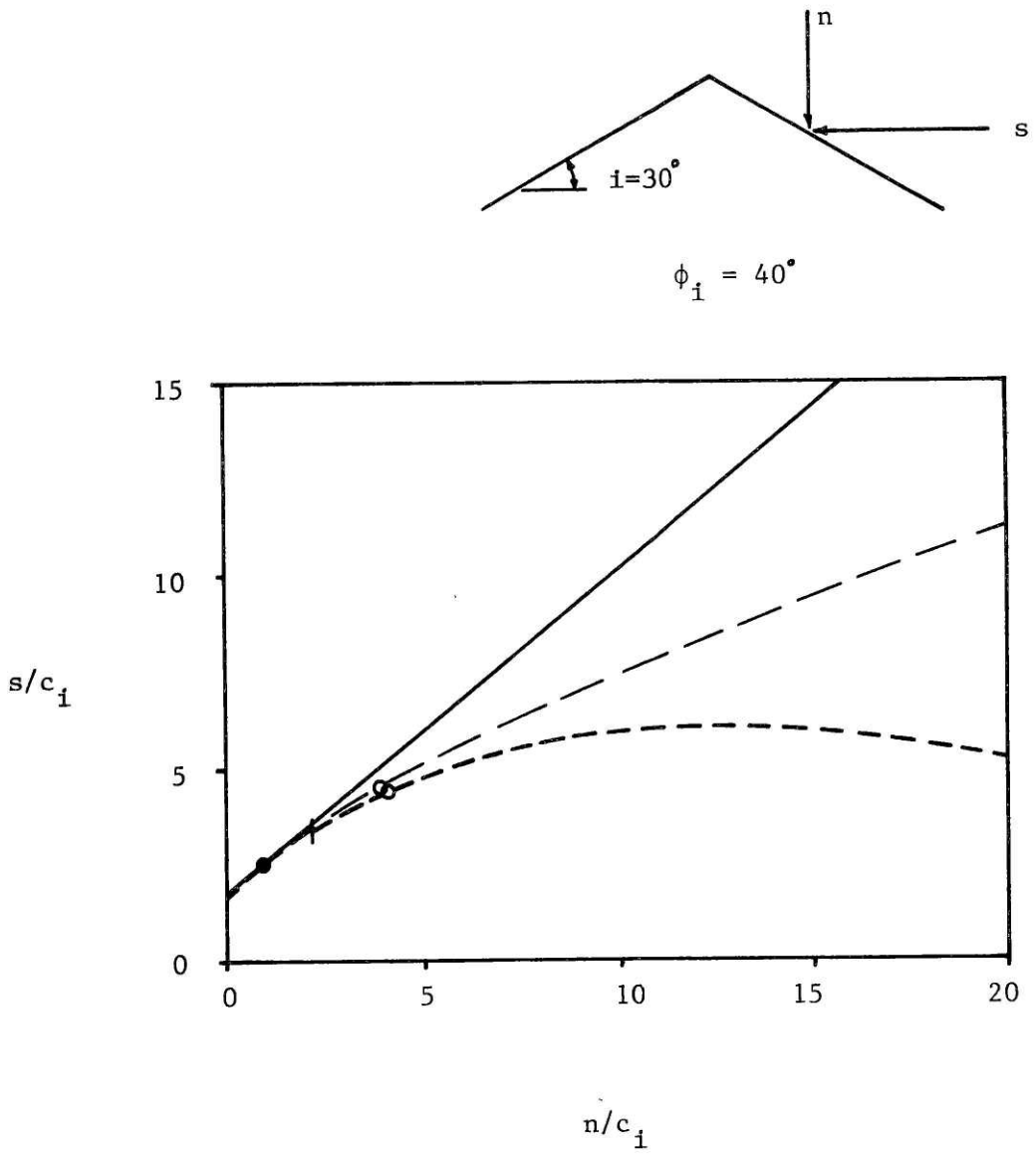

Figure 5-14 Plot of s/c_i vs. n/c_i for $i = 30^\circ$ and $\phi_i = 40^\circ$.

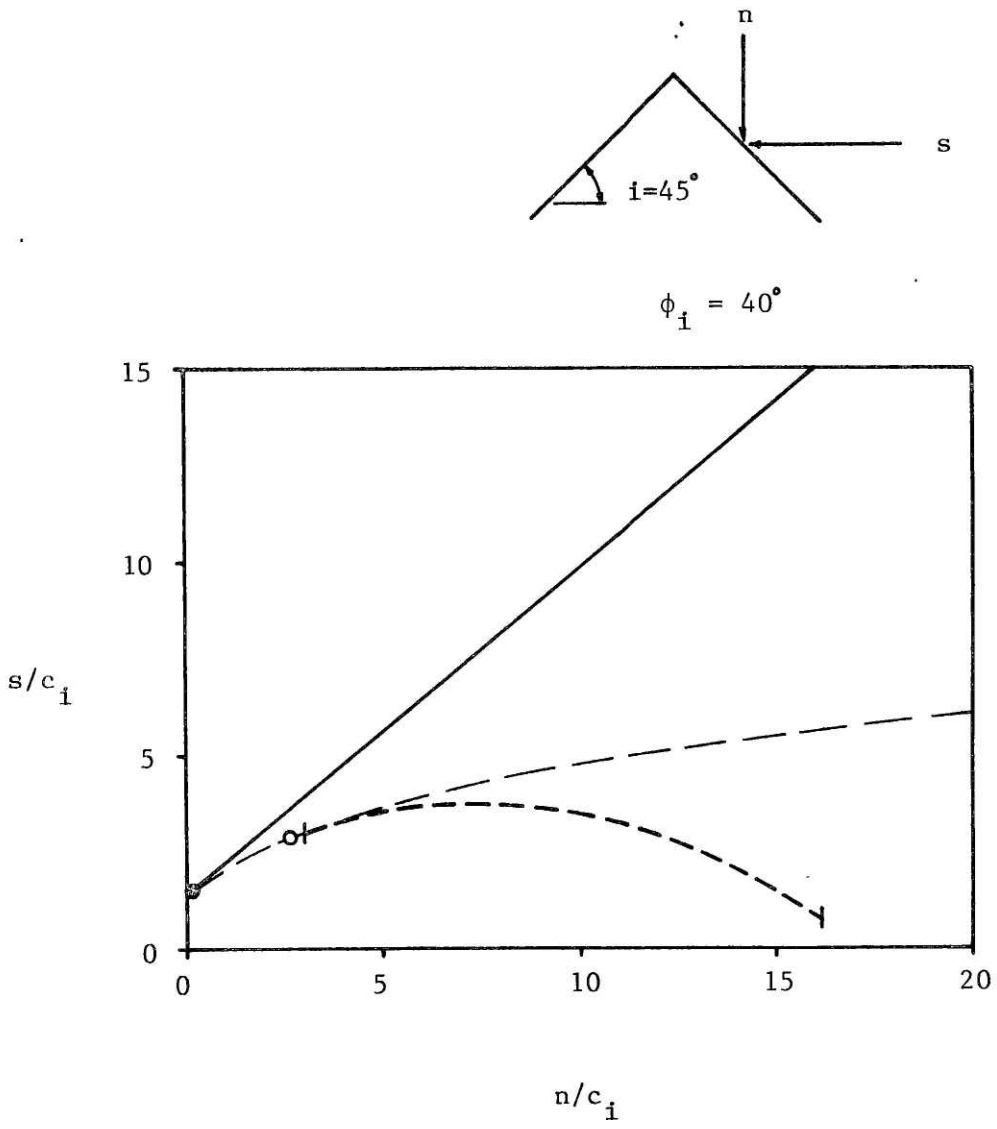

Figure 5-15 Plot of s/c_i vs. n/c_i for $i = 45^\circ$ and $\phi_i = 40^\circ$.

represents the inclination from the normal of the applied load q which causes asperity failure. The applied stress q will be applied to any given asperity by asperities on the opposite wall of the discontinuity. The forces transmitted by asperity-to-asperity contact will be limited by the frictional characteristics of the material. This means that α cannot be greater than ϕ_μ for the material, because sliding occurs if $\alpha > \phi_\mu$. Therefore, if a line with inclination i is drawn on an s/c_i vs. n/c_i plot through the origin, the only applicable region of the plot is bounded by the lines with inclination $i + \phi_\mu$ and $i - \phi_\mu$, as shown schematically in Fig. 5-16. This restriction can be significant for low values of ϕ_μ (20°) but high values of ϕ_μ (45°) do little to restrict the area of the plot.

Evaluation of Shear Mechanisms for an Individual Asperity

The three methods presented indicate two major limits to the shear resistance of a single asperity. The base shear method yields an upper limit, while the zone shear method yields a lower limit. The zone shear method is considered "exact", i.e. the method which gives the correct answer, within the assumptions set forth for all of the methods. However, there is an important limitation to the zone shear method which, in some cases, makes it incorrect to use. This limitation will now be discussed.

In the analyses made thus far, no consideration of the size of asperities has been made by specifying base length or height. In some situations the failure mechanism assumed by the zone and plane shear method is incompatible with asperity geometry, as illustrated in Fig. 5-17a. In this situation, the failure surface assumed by the plane and zone shear methods terminates within the intact material below the surface of the

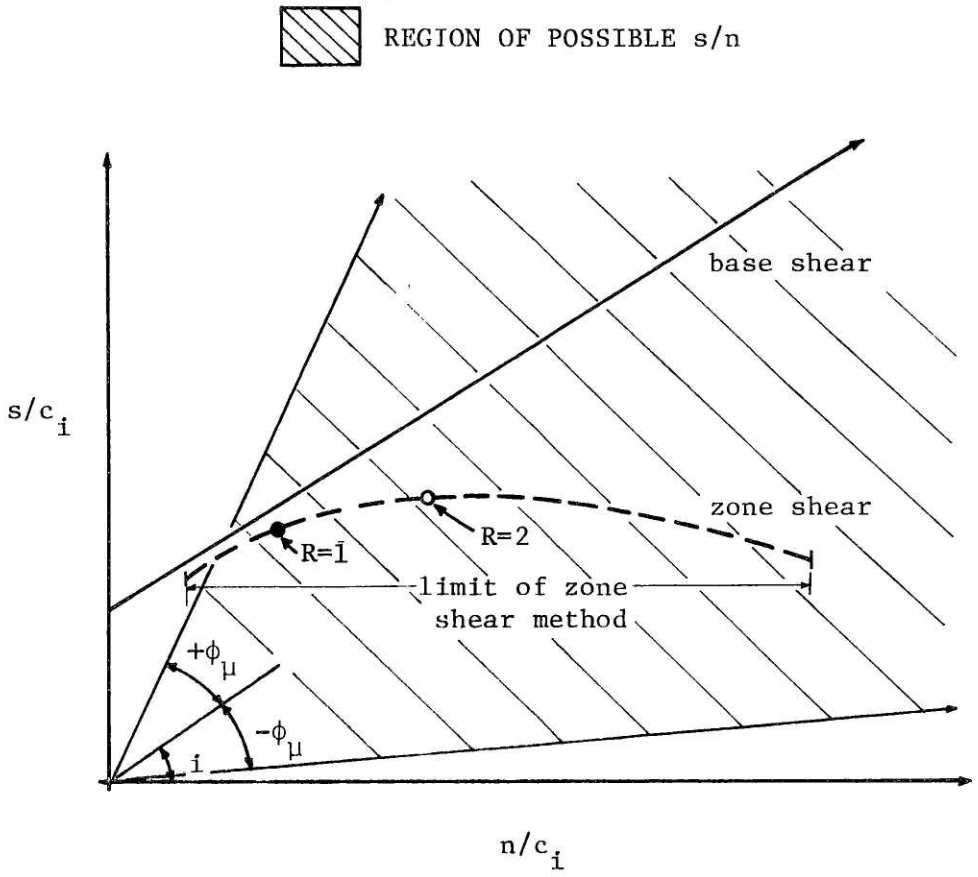

Figure 5-16 Schematic plot of s/c_i vs. n/c_i.

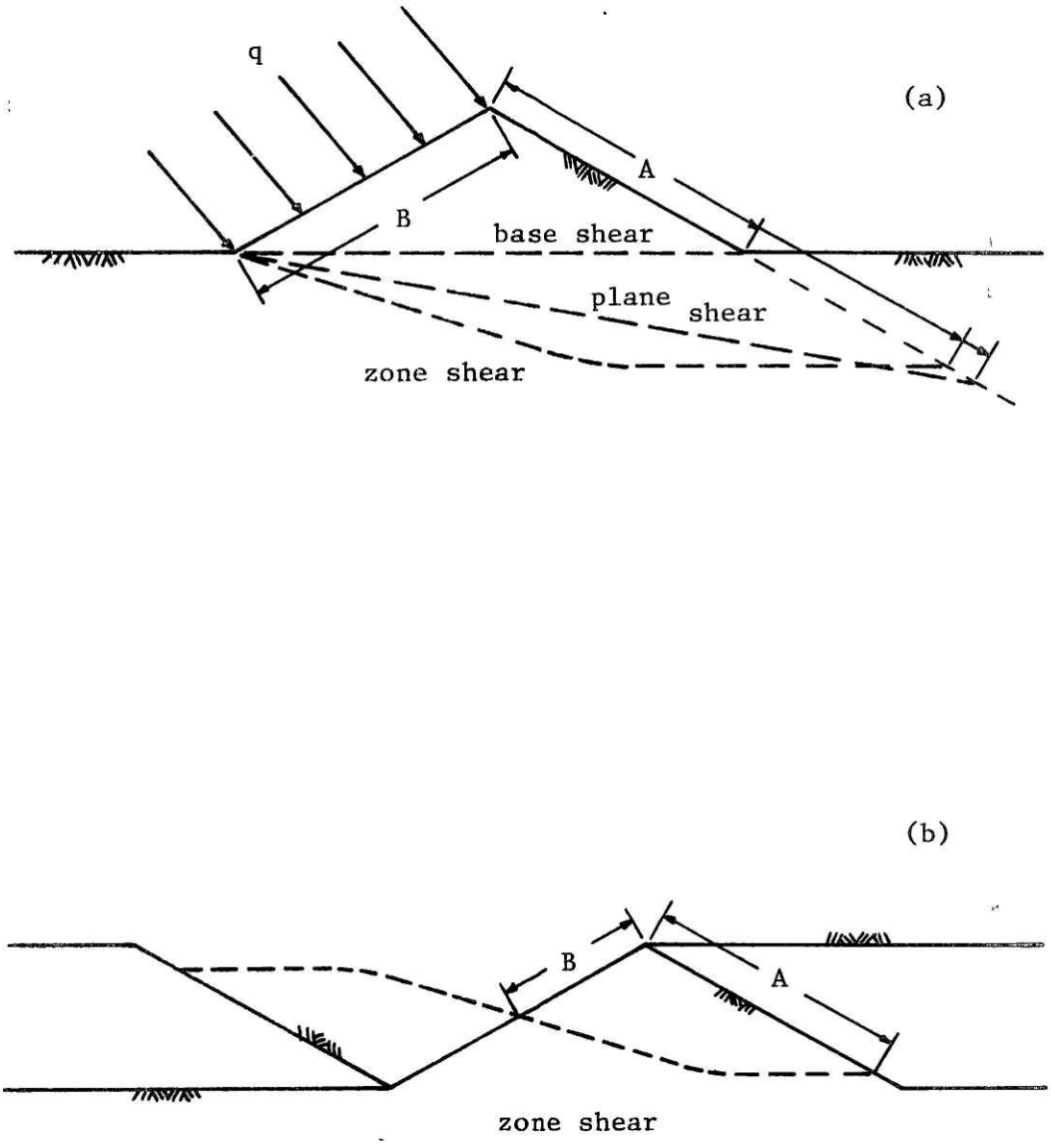

Figure 5-17 Shear methods applied to asperities on a discontinuity.

discontinuity, while the failure surface for the base shear method does not. For an asperity loaded along its entire face, as shown in Fig. 5-17a, this incompatibility of failure mechanism with asperity geometry will arise whenever R ($= \frac{A}{B}$) is greater than 1. If the asperity is not loaded along its entire face, then R can be greater than 1, the exact value depending on the ratio of loaded length to face length.

In cases where identical asperities on opposing surfaces of discontinuities bear against each other, failure surfaces could develop in both asperities, as illustrated in Fig. 5-17b. In this case, a failure mechanism with $R \leq 2$ would be compatible with asperity geometry.

In any case, the applicability of the zone and plane shear methods must be evaluated with consideration of the associated value of R, to determine if the failure mechanism is compatible with asperity geometry. In Figs. 5-7 through 5-15, the points on the zone and plane shear curves where R = 1 and R = 2 have been indicated. (Note that, by definition, R = 1 for the entire base shear curves.) For both the zone and plane shear curves, R changes continuously along the curves, increasing with increasing n/c_i. In all of the plots, $R > 1$ for $n/c_i > 5$, so that the greater portion of the curves shown represent points for which $R > 1$. This has important implications. For example, if the zone shear method is applied to an asperity which is loaded along its entire face, and the method indicates that $R > 1$, the actual failure surface will be different from that assumed in the analysis. This will result in an underprediction of the actual asperity shear resistance. An analysis which accounts for the actual asperity geometry in this case would provide a value of shear resistance which would lie somewhere inbetween the zone shear method and the base

shear method.

In summary, the base shear method provides an upper limit to asperity shear resistance which is always compatible with asperity geometry (for symetric asperities). The zone shear method provides a lower limit to asperity shear resistance which yields the exact value in some cases and a value which is too low in other cases. To determine whether the zone shear method is exact or too low, a comparison of the distance A required and the distance A available must be made.

It should be noted that there is physical evidence to support the type of shearing mechanism used in the zone shear method. Curved failure surfaces on both sides of the discontinuity, as suggested in Fig. 5-17b, have been observed on slicken-sided (previously sheared) discontinuities in rock. In addition, Archambault (1972, pp. 66,82) shows photographs of direct shear tests on model discontinuities with interlocking, identical asperities which show failure surfaces quite similar to those shown in Fig. 5-17b.

Further understanding of individual asperity shear related to discontinuity shear may be obtained by considering the behavior of discontinuities at very high normal stresses. It has been established by a number of researchers that the failure envelope of a discontinuity in rock approaches and possibly joins the failure envelope for the intact rock at a very high normal stress, defined as the transition stress (σ_T). This means that as σ approaches σ_T , individual asperity shear analysis will no longer be valid for predicting shear resistance.

5.6 CONCLUSIONS AND DISCUSSION

The base shear method and zone shear method have been shown to represent upper and lower limits, respectively, of asperity shear resistance. The region of the plots of s/c_i vs. n/c_i in which all methods describing asperity shear resistance are physically possible is defined by $-\phi_\mu < \alpha < +\phi_\mu$ as illustrated in Fig. 5-16, with certain exceptions as described below. Actual asperity shear resistance will be correctly given by the zone shear method, because it is an exact solution to the problem, except in cases where two important limitations affect the method. One limitation is that the zone shear method is only defined over limited ranges of n/c_i, due to asperity geometry which prevents development of the required shear zones. The other limitation is caused by insufficient asperity face length (as determined through the quantity R) which makes the assumed failure surface incompatible with actual asperity geometry. These two limitations further restrict the region of the s/c_i vs. n/c_i plots for which the zone shear method yields the correct result. Outside of this region, the zone shear method will yield a value of asperity shear resistance which is too low, as the value of actual asperity shear resistance will tend towards the base shear value because the base shear method does not suffer from these limitations.

The practical effect of using either the base shear method or the zone shear method in any particular case will depend on whether the zone shear method is physically possible (i.e., not affected by the above two limitations). If zone shear is possible, then the zone shear method is correct, and the base shear method will overpredict asperity shear resistance. If zone shear is not possible, then use of the zone shear method

will underpredict asperity shear resistance.

The fact that the base shear method will yield a value of asperity shear resistance which is too large has important implications for theoretical considerations of discontinuity shear resistance. An overprediction of discontinuity shear resistance will result when the base shear method is used to predict asperity shear resistance, as in cases where asperity shear resistance is obtained by multiplying shear area by specific shear strength. For example, Ladanyi and Archambault (1970) use this method to evaluate the shearing component S_4 in the development of their shear equation.

An overprediction of asperity shear resistance can also have an indirect effect on predicted discontinuity shear resistance because of dilation. An overprediction of asperity shear strength will cause an overprediction of the discontinuity dilation in cases where there is some sliding on asperities before shearing of asperities occurs. The asperities will actually be sheared "sooner" because their resistance is less than expected. This would be important if the normal stress on the discontinuity is dependent on normal displacement (dilation), in confined situations such as discontinuities around underground openings. In this case, the predicted normal stress at peak resistance would be greater than the actual normal stress at peak resistance, and a further overprediction of shear resistance would result.

A final comment on the implications of the results contained in this chapter is concerned with the dependence of asperity shear resistance on normal stress. From Figs. 5-7 through 5-15, it is apparent that shear resistance has a linear dependence on normal stress for the base shear

method, and a non-linear dependence on normal stress for the zone shear method. If the actual dependence of shear resistance on normal stress is non-linear, then the distribution of normal stresses on a discontinuity becomes increasingly important. Simplifications with respect to the distribution of normal stresses (e.g., assuming a uniform normal stress) when analyzing the results of direct shear tests or field observations may lead to erroneous conclusions regarding asperity shear resistance.

CHAPTER 6

MODELLING THE SHEARING OF DISCONTINUITIES

In the preceding two chapters, the two basic mechanisms of shear resistance in rock discontinuities were examined: the sliding mechanism and the shearing mechanism. In general, these two mechanisms take place simultaneously on different portions of a discontinuity to provide shear resistance. This chapter considers how the simultaneous occurrence of both shearing and sliding can be modelled for an irregular discontinuity.

6.1 DEVELOPMENT OF A DISCONTINUITY SHEAR EQUATION

This section presents the development of an analytical model which describes the shear resistance of rock discontinuities. As will be shown, the shear resistance can be described in a consistent manner only if it is related to the shear displacement. Analytic relationships describing the resistance due to the sliding mechanism and due to the shearing mechanism have been developed in previous chapters and will be recalled shortly. They will be briefly discussed separately, and then combined to obtain a relationship which accounts for both sliding and shearing.

Shear resistance due to sliding on inclined surfaces was discussed in Section 2.2, and can be expressed by

$$S_r = N_r \tan(i^* + \phi_\mu) \qquad (6.1)$$

where

S_r = shear resistance due to sliding

N_r = normal force which generates sliding resistance

i^* = dilation angle, the angle representing deviation of sliding direction from shear direction

ϕ_μ = friction angle for sliding on a flat surface

Equation 6.1 is equivalent to eq. 2.1 except that the notation has been changed. (S_r replaces S, N_r replaces N, and i^* replaces i.) This relationship accounts for resistance due to friction as well as dilation.

Shear resistance due to the shearing of asperities was discussed in Chapter 5, where different relationships representing different failure mechanisms were presented. When an assumption of base shear is made, shear resistance can be expressed by

$$S_s = c_i A_s + N_s \tan \phi_i \qquad (6.2)$$

where

S_s = shear resistance due to shearing of asperities

N_s = normal force acting on the asperities being sheared

A_s = shear area

c_i = cohesion of the intact material

ϕ_i = angle of internal friction of the intact material

Equation 6.2 is the same as eq. 5.12, except that A_s replaces ℓ, N_s replaces $Q \cos(i + \alpha)$, and S_s replaces $Q \sin(i + \alpha)$. (While the inaccuracies of the base shear assumption have been pointed out in Chapter 5, it is used here for simplicity in the formulation of the general shear equation which follows.)

Equation 6.2 was developed from consideration of statics, and does not account for possible dilation which may occur during shear. An

additional component of S_s is required when dilation against the normal force (N_s) is considered. This component is equal to the force required to do the work against N_s during dilation, as shown in Fig. 6-1, and is equal to $N_s \tan i^*$. (This component is equal to the component S_1 of Ladanyi and Archambault (1970), see Section 3.2.) The component can be added directly to eq. 6.2, resulting in

$$S_s = c_i A_s + N_s \tan \phi_i + N_s \tan i^*$$

or

$$S_s = c_i A_s + N_s(\tan \phi_i + \tan i^*) \qquad (6.3)$$

Thus, eqs. 6.1 and 6.3 account for resistance due to sliding and shearing, respectively, and both include the effects of dilation. Now the two equations can be combined to account for each of them occuring over different portions of the discontinuity at the same time.

The total shear resistance on a discontinuity (S) is the sum of sliding resistance (S_r) and shearing resistance (S_s), i.e.,

$$S = S_r + S_s \qquad (6.4)$$

Using eqs. 6.1 and 6.3 with eq. 6.4,

$$S = N_r \tan(\phi_\mu + i^*) + c_i A_s + N_s(\tan \phi_i + \tan i^*) \qquad (6.5)$$

(Both quantities of S_r and S_s depend on i^*, and i^* is identical for both S_r and S_s for a rigid discontinuity.)

The total normal force acting on the discontinuity (N) is the sum of the normal force acting on sliding portions (N_r) and the normal force acting on shearing portions (N_s), i.e.,

$$N = N_r + N_s \qquad (6.6)$$

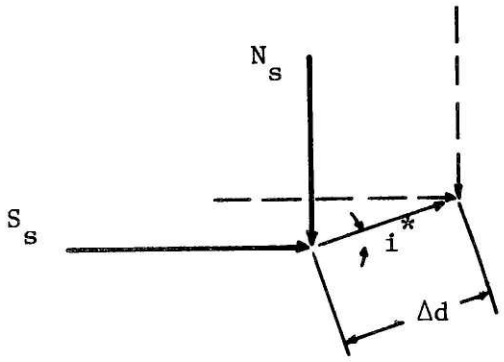

$$\text{work in} = \text{work out}$$

$$S_s \, \Delta d \cos i^* = N_s \, \Delta d \sin i^*$$

$$S_s = N_s \tan i^*$$

Figure 6-1 Derivation of shear force component due to dilation against normal force.

It is now necessary to make an assumption concerning the relative proportion of N_r and N_s to N. The actual distribution of normal force over the discontinuity is probably quite irregular in many cases. This distribution will depend on the surface geometry of both walls of the discontinuity, as well as the deformability of the intact material. To attempt to determine this distribution in a theoretical way would be very difficult and would not remove the uncertainities in the problem. In addition, there is no experimental information on this subject. Therefore, a simplifying assumption is made with respect to this distribution, where N_r and N_s are aportioned to N according to the areas on which they act:

$$N_r = \frac{A_r}{A_r + A_s} N \tag{6.7}$$

$$N_s = \frac{A_s}{A_r + A_s} N \tag{6.8}$$

where A_r = area of the discontinuity where sliding takes place

A_s = area of the discontinuity where shearing of asperities takes place

(Note that these conditions will be satisfied if the distribution of normal force is uniform over $A_r + A_s$.)

In some cases, $A_r + A_s = A$, such as the case of a tightly interlocking discontinuity. More generally however, $A_r + A_s \neq A$. In other words, some areas of the discontinuity are neither sliding nor shearing, i.e., not in contact.

It is convenient to define the contact area ratio (a_c) as

$$a_c = \frac{A_r + A_s}{A} \tag{6.9}$$

In addition, the shear area ratio (a_s) is defined as

$$a_s = \frac{A_s}{A} \tag{6.10}$$

so that eqs. 6.7 and 6.8 can be written in the following form:

$$N_r = \left(1 - \frac{a_s}{a_c} \right) N \tag{6.11}$$

$$N_s = \frac{a_s}{a_c} N \tag{6.12}$$

Equation 6.5 can be combined with eqs. 6.11 and 6.12 to give

$$\tau = \frac{S}{A} = \left(1 - \frac{a_s}{a_c} \right) \tan(\phi_\mu + i^*) + c_i a_s + \frac{a_s}{a_c} \sigma (\tan \phi_i + \tan i^*) \tag{6.13}$$

where $\sigma = N/A$. Equation 6.13 represents a relationship describing the shear resistance (τ) which accounts for sliding and shearing taking place at the same time on different portions of a discontinuity, properly accounting for the effects of dilation. The equation requires a number of parameters: ϕ_μ , c_i, ϕ_i, i^*, a_s, and a_c. The parameters ϕ_μ , c_i, and ϕ_i are relatively straightforward to evaluate. They are properties of the intact material and can be evaluated from sliding tests and strength tests on the intact material. The parameters i^*, a_s and a_c are much more

difficult to evaluate, and they will now be discussed in detail.

The parameters i^* and a_s are closely related to each other, as will be illustrated in Fig. 6-2. Figure 6-2a represents a portion of a discontinuity which is initially fully interlocked. (However, the comments which follow could be applied to a partially interlocked discontinuity as well.) If the discontinuity is "sheared" or displaced through a certain horizontal increment (Δu) and no shearing through of asperities occurs ($a_s = 0$), then sliding takes place on the most steeply inclined asperities, as in Fig. 6-2b. Thus, when $a_s = 0$, $i^* = i_1$, where i_1 is the inclination of the steepest asperities. For the case where there is only <u>one</u> steepest asperity on the discontinuity, sliding will take place on that steepest asperity alone <u>only</u> if there is no rotation of one of the discontinuity walls. If there is rotation, it is possible for sliding to take place on the steepest asperity <u>and</u> another less steep asperity.

For this case of no shearing, i^* is only dependent on the surface geometry of the discontinuity and the displacement of the discontinuity. (As displacement increases, asperities are overridden, the discontinuity contracts, and new asperities are contacted and slid upon.)

In the more general case, some of the asperities shear through. Figure 6-2c illustrates the case of $i^* = i_2$, where $i_2 < i_1$, for which $a_s \neq 0$. The two asperities with inclination i_1 are sheared in this case, while sliding takes place on the asperity with inclination i_2. Figure 6-2d illustrates the case of $i^* = i_3$, where $i_3 < i_2$. All asperities with inclinations greater than i_3 are sheared through, and sliding takes place on the asperity with inclination i_3. Therefore, it is apparent that the number of asperities sheared (and thus a_s) is dependent on the

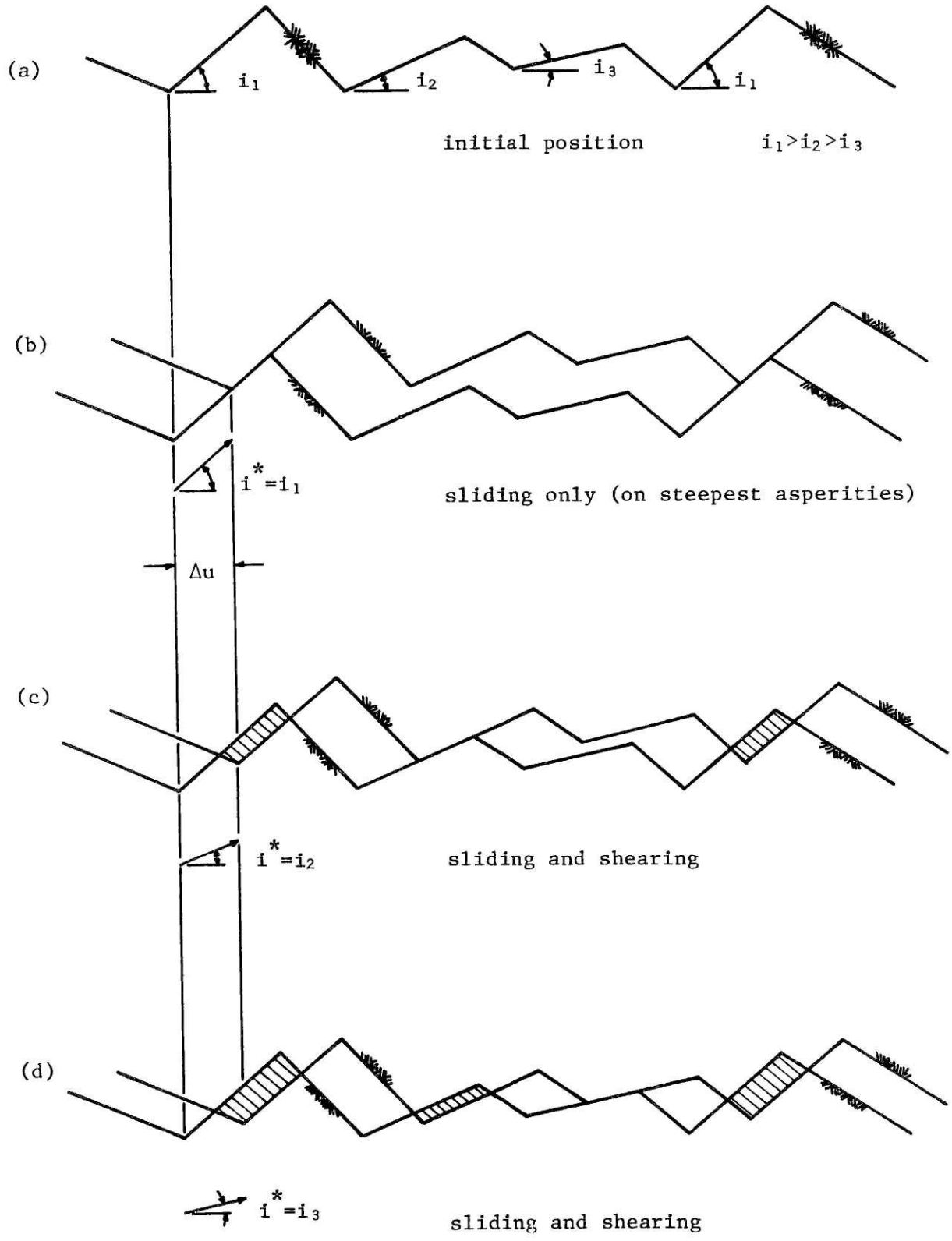

Figure 6-2 Illustration of the dependence of the shear area ratio (a_s) on the dilation angle (i*).

direction of displacement as given by i^*. As i^* decreases, a_s increases, and as i^* increases, a_s decreases.

Clearly, a_s depends on i^*: On a discontinuity where there are many contacting asperities with different inclinations, any particular direction of displacement will cause sliding or shearing on the various asperities. The total shear resistance of the discontinuity in that direction is the sum of the resistances provided by its asperities for displacement in that direction. Of all the possible directions of displacement, sliding actually takes place only in the direction of least resistance, and that is i^*. For this value of i^*, there is an associated value of a_s.

From the above discussion, it is apparent that all of the parameters which influence the resistance due to sliding or shearing also influence the dilation angle (i^*), and in turn, the shear area ratio (a_s). These parameters include σ, ϕ_μ, i, c_i, and ϕ_i. The effect of σ was clearly shown by Patton (1966), as discussed in Section 2.2, where low σ favors sliding and high σ favors shearing. The effects of the other parameters are not as clearly defined. However, in general, it is expected that high values of i and ϕ_μ and low values of c_i and ϕ_i will favor shearing, while low values of i and ϕ_μ and high values of c_i and ϕ_i will favor sliding. Because these parameters affect the relative amounts of sliding and shearing which takes place, they will also affect i^* and a_s.

Use of eq. 6.13 requires the evaluation of its parameters at the particular "moment" that a value of τ is desired. Because τ varies with shear displacement (see Fig. 2-2, for example), that "moment" corresponds to a value of displacement. If it is desired to predict τ at its peak value, (τ_p), then the required parameters must be evaluated at the

displacement corresponding to τ_p. Peak shear resistance for some discontinuities may occur at virtually no displacement, such as for tightly interlocked discontinuities. In general, however, some displacement of the discontinuity is likely to take place before peak resistance is reached. This means that there will be some sliding and/or shearing prior to peak resistance. This is likely to be true for discontinuities which are initially only partly interlocked, such as the discontinuity illustrated in Fig. 6-3. For this discontinuity, peak resistance does not occur immediately (Fig. 6-3a), but after some displacement takes place (Fig. 6-3b).

If τ_p occurs after a certain amount of displacement, then the parameters required in eq. 6.13 must be evaluated at that displacement. Since i^* and a_s change with displacement, their evaluation is a difficult task. As a discontinuity undergoes displacement, i^* and a_s are continuously changing as asperities make and break contact, and as the surface geometry of the discontinuity changes due to asperity shearing. Figure 6-3 provides an example of how i^* and A_s change as the discontinuity is displaced.

Evaluation of the parameters i^* and a_s clearly requires that the displacements of the discontinuity during shear be considered. Proper modelling of the different mechanisms of shear resistance requires consideration of the relationship between resistance and displacement. Resistance can be expressed through the parameters i^* and a_s, which in turn are dependent on a number of other parameters describing the discontinuity. Therefore, i^* and a_s must be related to displacement.

Just as i^* and a_s are a function of displacement, the contact area ratio (a_c) also depends on displacement. Initially, a_c depends on the surface geometry of the two walls of the discontinuity, the normal stress

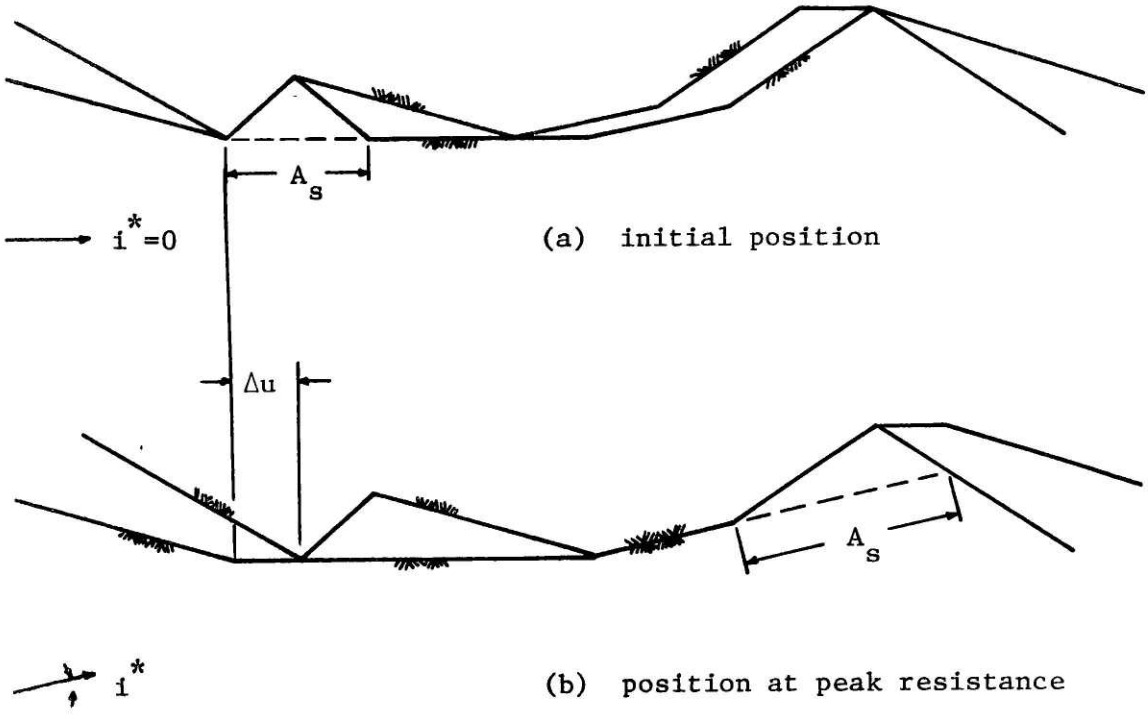

Figure 6-3 Partially interlocked discontinuity, with peak resistance occurring after some displacement.

acting on the discontinuity, and the deformability of the intact material. As the discontinuity undergoes displacement, a_c will change as asperities are slid upon and sheared through. From Fig. 6-2, it is readily seen that when the discontinuity is displaced from its initial position (Fig. 6-2a) to any of the other positions (Fig. 6-2b,c,d), the contact area (and therefore a_c) decreases.

From the above discussion, it is apparent that i^*, a_s, and a_c depend on a number of factors which describe the physical properties of the discontinuity, as well as being closely interdependent. At the present time, however, there is no method available to predict these parameters for a particular discontinuity. In addition, there is little experimental information on this subject:

Ladanyi and Archambault (1970) measured i^* and a_s on model discontinuities and proposed empirical relationships for each which described their dependence on normal stress (σ), (see Section 3.2). Barton (1971) measured i^* in model tests and presented an empirical relationship which described its dependence on normal stress (σ) relative to the unconfined compressive strength (σ_c) of the intact material, (see Section 3.3). These relationships were developed from very limited tests, and they may or may not apply to discontinuities in general.

In summary, a general relationship (eq. 6.13) was developed to determine discontinuity shear resistance (τ) which is dependent on a number of parameters. Some of these parameters (i^*, a_s, a_c) are very difficult to evaluate, because they are dependent on a number of physical factors describing the discontinuity and also on the displacement of the discontinuity as it is sheared. The shearing process of a discontinuity is a

highly complex one, due primarily to irregular geometry involving a combination of shearing and sliding mechanisms. The following section formulates a possible solution using a numerical modeling technique, whereby the shearing process of an irregular discontinuity is simulated.

6.2 SIMULATION OF DISCONTINUITY SHEAR

In the preceding section, the influence of displacement on shear resistance was pointed out. The direction of displacement (as given by i^*) and how this direction changes during displacement must be determined in order to predict shear resistance.

The direction of sliding, at any particular displacement position, is the direction of minimum shear resistance, as was discussed in the previous section. The shear resistance of the discontinuity in this direction, as well as any other direction, is the sum of resistances provided by individual asperities on the discontinuity. Individual asperity resistance can be due to the sliding mechanism or the shearing mechanism, depending on the displacement direction and the asperity geometry, as illustrated in Fig. 6-4. Figure 6-4a shows two asperities which contact one another across a discontinuity. If the dilation angle (i^*) is greater than the asperity inclination (i), as in Fig. 6-4b, then the upper asperity will lift off the lower asperity, and there is no resistance by that particular asperity. If $i^* = i$, as in Fig. 6-4c, the two asperities will slide over each other, and there is sliding resistance. If $i^* < i$, as in Fig. 6-4d, one or both of the asperities will be sheared through. On a discontinuity where there are many contacting asperities with different inclinations, any particular direction of displacement will cause a combination of

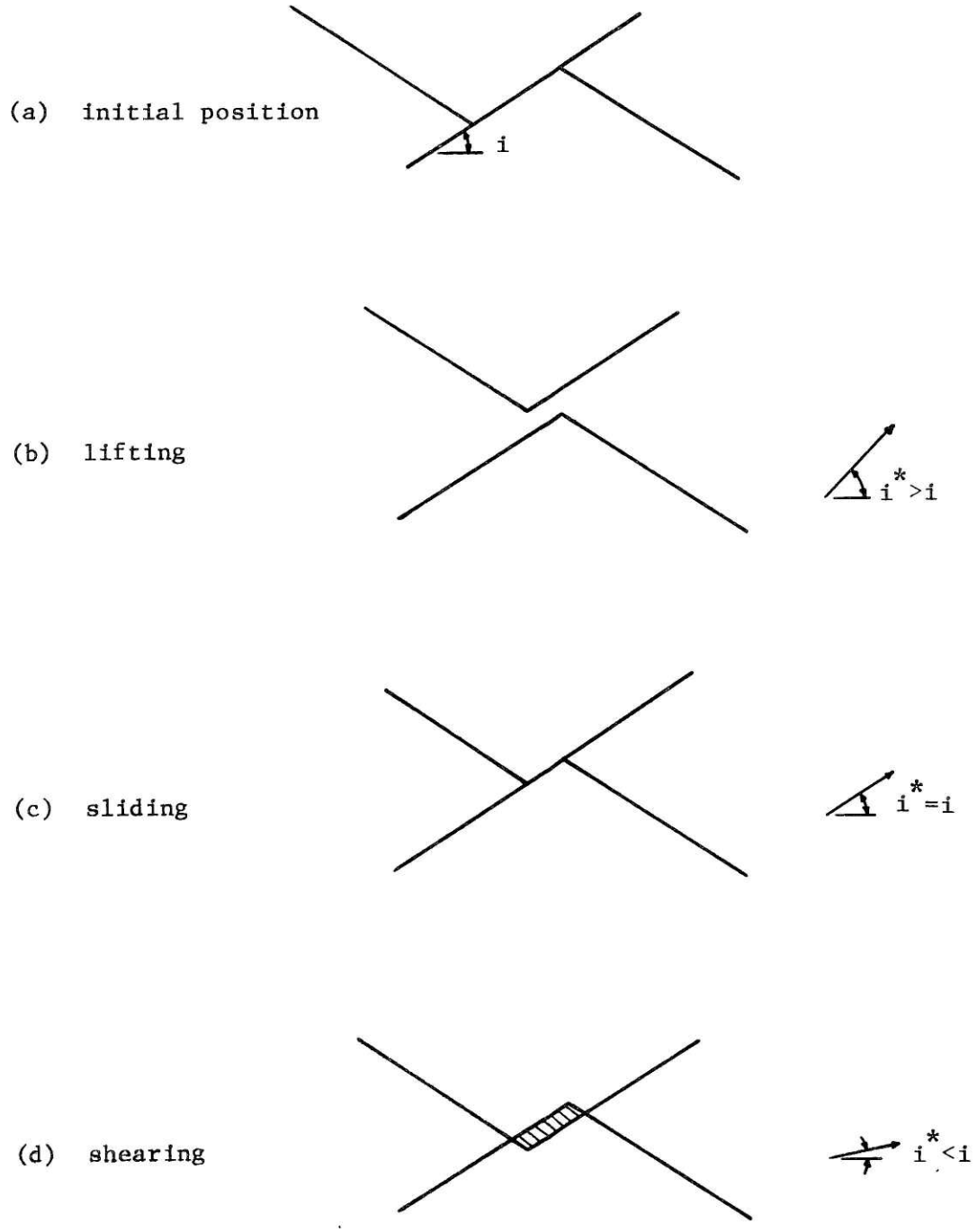

Figure 6-4 Asperity lifting, sliding, and shearing.

lifting, sliding, and shearing on different asperities. The total shear resistance of the discontinuity in that direction is the sum of the resistances provided by its asperities for displacement in that direction. Of all the possible directions of displacement, there is only one direction in which sliding actually takes place, the direction of least resistance. By determining the actual direction of displacement and how it changes during displacement, a complete description of the shearing of a discontinuity can be achieved.

The Simulation Process

A procedure will now be described whereby the shearing of a discontinuity is simulated to account for the displacement-dependence of shear resistance. Starting from a description of the physical properties of the discontinuity (geometry, material properties, loading conditions), the discontinuity is "sheared" in an incremental process. For each increment in the process, the displacement direction and the associated value of shear resistance are evaluated. The method by which the displacement direction is determined is an iterative one. Shear resistance is evaluated in different directions until the direction of least resistance is determined. This direction is then the actual displacement direction for the increment. The discontinuity is displaced through the increment, and the surface geometry of the discontinuity is altered to account for any asperity shear in the increment. The process is then repeated in the same way for the next increment.

The procedure just described can be divided into three major steps, as illustrated in Fig. 6-5. The three steps are: 1. discontinuity

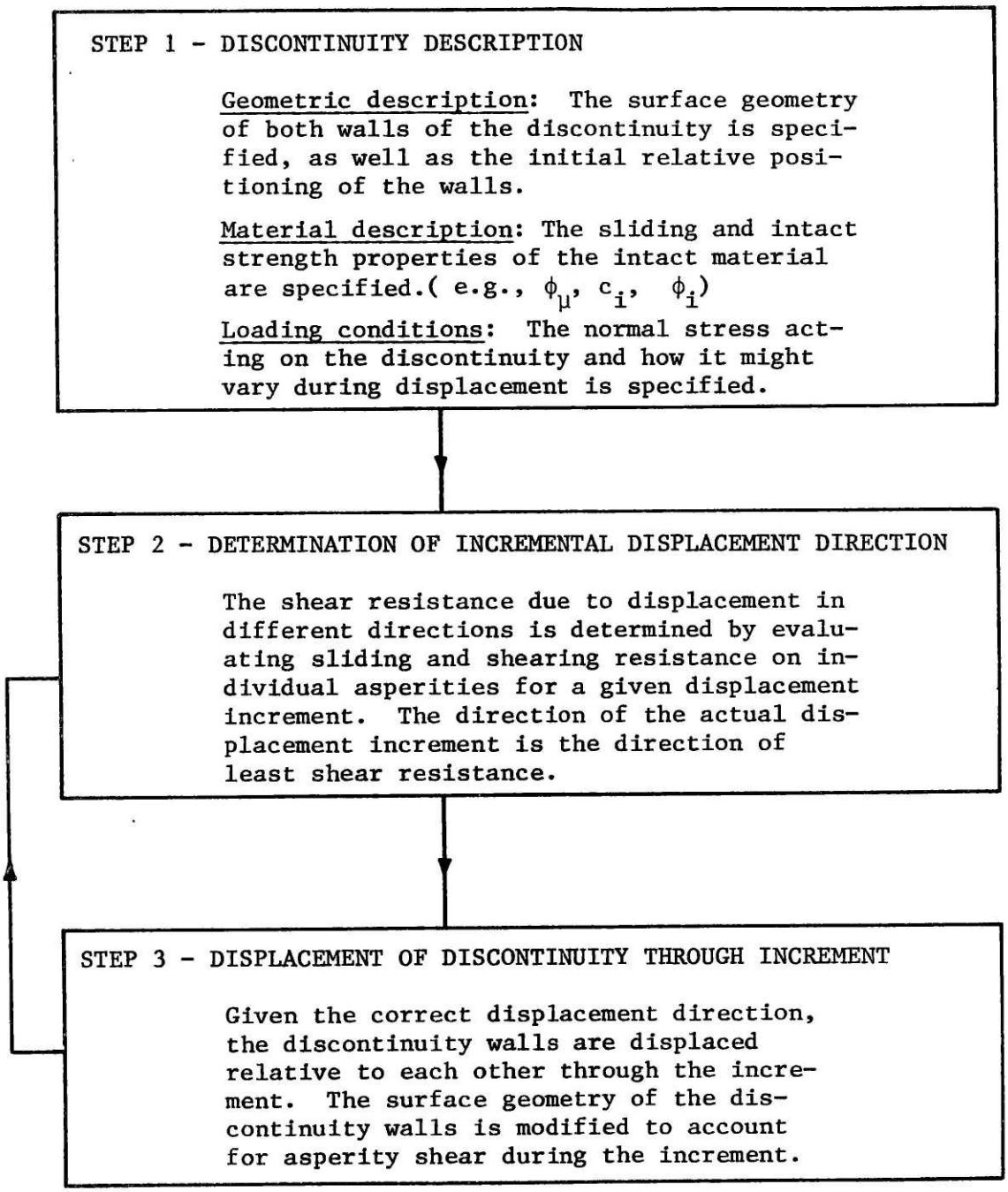

Figure 6-5 Steps in the shear simulation process.

description, 2. determination of incremental displacement direction, and 3. displacement of discontinuity through increment. These steps follow each other in order, after which steps 2 and 3 are repeated in a cycle so that the discontinuity is "sheared" through as many increments as desired.

Procedures for performing the above-described steps will now be presented.

Step 1 - Discontinuity Description

To describe the surface geometry of the discontinuity, a two-dimensional representation of the two walls of the discontinuity is proposed. The geometry of each wall is represented by a "profile". For convenience, these profiles are discretized such that they consist of straight line segments which join at specified locations called "nodes". This is illustrated in Fig. 6-6a. The nodes are located at coordinates which are multiples of certain horizontal and vertical increments. The profiles are defined by specifying the vertical coordinate of the profile at every horizontal node coordinate, with straight lines assumed between adjacent nodes. A discontinuity will have an "upper" profile and a "lower" profile defined in this way.

The reason for choosing this type of discretized geometric description is to simplify manipulation of the profiles during the simulation process. This will be apparent as the process is further described. This type of approach can closely approximate any profile if the node spacing is chosen small enough. One difficulty which does arise, however, is due to the fact that rotation of the profiles is very difficult to model with

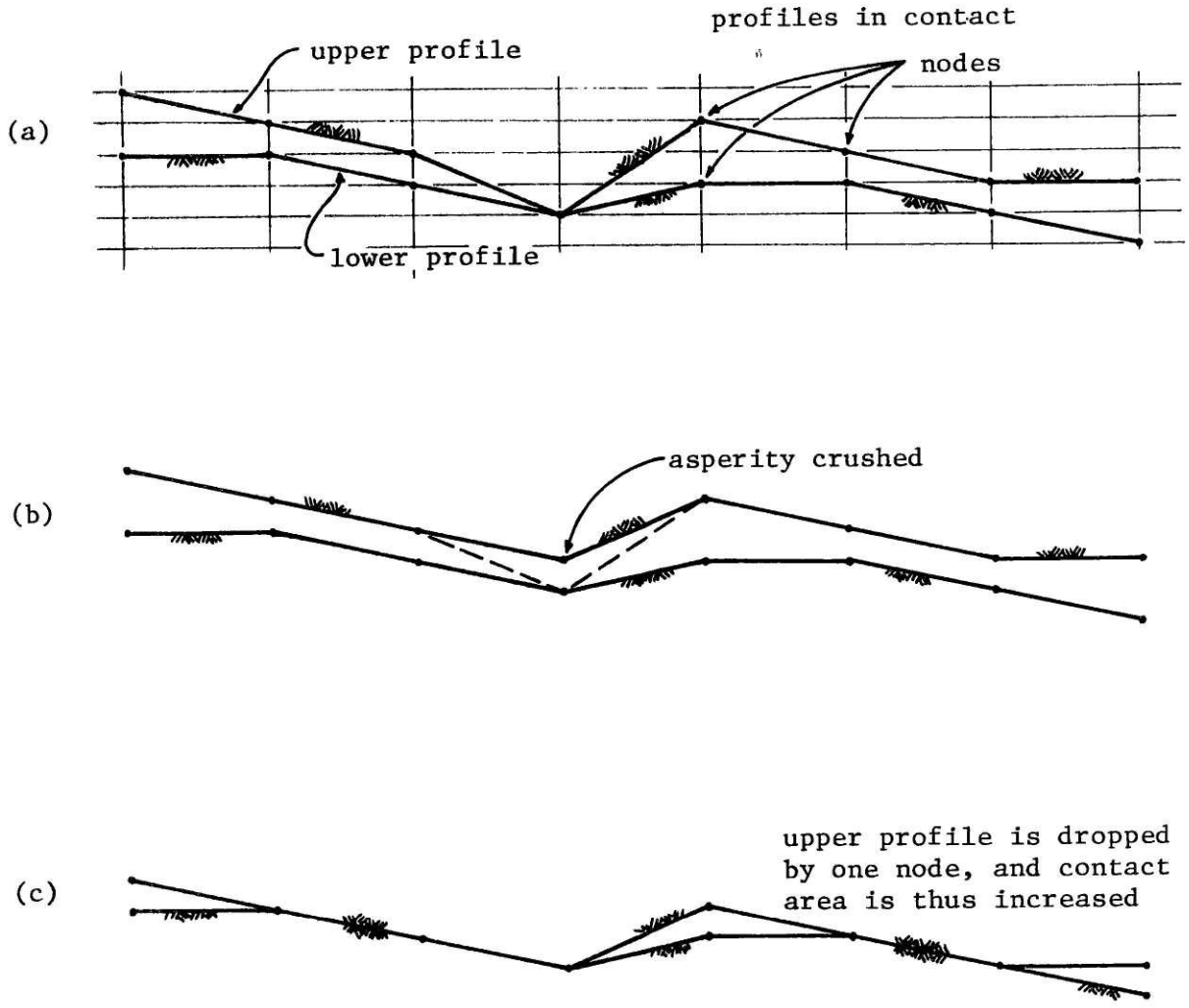

Figure 6-6 Discretized discontinuity profiles, with illustration of the "crushing" process.

this type of approach. While incremental horizontal and vertical displacements of the nodes on the profile can be accounted for, rotation of the entire profile cannot be accurately described by a discretized system of nodes.

The material composing the walls (profiles) of the discontinuity are considered rigid, with sliding properties given by ϕ_μ and intact strength properties given by c_i and ϕ_i. The exact manner in which these parameters are used is described subsequently under step 2.

The relative positions of the upper and lower profiles must be specified prior to shearing. This can be done by simply placing the two profiles in contact with one another. However, in some cases, this will result in very little contact <u>area</u> between the profiles. For example, the two profiles in Fig. 6-6a are in contact with one another, but there is no contact area between them. Under the application of normal force to the discontinuity, there is likely to be crushing of the contacting asperity due to the high localized stresses at the asperity tip. The asperity will crush until the contact area across the discontinuity has increased sufficiently to reduce the contact stresses to an acceptable level.

This type of crushing action to cause an increase in the contact area can be modelled in the following way. It will be assumed that there is some minimum contact area (A_m) across the discontinuity at all times, and that this minimum contact area is directly proportional to the normal force (N) on the discontinuity. A quantity defined as the asperity crushing strength (σ_{cr}) will be used to determine A_m through the following relationship:

$$A_m = \frac{N}{\sigma_{cr}}$$

If the actual contact area (A_c) between the two profiles is less than A_m, then crushing of the contacting asperities will occur until $A_c \geq A_m$. An illustration of this process is presented in Fig. 6-6. At the point of contact between the profiles in Fig. 6-6a, one of the profiles is "crushed" or "reduced" by one vertical node increment. In this case, it is obvious that the upper profile should be "crushed", as shown in Fig. 6-6b. In general, the decision as to which profile is crushed can be made by evaluating the slopes of the asperity faces on each side of the contact node for each profile. In this way, a quantitative assessment of the "steepness" of the contacting asperities can be made. The "steepest" asperity is the one which should be crushed.

Once all of the contacting nodes along the discontinuity have been crushed by one vertical node increment, the entire upper profile is decreased by one vertical node increment to bring the profiles in contact with each other, as illustrated in Fig. 6-6c. This will result in an increase in actual contact area (A_c). If A_c is still less than A_m, then the crushing procedure must be repeated until $A_c \geq A_m$. The discontinuity will then be "ready" for the next step in the simulation process.

Step 2 - Determination of Incremental Shear Direction

As stated previously, the incremental shear direction is determined by evaluating the resistance due to displacement in different directions, and choosing the direction of minimum resistance. A procedure for determining the resistance to displacement for a given direction will now be described.

Figure 6-7a shows a portion of a discontinuity at the initial position

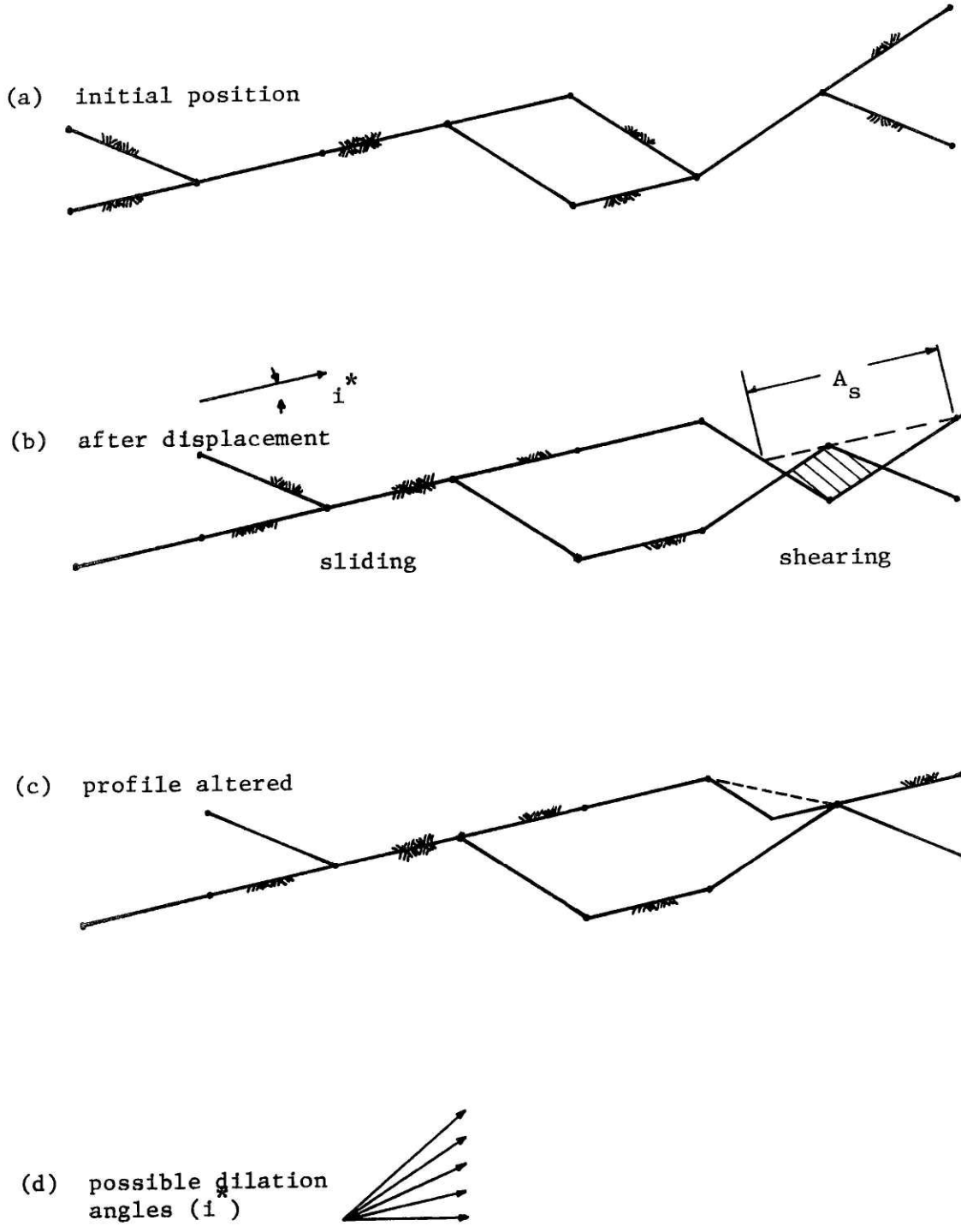

Figure 6-7 Displacement increment for a discontinuity, involving sliding and shearing.

of an increment, with a given displacement direction given by i^*.

(Possible directions of displacement must be limited to certain discrete directions, in order that the upper profile always passes through nodal locations. In other words, the dilation angle (i^*) is restricted to angles whose tangents are multiples of the ratio of one vertical node increment to one horizontal node increment, as illustrated in Fig. 6-7d. This limitation will not be serious as long as the vertical nodal increments are small enough relative to the horizontal nodal increments.)

In Fig. 6-7b, the upper profile has been displaced through the increment in the direction given by i^*. Over this displacement, it is apparent that sliding takes place at one location, while shearing takes place at another. As previously discussed and illustrated in Fig. 6-4, in general, contacting asperities will either lift, slide or shear during a displacement increment. Only sliding and shearing provide resistance to displacement, so a method by which these resistances can be evaluated must be formulated.

To account for sliding resistance on an asperity, eq. 6.1 as developed in Section 6.1 can be used.

$$S_r = N_r \tan(i^* + \phi_\mu) \qquad (6.1)$$

To evaluate S_r, it is necessary to know N_r, i^*, and ϕ_μ. i^* is specified for the increment, and ϕ_μ is a material property, so that only N_r needs to be determined. This will be discussed later in this section.

To account for resistance due to asperity shear, eq. 6.3 as developed in Section 6.1 can be used.

$$S_s = c_i A_s + N_s(\tan \phi_i + \tan i^*) \qquad (6.3)$$

To evaluate S_s, it is necessary to know c_i, ϕ_i, i^*, N_s, and A_s. N_s and A_s are the only parameters which need to be determined, as i^*, c_i, and ϕ_i are already known.

Equation 6.3 assumes a failure plane which is parallel to the shear direction, i.e., horizontal. Alternatively, a planar failure surface could be assumed to be parallel to the direction of displacement. These two types of failure planes are illustrated in Fig. 6-8a. An analysis of the case where the failure plane is inclined at an angle equal to i^* is presented in Fig. 6-9, resulting in the following relationship for resistance due to asperity shear:

$$S_s = \frac{c_i A_s}{\cos i^* - \sin i^* \tan \phi_i} + N_s \tan (i^* + \phi_i) \qquad (6.14)$$

The same parameters required in eq. 6.3 are also required in eq. 6.14, except that A_s is different for each equation (see Figs. 6-8c and 6-8b).

As discussed in Chapter 5, the assumed mechanism of failure (the form and position of the failure surface) can have an important effect on the calculated value of asperity shear resistance. To obtain an accurate value of asperity shear resistance for each asperity being sheared on a discontinuity during an increment, it would be necessary to examine each one individually to determine the appropriate failure mechanism. For the proposed sumulation process, involving many asperities, this would be practically impossible. A simplified method must be adopted, such as one of the methods just described above. Both of these methods are recognized as being approximate, and it is not known which of them will yield the more correct answer. However, from consideration of the "after shear"

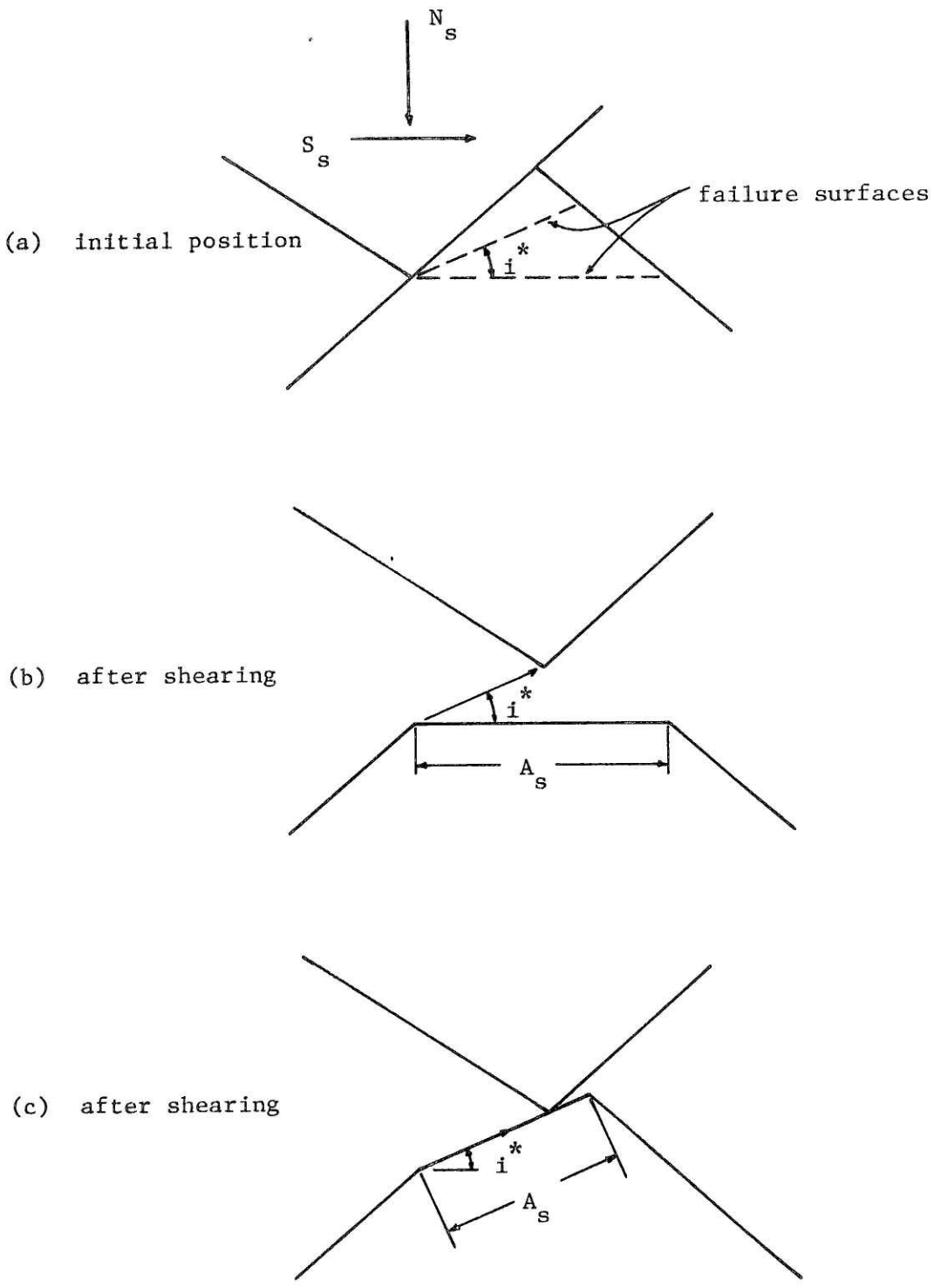

Figure 6-8 Two different failure plane assumptions for asperity shear.

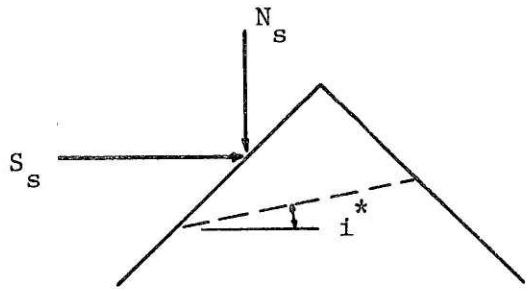

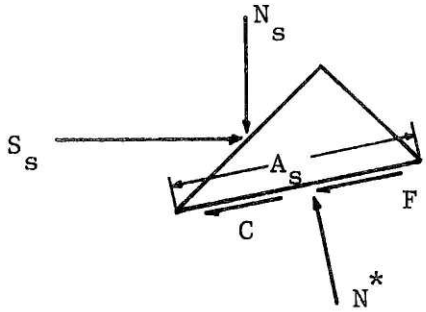

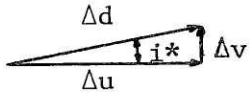

$$C = c_i A_s$$

$$F = N^* \tan \phi_i$$

$$N^* = N_s \cos i^* + S_s \sin i^*$$

work in = work out

$$S_s \Delta u = N_s \Delta v + (C + F) \Delta d$$

$$S_s \Delta d \cos i^* = N_s \Delta d \sin i^* + \{ c_i A_s + (N_s \cos i^* + S_s \sin i^*) \tan \phi_i \} \Delta d$$

$$S_s = N_s \tan i^* + (c_i A_s)/\cos i^* + N_s \tan \phi_i + S_s \tan \phi_i \tan i^*$$

$$S_s (1 - \tan \phi_i \tan i^*) = (c_i A_s)/\cos i^* + N_s (\tan \phi_i + \tan i^*)$$

$$S_s = \frac{c_i A_s}{\cos i^* - \sin i^* \tan \phi_i} + N_s \tan(\phi_i + i^*)$$

Figure 6-9 Derivation of asperity shear resistance for a failure plane inclined at an angle equal to the dilation angle.

geometry of the sheared asperities, a failure plane inclined at an angle i^* appears to produce a more reasonable result. Figures 6-8b and 6-8c indicate how the lower asperity in Fig. 6-8 would appear after shear according to the two different failure plane assumptions. (The procedure for establishing after-shear geometry is discussed in step 3 , which follows below.) If the failure plane is horizontal, as in Fig. 6-8b, the asperities separate from one another during the increment. If the failure plane is inclined at i^*, as in Fig. 6-8c, then there is a contact point between the asperities at the end of the increment. From a geometric standpoint, it appears more reasonable to assume an inclined failure plane at an angle i^*. This assumption will be used for this simulation process.

In addition to specifying the inclination of the failure plane, its exact location must be known in order to determine A_s. An inclined failure plane has been drawn in Fig. 6-7b (shown as a dashed line) through the asperity on the upper profile, although it could have been drawn as well through the lower asperity, or through both asperities. Figure 6-10 shows an enlarged view of the two shearing asperities from Fig. 6-7, showing possible failure planes. The failure planes must be inclined at an angle i^*, and must also pass through possible nodal locations. (This last requirement that the failure plane passes through nodes is necessary because the failure plane eventually becomes part of a profile.) Among all of the possible failure planes, the actual failure plane chosen is the one which has the least area (or length in this two-dimensional profile). From Fig. 6-10, the failure plane with minimum length is the uppermost, and it has been drawn in Fig. 6-7b. This procedure provides a value of A_s to use in eq. 6.14. If there is more than one failure plane of minimum

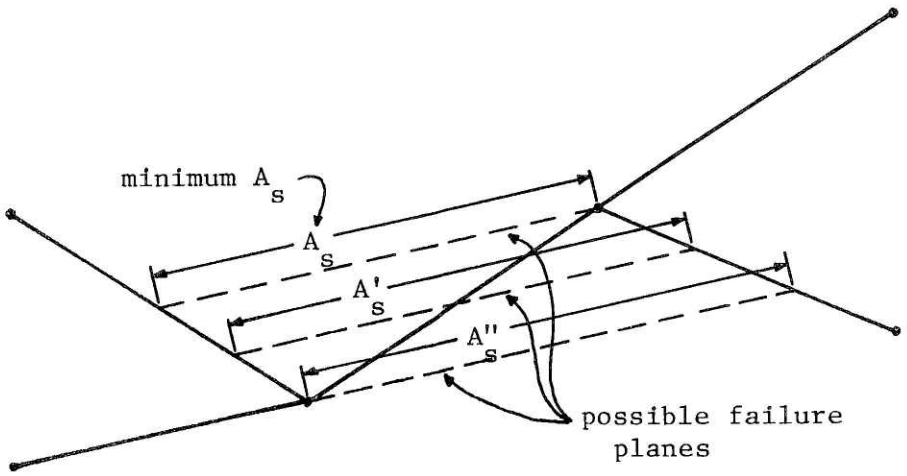

Figure 6-10 Possible failure planes for two shearing asperities.

size, then it seems that any arbitrary procedure for choosing among them would be acceptable.

Use of eqs. 6.1 and 6.14 requires that the normal force on each sliding and shearing asperity be known. As discussed in Section 6.1, the actual distribution of normal force over an irregular discontinuity depends on a number of factors and is difficult to evaluate. For reasons of simplification, a uniform distribution of normal force over the contact area of the discontinuity is assumed for the shear simulation process. This means that the normal force acting on an asperity is directly proportional to the contact area on the asperity.

$$N(\text{asperity}) = \frac{A_c(\text{asperity})}{A_c(\text{discontinuity})} \quad N$$

However, since the contact area changes during a displacement increment, the quantities A_c(asperity) and A_c(discontinuity) must be average values for the increment.

From the above considerations, the resistance due to sliding (S_r) or shearing (S_s) can be calculated for individual asperities on a discontinuity. Before these individual resistances can be combined to determine discontinuity resistance, the way in which S_r and S_s might change during the displacement increment must be considered.

Figure 6-11 illustrates in a conceptual way how S_r and S_s are expected to change with displacement.

Sliding resistance (S_r) is constant during displacement provided that N_r, i^*, and ϕ_μ are constant. The two submechanisms of the sliding mechanism, friction and dilation, provide resistance which is constant

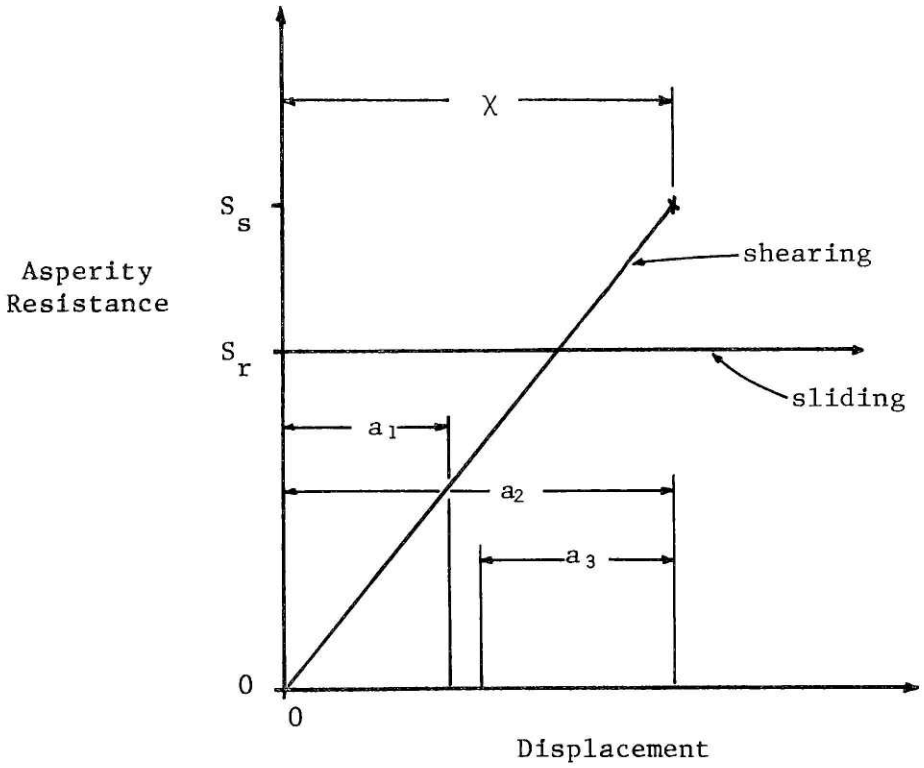

Figure 6-11 Sliding resistance and shearing resistance as a function of displacement.

with displacement, as shown in Fig. 6-11.

Resistance due to asperity shearing has a quite different form. As the asperity is displaced, the resistance will increase from zero to a maximum value of S_s. For a brittle material, the asperity will break when $S = S_s$, and the resistance will drop. The average value of S which a shearing asperity provides over a certain displacement "a" will depend on the magnitude of "a" relative to the displacement required to cause asperity failure (χ), as well as depending on the position of the increment "a"relative to the position of the increment χ. From Fig. 6-11, it is apparent that the average value of S due to asperity shear is different for $a = a_1$, $a = a_2$, and $a = a_3$. In contrast, the average value of resistance due to sliding is always equal to S_r, independent of a.

It is therefore quite important to consider the deformation characteristics of shearing asperities on a discontinuity in order to properly model their resistance for a displacement increment. This is true in spite of the fact that the material has been modelled as a rigid material thus far. The deformation that an asperity undergoes prior to failure is expected to be dependent on a number of factors: asperity size and shape, deformability of the intact material, and the direction and magnitude of the applied stresses causing failure. In order to estimate how the quantity χ might vary due to changes in these parameters, a deformation analysis of different sizes and shapes of asperities was performed. A description of the analysis and the results are given in Appendix A. For asperities composed of the same material, it is concluded that χ can be expected to vary as much as an order of magnitude, depending on the level of normal stress and the size and shape of the asperity. However, it is

noted that χ increases with increasing asperity size and decreases with decreasing asperity inclination. Measurements of size and inclination of asperities on actual discontinuities indicate that as size increases, inclination decreases. Therefore, these two effects have the opposite effect on χ, and tend to cancel each other. (see Appendix A for more details)

Although χ is probably different for different asperities, it is suggested that an average value of χ could be estimated for all the asperities on the discontinuity. If this average value of χ is used as the displacement increment (i.e., $a = \chi$), then the average value of resistance due to asperity shear for the increment will be equal to $\frac{1}{2} S_s$.

A summary of the overall procedure which has been outlined in Step 2 is as follows: Equations 6.1 and 6.14 can be used to evaluate individual asperity resistance for a given displacement direction and increment. N_r and N_s are evaluated from the contact area of the asperity. A_s is evaluated from the length of the failure plane through the sheared asperity. Individual asperity resistances from sliding and shearing are then added to produce the total shear resistance for the discontinuity in the given direction. The entire procedure is then repeated for different displacement directions until the direction of minimum resistance is determined.

Step 3 - Displacement of Discontinuity Through Increment

Once the displacement direction has been established in Step 2, the upper profile is displaced through the increment. The shear resistance of the discontinuity for that increment is the resistance determined in Step 2.

The upper and lower profile must now be changed to account for

asperity shear which has taken place. This is done by taking the failure planes as the new profile in that asperity. Figure 6-7c illustrates how the failure plane (dashed line in Fig. 6-7b) now becomes part of the upper profile. The sheared portion of the asperity is simply eliminated. In effect, this procedure simplifies the process by ignoring the influence of sheared material (gouge) on the behavior of the discontinuity.

From Fig. 6-7c, it is apparent that the failure surface, which now represents part of the upper profile, does not have both endpoints on nodes. The left endpoint is halfway between nodes, and therefore cannot be described with the present system of nodes. It is necessary to re-define this portion of the asperity, as shown by the dotted line in Fig. 6-7c, so that a straight line between adjacent nodes is obtained. This is a necessary approximation to satisfy the discrete nature of the profile description.

In general, the contact area between profiles will decrease over a displacement increment. Comparison of Fig. 6-7a with 6-7c shows how contact area is decreases through both sliding and shearing. It is possible that the contact area may decrease below the minimum allowable value of A_m, as discussed in Step 1. In this event, the crushing procedure (also discussed in Step 1) must be implemented to increase the contact area.

The discontinuity is now ready to be displaced through another increment, and the process returns to Step 2. Steps 2 and 3 (and possibly Step 1) are repeated until the discontinuity has been sheared through the desired number of increments.

6.3 DISCUSSION OF THE SHEAR SIMULATION PROCESS

Section 6.2 presented a procedure for simulating the shearing of an irregular discontinuity. Using this procedure, the complete shear resistance-displacement behavior of a discontinuity can be modelled. The important steps in the procedure have been described in some detail, but the development at this point is still conceptual and further work must be done before the simulation process can be actually implemented. It is intended that the simulation be performed numerically with a computer.

The simulation process employs a number of approximations and simplifications in its present form, and some of these deserve further theoretical consideration. Probably the most important of these is the method of evaluating the resistance of a shearing asperity during an increment. The deformability of the asperities and how this influences incremental shear resistance (and therefore the incremental discontinuity resistance) should be examined further. Another important aspect of asperity shear is the failure mechanism assumption. Chapter 5 pointed out some of the inaccuracies involved in various failure mechanism assumptions, which indicates a need for attempting to evaluate the influence of asperity failure mechanism on the simulation process.

Successful implementation of the simulation process will provide a valuable tool with which to study the shear behavior of discontinuities in rock. The process would lend itself readily to a parametric study of the influence of various factors on discontinuity shear resistance-displacement behavior. For example, the influence of different distributions of asperity sizes and shapes for a given discontinuity could be investigated without difficulty. This type of information is important for probabilistic considerations of discontinuity behavior.

CHAPTER 7

SUMMARY AND CONCLUSIONS

This thesis has employed a mechanistic approach to analytically describe the shear resistance of rock discontinuities. Two basic shearing mechanisms have been identified: the sliding mechanism and the shearing mechanism.

The sliding mechanism represents sliding on horizontal and inclined surfaces of the discontinuity. Friction, as an important part of the sliding mechanism, has been studied in detail. Investigation of friction theory and observations of rock friction from stick-slip experiments have revealed that friction in rocks is not clearly understood. Experimental observations of friction in minerals indicate that test conditions have an important influence on sliding behavior. In particular, surface conditions of cleanliness, roughness, and moisture play an important role in controlling sliding resistance.

The shearing mechanism represents shearing through asperities on the discontinuity. Different methods for theoretically calculating single asperity shear resistance have been presented and compared. The base shear method, a simple and commonly used method which assumes a failure surface parallel to the plane of the discontinuity, has been shown to significantly overestimate asperity shear resistance in some cases.

The two mechanisms of sliding and shearing have been combined in an analytical relationship describing the shear resistance of a discontinuity. The parameters affecting this relationship are difficult to evaluate, since they are strongly dependent on the displacement of the discontinuity during shear. Therefore, in order to properly model the dependence of shear resistance on displacement, a shear simulation process has been proposed, in which a geometric representation of the discontinuity is sheared in increments of displacement. The direction of displacement for each increment is the direction resulting in the least resistance, and is determined in an iterative procedure. The major steps in the shear simulation process have been formulated in this thesis, and it promises to be a useful tool in the study of shear behavior of rock discontinuities. Further development on a detailed level is required before the process can be implemented.

REFERENCES

Archambault, G. (1972) "Comportement Méchanique Des Massifs Fracturés", Thèse de doctorat, Ecole Polytechnique de Montréal.

Barton, N. R. (1976a) Personal communication.

Barton, N. R. (1976b) "The shear strength of rock and rock joints", International Journal of Rock Mechanics and Mining Sciences, Vol. 13, pp. 255-279.

Barton, N. R. (1973) "Review of a new shear strength criterion for rock joints", Engineering Geology, Vol. 7, No. 4, pp. 287-332.

Barton, N. R. (1971) "A relationship between joint roughness and joint shear strength", Paper I-8, Proc. Sym. on Rock Fracture, Nancy.

Bathe, K. -J. (1976) "ADINA - A finite element program for automatic dynamic incremental nonlinear analysis", Report 82448-1, Acoustics and Vibration Laboratory, Mechanical Engineering Department, M.I.T., May.

Bowden, F. P. and Tabor, D. (1964) Friction and Lubrication of Solids, Part II, Oxford University Press, London.

Brace, W. F. (1972) "Laboratory studies of stick-slip and their application to earthquakes", Tectonophysics, Vol. 14, pp. 189-200.

Brace, W. F. (1963) "Behavior of quartz during indentation", The Journal of Geology, Vol. 71, No. 5, pp. 581-595.

Brace, W. F. and Byerlee, J. D. (1966) "Stick-slip as a mechanism for earthquakes", Science, Vol. 153, pp. 990-992.

Brinch Hansen, J. and Lundgren, H. (1960) Hauptprobleme der Bodenmechanik, Springer-Verlag, Berlin.

Bromwell, L. G. (1966) "The friction of quartz in high vacuum", Research Report R66-18, Department of Civil Engineering, M.I.T.

Byerlee, J. D. (1970) "The mechanics of stick-slip", Tectonophysics, Vol. 9, pp. 475-486.

Byerlee, J. D. (1976a) "Frictional characteristics of granite under high confining pressure", Journal of Geophysical Research, Vol. 72, pp. 3639-3648.

Byerlee, J. D. (1967b) "Theory of friction based on brittle fracture", Journal of Applied Physics, Vol. 38, pp. 2928-2934.

Byerlee, J. D. (1966) "The frictional characteristics of Westerly granite", Ph.D. Thesis, M.I.T., Department of Geology and Geophysics.

Byerlee, J. D. and Brace, W. F. (1968) "Stick-slip, stable sliding, and earthquakes - effect of rock type, pressure, strain rate, and stiffness", Journal of Geophysical Research, Vol. 73, No. 18. pp. 6031-6037.

Dieterich, James H. (1972) "Time-dependent friction in rocks", Journal of Geophysical Research, Vol. 77. No. 20, pp. 3690-3697.

Dickey, J. W. (1966) "Frictional characteristics of quartz", S.B. Thesis, Department of Chemical Engineering, M.I.T.

Dokos, S. J. (1946) "Sliding friction under extreme pressures", Journal of Applied Mehcanics, Vol. 13, pp. A148-A156.

Drennon, C. B. and Handy, R. L. (1972) "Stick-slip of lightly loaded limestone", International Journal of Rock Mechanics and Mining Sciences, Vol. 9, pp. 603-615.

Fairhurst, C. (1964) "On the validty of Brazilian test for brittle materials", International Journal of Rock Mechanics and Mining Sciences, Vol. 1, pp. 535-546.

Hardy, W. B. and Doubleday, I. (1922) "Boundary lubrication - the temperature coefficient", Proc. of the Royal Soc., A101, pp. 487-492.

Hill, R. (1950) The Mathematical Theory of Plasticity, Oxford University Press, New York.

Horn, H. M. and Deere, D. U. (1962) "Frictional characteristics of minerals", Geotechnique, Vol. 12, No. 4, pp. 319-355.

Hoskins, E. R., Jaeger, J. C., and Rosengren, K. J. (1968) "A medium-scale direct friction experiment", International Journal of Rock Mechanics and Mining Sciences, Vol. 5, pp. 143-154.

Ladanyi, B. and Archambault, G. (1970) "Simulation of shear behavior of a jointed rock mass", Proc. 11th U.S. Symposium on Rock Mechanics, Berkeley, pp. 105-125.

Meyerhof, G. G. (1953) "The bearing capacity of foundations under eccentric and inclined loads", Proc. 3rd International Conference on Soil Mechanics and Foundation Engineering, Vol. 1, pp. 440-445.

Meyerhof, G. G. (1951) "The ultimate bearing capacity of foundations", Geotechnique, Vol. 2, pp. 301-332.

Patton, F. D. (1966) "Multiple modes of shear failure in rock and related materials", Ph.D. Thesis, University of Illinois, (also see: "Multiple modes of shear failure in rock", Proc. First Cong. Int. Soc. Rock Mech., Vol. 1, pp. 521-524, Lisbon, 1966.)

Penman, A. D. M. (1953) "Shear characteristics of a saturated silt, measured in triaxial compression", Geotechnique, Vol. 3, pp. 312-328.

Prandtl, L. (1920) "Über die Härte plastischer Körper", Nachr. kgl. Ges. Wiss. Göttingen, Math. phys. Klasse., p. 74.

Rabinowicz, E. (1965) Friction and Wear of Materials, Wiley, New York.

Rengers, N. (1970) "Influence of surface roughness on the friction properties of rock planes", Proc. 2nd Cong. Int. Soc. Rock Mech., Belgrade, Vol. 1, paper 1-31.

Rowe, P. W. (1962) "The stress-dilatancy relation for static equilibrium of an assembly of particles in contact", Proc. of the Royal Society, A269, pp. 500-527.

Rowe, P. W., Barden, L., and Lee, I. K. (1964) "Energy components during the triaxial cell and direct shear tests", Geotechnique, Vol. 14, No. 3.

Scholz, C., Molnar, P., and Johnson, T. (1972) "Detailed studies of frictional sliding of granite and implications for the earthquake mechanisms", Journal of Geophysical Research, Vol. 77, No. 32, pp. 6392-6406.

Sokolovskii, V.V. (1965) Statics of Granular Media, Pergamon Press, Oxford.

Stesky, R. M., Brace, W. F., Riley, D. K., and Robin, P.-Y. F. (1974) "Friction in faulted rock at high temperature and pressure", Tectonophysics, Vol. 23, pp. 177-203.

Terzaghi, K. (1925) Erbaumechanik, Franz Deuticke, Vienna.

Tschebotarioff, G. P. and Welch, J. D. (1948) "Lateral earth pressure and friction between soil minerals", Proc. 2nd Int'l. Conf. Soil Mech., Vol. 7, p. 135.

APPENDIX A

ASPERITY DEFORMATION ANALYSIS

This appendix presents the method and results of an analysis to determine the magnitude of displacements which an asperity on the surface of a discontinuity undergoes prior to shear failure. These deformations are approximated by computing the elastic deformations of an idealized asperity under the application of stresses which would cause failure according to an assumed failure mechanism.

Figure A-1a illustrates the idealized asperity shape and loading conditions assumed in the analysis. A symetric asperity on the surface of a discontinuity is loaded by uniform normal and shear stresses equal to those which cause shear failure of the asperity. The horizontal displacement of the asperity tip (χ) is a measure of the deformation of the asperity, and is the quantity which is calculated in the following analysis. The asperity material is modelled as being a linearly elastic, brittle material under the applied stresses, so that the shear resistance-deformation curve is linear as shown in Figure A-1b. This is an approximation to actual asperity deformation, where the curve is expected to be non-linear due to inelastic, non-linear material behavior.

The horizontal displacement χ is a function of the size and shape of the asperity (as given by i and B), the elastic material constants (E,ν), and the applied stresses (n,s). The deformations of an asperity

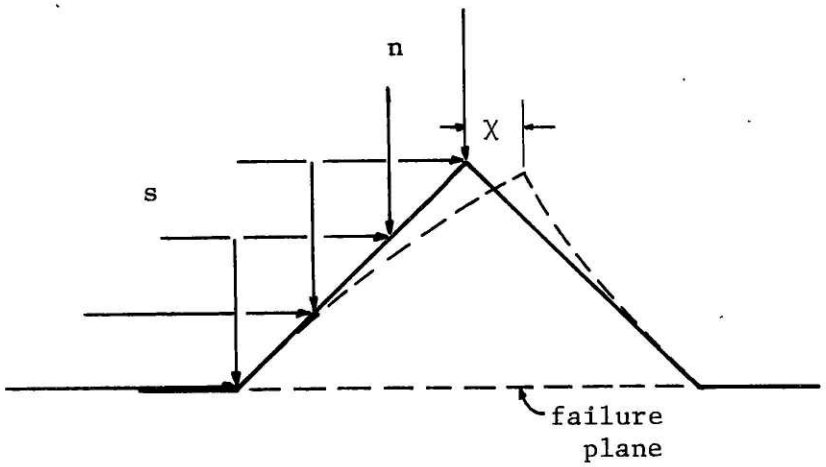

(a)

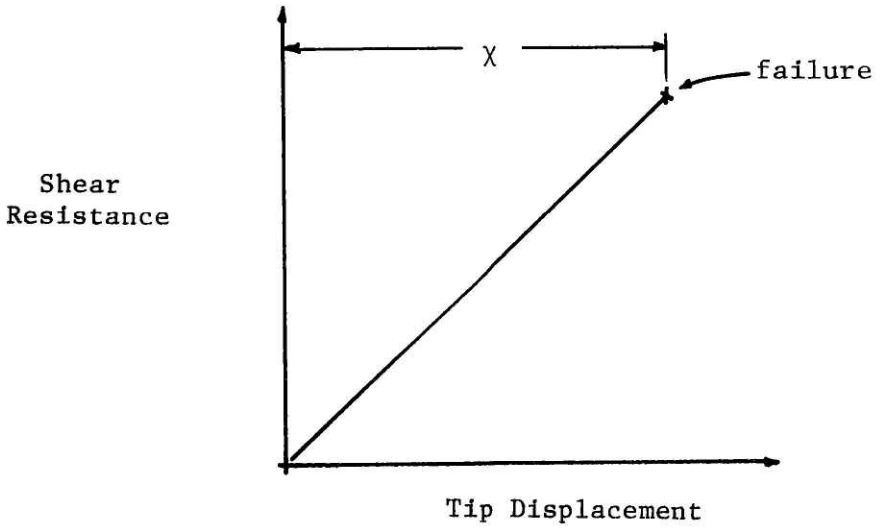

(b)

Figure A-1 Idealized asperity shape, loading conditions, and relation between shear resistance and asperity tip displacement.

were modelled by the finite element method. The finite element program ADINA (Bathe, 1976) was used for the analysis. The grid used to represent an asperity is presented in Fig. A-2a. The asperity is divided into twelve elements, with each element having seven or eight nodes, depending on its location. A linear, elastic material model was used, with elastic constants E and ν .

Asperity deformations for all combinations of B, E, n, and s were obtained by analysing and then combining two different loading cases for each asperity inclination (i), as will be shown below. In one loading case, unit normal loading (n = 1) was applied, as in Fig. A-2b. In the other loading case, unit shear loading was applied (s = 1), as in Fig. A-2c. In both cases, values of E = 1.0, ν = 0.3, and B = 1.0 were used. (The exact value of ν has little influence on the displacements of the asperity.) These two loading cases yield values of horizontal tip displacement which are designated I_n and I_s, where I_n is the influence value (= displacement under unit loading) for normal loading and I_s is the influence value for shear loading.

Values of χ for different values of B, E, and n (or s) can be obtained directly, due to elastic proportionality. That is,

$$\chi = \frac{B\ n}{E} I_n$$

and

$$\chi = \frac{B\ s}{E} I_s$$

The principle of superposition enables a combination of normal and shear loading to be expressed by

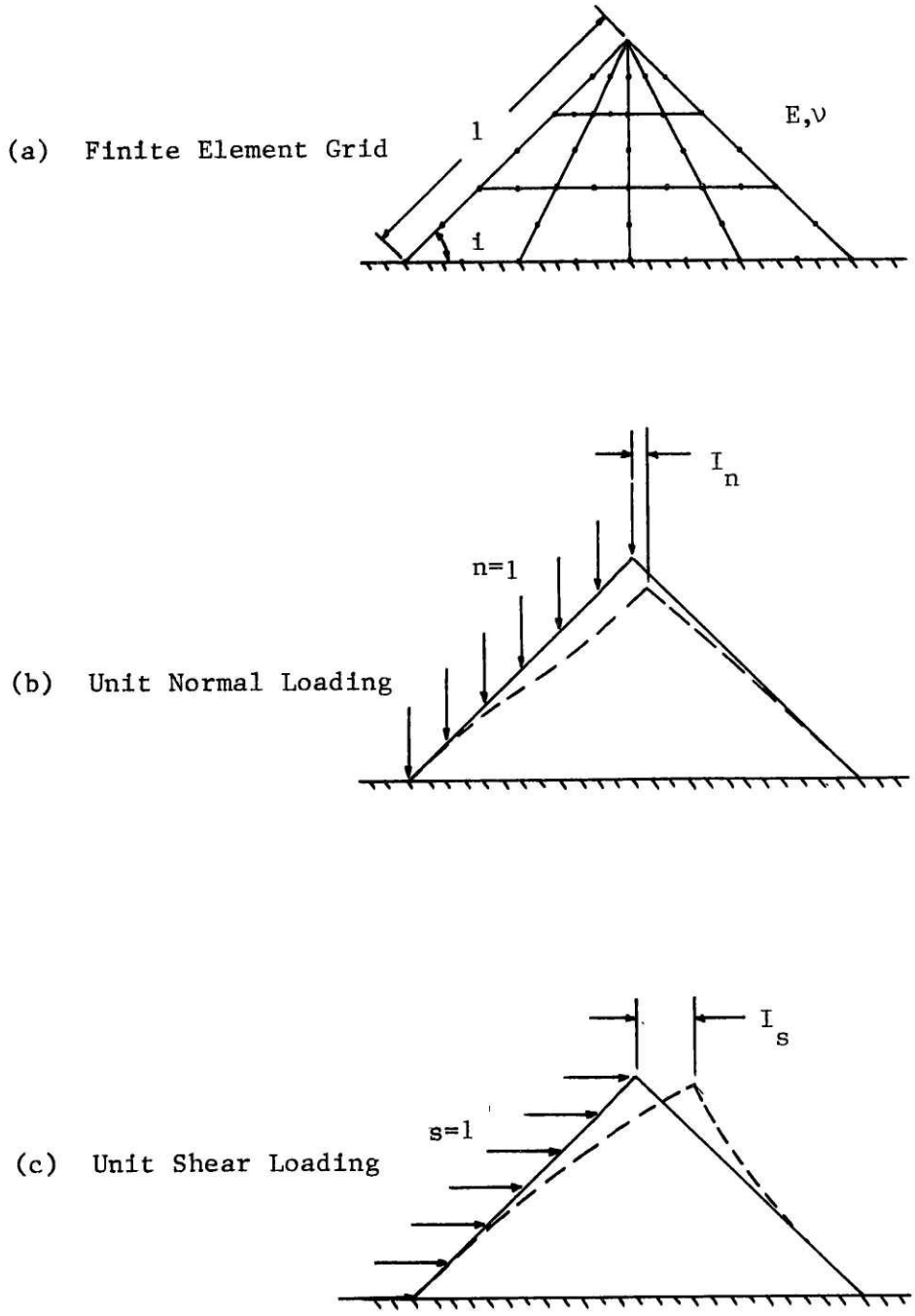

Figure A-2 Finite element grid for asperity, and the two loading cases.

$$\chi = \frac{B\ n}{E} I_n + \frac{B\ s}{E} I_s$$

or

$$\chi = \frac{B}{E} (n I_n + s I_s) \qquad (A.1)$$

In this way, the elastic horizontal tip displacement of an asperity (χ) can be calculated directly from the two influence values obtained for a given asperity inclination. Influence values were computed by the finite element method for four different asperity inclinations: i = 15°, 30°, 45°, 60°, and are listed in the following table:

i =	15°	30°	45°	60°
I_n =	-0.02	-0.15	-0.49	-1.47
I_s =	0.35	0.84	1.80	4.81

The relationship between n and s at failure of the asperity can be determined with one of the methods of calculating asperity shear resistance described in Chapter 5. Here the base shear assumption is used, where the failure surface is a horizontal plane through the base of the asperity, as shown in Fig. A-1a. Section 5.2 presented the analysis for this method, the following relationship between n and s at failure was developed:

$$s = 2 \cos i\ c_i + n \tan \phi_i \qquad (5.10)$$

This equation can be substituted into eq. A.1 to yield

$$\chi = \frac{B}{E}\left(n I_n + (2 \cos c_i + n \tan \phi_i) I_s \right)$$

or $$\chi = \frac{B\, c_i}{E} \left(\frac{n}{c_i} I_n + (2 \cos i + \frac{n}{c_i} \tan \phi_i)\, I_s \right) \qquad (A.2)$$

For convenience, a quantity U is defined as

$$U = \frac{n}{c_i} I_n + (2 \cos i + \frac{n}{c_i} \tan \phi_i)\ I_s \qquad (A.3)$$

so that $$\chi = \frac{B\, c_i}{E}\ U \qquad (A.4)$$

From eq. A.4, it is seen that the horizontal displacement of the asperity tip at failure (χ) is directly proportional to the size of the asperity (B), the cohesion of the intact material (c_i), and the quantity U, and is inversely proportional to the elastic modulus (E). The quantity U, as indicated by eq. A.3, is a function of the asperity inclination (i), the ratio of normal stress to cohesion ($\frac{n}{c_i}$), and the angle of internal friction (ϕ_i). Figure A-3 illustrates the variation of U with $\frac{n}{c_i}$ for different values of i, with $\phi_i = 30^\circ$.

The results of the above analysis can now be applied to the asperities of a given discontinuity. If the intact material of the discontinuity is homogenous, then E, c_i, and ϕ_i are identical constants for all of the asperities. Therefore, differences in χ for different asperities will be due to differences in B and U, with U depending on i and $\frac{n}{c_i}$.

From eq. A.1 and Fig. A-3, it can be seen that χ increases with increasing B and increasing i. Measurement of asperity size (B) and inclination (i) of asperities on actual rock discontinuities (Rengers, 1970) indicate that as B increases, i decreases. In other words, asperities

$$U = (n/c_i)\ I_n + \{\ 2 \cos i + (n/c_i) \tan \phi_i\ \}\ I_s$$

$$\chi = \frac{B\ c_i}{E}\ U$$

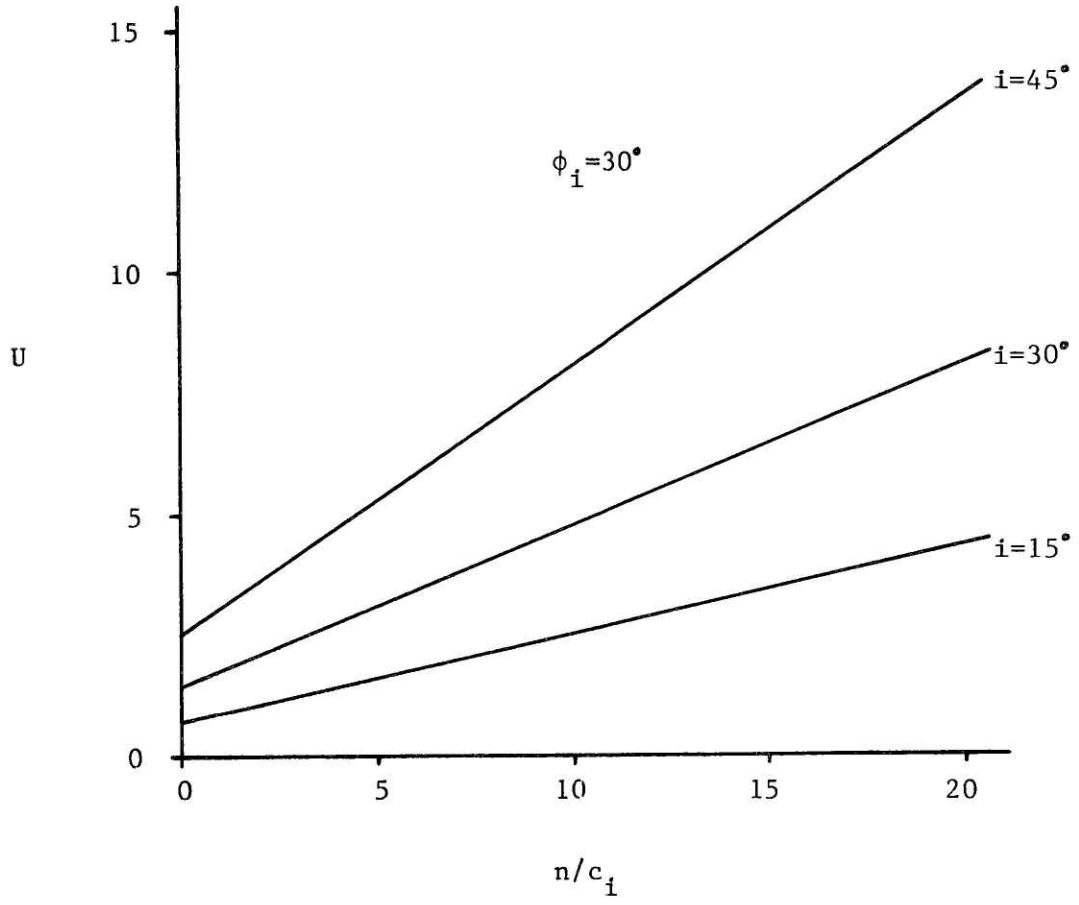

Figure A-3 Plot of U vs. n/c_i for i = 15°, 30°, 40°, with ϕ_i = 30°.

with large B are likely to have small i, and asperities with smaller B are likely to have larger i. These two factors thus have a cancelling effect on each other, and values of χ for different asperities will tend to be more similar because of this.

From Fig. A-3, it can also be seen that U (and therefore χ) increases as n/c_i increases. The effect is different for different values of i, being more pronounced for the larger values of i.

In summary, on a given discontinuity the variation in horizontal tip displacement (χ) of asperities at failure depends on asperity size (B), asperity inclination (i), and normal stress (n). While it is difficult to make definite quantitative conclusions, possible variations in B, i, and n on a discontinuity suggest that χ may vary as much as an order of magnitude for different asperities on a discontinuity.